ELSEVIER Solar Energy Materials & Solar Cells 58 (1999) 1–131

Solar Energy Materials & Solar Cells

www.elsevier.com/locate/solmat

Colouration of tungsten oxide films: A model for optically active coatings

K. Bange*

Schott Glas, R&D, Otto-Schott-Straße 2, 55127 Mainz, Germany

1. Introduction

Optically active thin-film coatings can alter their optical properties as a function of changes in external conditions. The changeable optical characteristics can be obtained by different physical and chemical processes in a large number of materials. These substances, recently named "chromogenics" [1], embrace both inorganic and organic materials. The mechanisms responsible for the reversible variation of the optical properties of films may basically be divided in three different types:

Thermochromic films change their optical properties as a function of substance temperature. The films alter their optical data reversibly when heated, and return to their original properties when cooled to the starting temperature.

Photochromism may be defined as a reversible absorption change triggered when a film is exposed to different types of irradiation, and it regains the original properties

* Tel.: 49-6131 667231; Fax: 49-6131 667380; e-mail: bge@schott.de

0927-0248/99/$ - see front matter © 1999 Elsevier Science B.V. All rights reserved.
PII: S0927-0248(98)00196-2

without irradiation. This type of material has been investigated primarily in glasses so far, but not very extensively in thin films.

Electrochromism is a unique property of thin films or thin film systems to change colour, due to an applied potential, and change back to the original state by a potential reversal. From a technological point of view, thin electrochromic films are best investigated, and they are the most promising candidates for various applications in the proximate future.

Materials with controllable light absorptance, transmittance or reflectance possess a great technical relevance, because of their high potential applications. Single layers, or layer systems can be used for different types of devices, that can modulate their optical characteristics as a function of temperature, intensity of irradiation, applied external potentials, gases, etc. In the near future, optically active thin films may be utilized to regulate the throughput of radiation energy for windows in buildings and cars, to maintain comfortable lighting and temperature, in sun glasses, as an optically active filter, or in systems with variable reflectance, as automotive rear-view mirrors, in displays, in sensors or detectors, as road signs, and so forth.

The physical and chemical processes occurring in chromogenic materials and devices are of considerable scientific interest; because of electronic and ionic transport, changes in material composition, variation in structure or chemical potential, the formation of colour center, or small polarons and interfacial barrier effects, are all interrelated, i.e. the processes during the reversible optical switching are highly complex. For an understanding of the several processes, effects and mechanism, fundamental knowledge is required in solid-state chemistry and physics, thin-film science and technology, surface and interface physics with emphasis on the interaction of gases and liquids with solid-state surfaces, electrochemistry, techniques for material characterization and, sometimes, polymer physics.

A wide variety of optically active coatings have been discovered so far, and many alternatives are available for making thin films. Most of the investigations are documented on oxide films of transition metals and, generally, the electrochromism is studied in larger detail. Fairly recently, the first book, a comprehensive treatise on inorganic electrochromic materials, is published by Granqvist [2]. One type of chromogenism is mainly reported in the majority of communications, however, a detailed *survey of different chromogenic effects* on one film material which combine and compare systematically the processes under fundamental aspects is not available so far. But a comparative analysis of the results, on changes in optical properties produced by different colouration procedure can elucidate the principles and lead to a better understanding of basic chromogenic processes. To enlighten the essential colouration mechanism, *tungsten oxide films* are an ideal choice for such an approach, because

(i) tungsten oxide films exhibit the different types of chromogenism, i.e. thermochromism, photochromism and electrochromism and, in addition, some nonreversible colouration processes;
(ii) tungsten oxide films have been studied in much greater detail than any other chromogenic material;

(iii) tungsten oxide films are the most relevant of optically functioning layers in most of electrochromic devices studied thus far;
(iv) the physics and the chemistry of many other optically active oxides are fairly similar, so that tungsten oxide can serve as a more convenient model for elucidating salient properties of the whole class of optically active layers.

Despite the large amount of work on the different colouration effects of tungsten oxide films, many contradictory results are still reported and the interpretation of the experimental data is still disputed. For example, the colouration of tungsten oxide film is explained by several models [3–7]; two of which, more acceptable than the others, are the intervalence charge transfer transition between W^{5+} and W^{6+} sites [3] and the small polaron absorption [4]. But the question as to whether the electron actually distorts the lattice around the tungsten to further lower its energy is still unclear. Another open subject is the explanation of the charge transfer across the solid-state interface. The electrochromic reaction is usually described by a double injection of a proton and an electron in the tungsten oxide films [8]:

$$WO_3\ (\text{transparent}) + xH^+ + xe^- \rightleftharpoons H_x\,WO_3\ (\text{coloured}). \tag{1.1}$$

Although the model is quite attractive and leads to kinetic models for colouration and bleaching, which are in reasonable agreement with the experimental results, its assumptions are not verified at all [9]. The fact that there is an agreement to the observed colouration is attributable to the optical properties being governed by the electron insertion or extraction, i.e. the term xe^- is the most important part in reaction (1.1). But, nevertheless, the chemical formula is mostly used, because it explains in a simple way, under tutorial aspects, the necessary charge compensation in the film.

In addition, chromogenic tungsten oxide films are not stoichiometric (WO_3); they are substoichiometric and contain hydroxyl groups and water in high concentration. While the injection of an electron for colouration is not debated, the intercalation of hydrogen from an external medium as described in reaction (1.1) has to be questioned, because up to now there exists no direct substantiated experimental proof that hydrogen concentration in the film increases during colouration [9]. Therefore, reaction (1.1) can certainly be only an oversimplified version of the more complex reality in the colouration process.

One of the reasons for that dilemma is that results are compared from experiments carried out on, in principle, "different" materials, although all films are named tungsten oxide or WO_3. The various deposition techniques used to produce the films on different substrates are creating very different film properties. In general, the as-deposited state, which is the basis for the chromogenic behaviour, is different in terms of density, composition, structure (amorphous, nanostructured clusters, polycrystalline, crystalline), etc. From the broad spectrum of deposition techniques, *evaporation* is the one most used to produce tungsten oxide films, and the films exhibit good optical switching capacity. Not as many changeable deposition parameters are available in this traditional vacuum technique as in other modern deposition methods. The main variables are the substrate temperature, the total pressure and the

deposition rate, which can manipulate the film properties only in a certain range. Therefore, tungsten oxide films deposited by evaporation seem an ideal candidate to develop a reasonably certain and specific model for the colouration in optically active coatings. Results obtained from the various analytical techniques on these film materials should be compared systematically for films coloured in accordance with different procedures.

Various possible procedures can create colouration in very different surroundings. Therefore, a further difficulty in obtaining a more unified description of the colouration mechanism is the *medium in the direct film neighbourhood*. Often, the interaction with environment is not considered in detail at all. Only some results comparable to the chromogenic colouration in a defined atmosphere can be found in the presence of hydrogen and oxygen-containing species. Photochromism and electrochromism are investigated in air or other oxygen or hydrogen-containing gases, or in liquid reservoirs. Thermochromism is reported in oxygen-free atmosphere. Electrochromism is also studied with solid state electrolytes containing hydroxyl groups, without changing the general nature of the effect. To overcome the problems with ill-defined films and environmental conditions, in this case study, the *chromogenism of evaporated tungsten oxide films* is considered essentially *in hydrogen, oxygen and water-containing reservoirs.*

Coloured tungsten oxide films create principally a new state able to be realized in optically non-active layers only by the use of a different material or deposition conditions. The changes in the optical data, i.e. the optical density, or the absorption and refractive index, is evoked by changes in the electron structure. This can be combined by variations in structure or in composition. Independent of the fact, that x is not a stoichiometry parameter for hydrogen in reaction (1.1), changes in other elements probably occur, especially in the electrochromic processes since charge compensation of the film is necessary.

Various types of information are necessary for a powerful description and a scientific understanding of the different effects, i.e. they have to be accessible to various experimental analyses. Since the as-deposited material is the basis for the optical switching behaviour, the influence of the actual deposition conditions on the film properties has to be known. Thin films are, in general, ill-defined systems, i.e. material characterization is important, both in transparent and coloured state. A sufficient analysis with different tools is necessary, since, for example, the film density, or the film composition, plays a dominant role in the optical efficiency. The most interesting films are highly disordered, but not truly amorphous, i.e. the nanoscale clusters and their changes during colouration have to be analysed to explain chromogenism on a molecular level. Additionally, results on the interactions of liquids, gases, or particles with solid-state surfaces are important, as they are describing the charge transfer mechanism in the interface of the different types of processes. Generally, a multimethod approach has to be used to obtain a better understanding of the various effects.

To add a new view to the scientific discussion, the main part of this contribution gives a detailed survey of different chromogenic effects of tungsten oxide films on tungsten oxide films deposited by evaporation which are coloured and bleached in

hydrogen and oxygen-containing reservoirs (Section 3).[1] To integrate this work in the overall picture of optically active coatings, Section 2 gives a short *overview on other relevant chromogenic thin-film materials* and provides some remarks on system design and applications, since electrochromism is not found in a single layer, but usually requires several of these, i.e. electrochromism is, strictly speaking, a device property. Different types of interactions are described in Section 2, which are responsible for changes in optical properties, and some key concepts characterizing the colouration effects are depicted. Some principles of device design are discussed, with emphasis on reflective and solid-state systems produced and investigated in our labs.[2]

The *as-deposited state* of evaporated tungsten oxide films is described in detail in Section 3.1, and the influence of the deposition conditions is treated for the density, structure, composition and the optical properties. Our "standard"[2] film, which exhibits excellent colouration features with good cycle stability in hydrogen and oxygen-containing reservoirs, is substoichiometric, WO_{3-z}, and contains high H, OH and H_2O content in bleached (as-deposited) state. The material appears "amorphous" in XRD, Raman and electron microscopy investigations, but a local cluster model based on SAXS investigation is presented [10].

Various *procedures* for reversible and non-reversible *colouration* are presented in Section 3.2. The influence of the reservoir conditions on the change in optical density and the kinetics of the switching behaviour is discussed. Ten different ways to realize the blue colour in WO_{3-z} are considered. Results of own studies represent the main part of Section 3.2. The electrochromism (Section 3.2.3) of our "standard" films is investigated in detail in gases, liquid electrolytes, and in the presence of solid-state films. The obtained findings, which create the basis of these contributions, are combined with data available in the literature on the colouration of tungsten oxide films by temperature, UV illumination, electron and ion beam bombardment. Independent of the applied colouration technique, the analysed changes in spectral absorption are essentially identical.

The *coloured state* is characterized in Section 3.3, and the differences between bleached and coloured material in electron configuration and optical properties, structure and composition are reported. For our "standard" films, a decreased vibration intensity is detected for the terminal W=O bond, and a linear relation is found between the injected charge and the W^{5+} content and the changes in optical density. The hydrogen concentration remains constant in the films during the colouration, while the oxygen content is decreased. To stimulate the discussion, unified models for material transport during colouration procedures are developed, which explain the different experimental data and also consider the influence of the composition on the reservoir in the colouration process.

[1] To help the reader each section and subsection starts with an abstract.

[2] Our "standard" films are produced with the "standard" parameters given in Section 3.1. All data not referred to any references are related to own investigations carried out on "standard" material.

Differences for *reversible* and *not completely reversible colouration* processes are discussed in Section 3.4. While in the not completely reversible processes oxygen desorption is prevailing, more complex reactions occur in reversible colouration. Tendencies for the detection of small polarons, and in changes in terminal W=O bond, are discussed and are related to the properties of as-deposited materials. The dominant role of the interface potential, which depends on the reservoir conditions, is discussed for the various effects. A unified view on the different interface potential is presented on the basis of the Fermi level concept for various media. Finally, Section 4 summarizes the chromogenism of coatings, with focus on optically active tungsten oxide films deposited by evaporation, and a new perspective of the different reaction channels for reversible and non-reversible colouration is depicted.

2. Chromogenic thin films and applications

This section gives a short overview on thin films with changeable optical features. Some key concepts to characterize the colouration are presented and some prototypes of device design are depicted.

Different types of mechanism are described as being responsible for the reversible variation of optical properties in optically active thin films. Thermochromism in thin film materials is summarized in Section 2.1. Changes in optical characteristics evoked by UV illumination are outlined in Section 2.2 demonstrating the photochromism in thin films. Electrochromism in cathodically or anodically colouring films are discussed in Section 2.3 with focus on the oxides of the transition metals. The colouration in organic and inorganic thin-film materials are dealt with in a short overview to give an impression on the various processes. Since, especially, electrochromism is in general a system property some principles on device design with focus on systems realized by ourselves and possible applications are given in Section 2.4. Different types of reflective configurations are depicted which can be used as car rear view mirrors.

2.1. Thermochromism

Temperature-induced changes in optical characteristics of coatings are considered briefly and the mechanism responsible for colour changes is summarized. Thermochromism in organic and inorganic thin-film materials is described. The most common transition metal compounds, especially the different oxides of vanadium, are discussed.

Thermochromism may be defined as the notable change in optical properties of materials, as a function of a substance's temperature. Since the variation of temperature is one of the simplest methods of attempting to change the state of materials, it is convenient to use the observation of thermochromism, especially in the visible range, as an indication of the possible existence of effects that can be induced by other means. Therefore, systematic studies of this phenomenon date back at least to the

1870s. Thermochromism is now observed in polymers, organic materials, compounds containing metals and, last but not least, in inorganic materials [11].

Of considerable interest are thin films changing their optical properties reversibly when heated, and returning to their original properties when cooled down to the starting temperature. Certain transition metal oxides and related compounds are candidates for such kind of behaviour. They transform from semiconducting to metallic state when a certain "critical" temperature is exceeded. For large-area devices, as, for example, the so-called "smart windows", thermochromic vanadium oxide, discovered in 1959 [12], is one of the most relevant materials. But also polymer-based thermochromic "cloud gels" are being developed for window applications.

Thermochromism of the different types of materials is based on a very different mechanism; it can, for example, be due to the equilibrium between different molecular species, cis–trans isomerization, crystal-face transitions, etc. The thermal behaviour of the different materials may be divided into two categories. One exhibits thermochromism over a wide temperature range, the other a sharp change in optical properties at a definite temperature. A gradual change in optical quantities over a wide temperature range may arise due to changes in the absorption band width, equilibrium between two forms of a molecule, especially in solutions, the degree of ionization, or any other chemical equilibrium process, but also to a change in the degree of order or extent of crystallinity. A sharp change in the optical data at a definite temperature generally signals a phase change, such as a melting or one change in crystal structure. Phase transitions are often associated with a change in the ligand field strength or in the coordination geometry.

Various *polymeric* materials exhibit thermochromism. Unusual optical properties have been reported for polydiacetylenes, which contain series of conjugated double and triple bonds. It is stated that substituents on the carbon chain have a considerable effect on the geometry, hence the energy state of the unsaturated backbone, so that polymers have a varying degree of thermal behaviour. A reversible colour change below 130°C is reported on polymers based on this system [13]. Transition temperatures between 16°C and 50°C are reported [14]. A number of other polymeric systems have been reported to be thermochromic as, for example, poly(3-alkylthiophene), poly(p-xylyleneviologen dibromide), acrolyl-L-valine, and spirooxazine [15–18]. Also several silicon-based polymers exhibit thermochromism, including silanes and siloxanes [19].

Other types of *organic* thin-film systems have been investigated. The thermochromic behaviour of spiropyran films is continuously studied. It is suggested that the properties of the thermochromism do not depend on the planarity of the molecules, but on the electron density of the lone pair of electrons in the imino nitrogen atom [20]. Rhodamine B in solution exhibits, for example, an absorptance spectrum (maximum at 550 nm) which depends on solvent and concentration, as well as on temperature [21].

Another type of thermochromism has been exhibited in compounds containing *metals*. The spectra of Cu_2HgI_4 and Ag_2Hgl_4 show, for example, the presence of an absorption band edge position that depends on the temperature. The band edge

moves to the red with increasing temperature, though the red shift is not linear with temperature, but shows a marked increase at about 50°C for the silver salt, and at 70°C for the copper compounds [22,23].

A different class of thermochromic materials are the *transition metal oxides* which exhibit a dielectric-to-semiconductor transition. Typically, the transition from one state to another is accompanied by a sharp change in electrical conductivity, as well as changes in other physical properties, such as crystalline symmetry. A change in the properties during the transition has been observed in Ti_2O_3, Ti_3O_5, Ti_4O_7, Ti_5O_9, Ti_6O_{11}, V_2O_3, V_3O_5, V_5O_9, V_6O_{11}, V_8O_{15}, VO_2, V_6O_{13}, NbO_2, Fe_3O_4, amongst others [24]. But also doped compounds, such as tungsten-doped VO_2 thin films, have been investigated [25]. The transition temperature in such compounds is reduced (10–18°C).

Inorganic thermochromic materials have been the subject of intensive experimental and theoretical study. Several theoretical models were developed in an attempt to interpret experimentally observed behaviour. Major theories include the excitonic dielectric theory [26] and a model developed by Hubbart [27] and extended by Mott [28] and Adler [29]. The most common inorganic thermochromic thin-film materials, in terms of how much they have been investigated, are crystalline transition metal compounds, especially the different oxides of vanadium [30–34]. VO_2 exhibits a sharp semiconductor–metal transition at ~ 68°C. Below the transition temperature, the structure of VO_2 is monoclinic (perovskite structure), and above the transition temperature the symmetry is rutile, with vanadium atoms occupying the body-centred tretragonal positions. The conductivity changes, at the transition temperature, over several orders of magnitude. The spectral switching characteristic of VO_2 films deposited on glass shows that the change in the transmittance and reflectance is quite low in the visible range and occurs mainly in the near-infrared region. These materials seem, at the moment, the best candidates for commercial applications.

2.2. Photochromism

This section outlines the colouration of thin films evoked by UV illumination. Organic and inorganic materials exhibiting changes in optical characteristics are briefly described.

Many materials and compounds exhibit a change in optical properties when exposed to a certain type of irradiation, but regain their original properties when placed in the dark [35]. This reversible process has been called photochromism. Thus, photochromism may be defined as a reversible absorption change undergone by a system when a suitable activation source irradiates the substance. The induced absorption disappears spontaneously upon removal of the activation source. Since many compounds exhibit this phenomenon, a broader definition for photochromism has been established. This definition can be represented by the equation given in Fig. 1.

A and B represent energy states of the respective material, with energies E_i and E_j, and hv is the energy of electromagnetic radiation. The two energy states possess

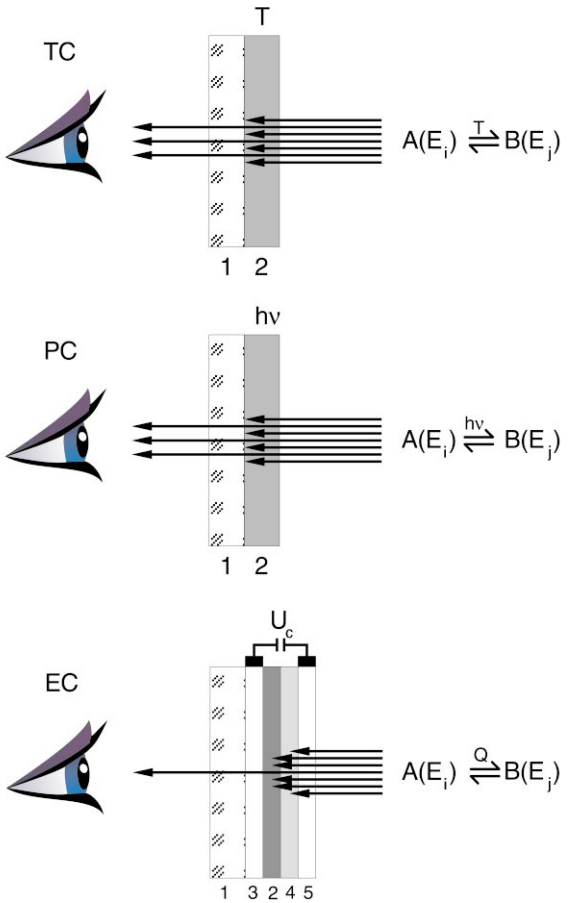

Fig. 1. Schematic representation of different types of (TC: thermochromic, PC: photochromic, EC: electrochromic) devices with optically active thin films. The illustrated basic device configurations consist of different components denoted as follows: 1 marks the glass, 2 the optically active coating, 3 and 5 the electrodes, and 4 the electrolyte.

distinct, different absorption spectra, and a reversible change is induced in at least one direction by the action of electromagnetic radiation. The photochromic phenomenon has been observed in various organic and inorganic substances in solid form and/or solution. The energy of the electromagnetic irradiation *hv*, which induces the formation of the coloured (activated) species, is usually situated in the blue region and/or in the UV range of the spectrum. The coloured state of the substances typically absorbs in the visible region, with few exceptions, which absorb in the near-infrared.

Although, the photochromism was first phenomenologically observed in inorganic materials, subsequent developmental work has proliferated the number of *organic materials* considerably. Though a rather large number of organic materials exhibit

photochromism, the important photochromic processes of these diverse organic substances can still be classified into four categories on the basis of process mechanisms: heterolytic cleavage, homolytic cleavage, cis–trans isomerization, and tautomerism [36]. In addition to these processes, the photophysical process involving excited state absorption, particularly triplet–triplet absorptions, is responsible for photochromism of many materials.

The heterolytic cleavage process is the most extensively studied photochromic mechanism so far. Organic compounds, which undergo heterolytic cleavage, are spiropyrans and triarylmethanes. The electromagnetic radiation energy breaks a single heterolytic bond of a molecule, forming a charged part which exists as an isolated ion or may be connected to other chemical bonds. These charged moieties are relatively stable and can recombine thermally to regenerate the original molecule.

Different deposition methods have been used for the production of spiropyran films. Some investigations have been made on spiropyran films prepared by vacuum deposition [37,38]. The thickness of the deposited films varied between 300 and 1000 nm, and the evaporation rate between 3 and 8 nm s^{-1}. But also a plasmapolymerization process is reported [39]. Film thicknesses of about 500 nm are obtained and the absorptance in the as-deposited films depends slightly on the used rf power, but is very similar to that of vacuum-deposited films. The possibility of controlling photochromic reactions has been investigated in Langmuir–Blodgett spiropyran films, too [40,41].

Homolytic cleavage produces free radicals which rapidly undergo side reactions. Thus, photochromic compounds of this class are not commercially useful. Photochromism, created by cis–trans isomerization of carbon–carbon double bonds, is observed, for example, in polyenes. Generally, the trans-isomer is a thermodynamically more stable state and is photochemically converted to the cis-isomer. Tautomerism involves shifting the equilibrium between isomers, similar to the case of cis–trans isomerization. One example of organic compounds exhibiting photochromism by hydrogen transfer tautomerism are anils.

Photochromism in *inorganic materials* invariably involves imperfections of the substances. Localized defects, impurities, and dislocations are responsible for formation of electron–hole pairs in the excitation process and for forming colour centers, by the trapping of free carriers. The energy for bleaching colour centers can be obtained either by illumination with light in the energy range of the induced absorption band of the colour centre, or thermally by heating. Typical examples for inorganic photochromic materials are photochromic glasses or alkali halide crystals.

The photochromism in inorganic thin films has not been investigated very well so far. It seems to be difficult to prepare the complex molecular structure in certain films by the standard methods of vacuum evaporation or by sputtering methods. Since the photochromic compounds have the tendency to decompose when heated, only few investigations are reported on photochromic coatings.

One class of photochromic coatings is based on Ag and Cu halides, and silver complex oxides [42,43]. The process observed on photochromic glasses containing silver halide as a light-sensitive component has been tried to be simulated in that type of films. Such photochromic thin films have been obtained by simultaneous

deposition of the silicon oxide, lead silicate, aluminium chloride and copper-sensitized silver halide. The photochromism in the films has been activated by a heat treatment in the dark and in air, at 100 to 200°C, lasting several hours [42]. The photochromic response of the system depends on the kind and the content of the halides, the crystal size and the intensity and the wavelength of the light. Photochromism is also obtained in silver complex oxide thin-films synthesized by anodic oxidation. It was found that A_3VO_4, Ag_4SiO_4 and Ag_3PO_4 films show photochromic properties in the visible, but mainly in the infrared region [44].

Photochromism is also observed in amorphous transition metal oxide films known to be electrochromic. So, for example, in a-MoO_3 and a-WO_3 films a blue colouration is reported when the films are irradiated with light ($h\nu > 3.4$ eV) for several hours. Blue colour develops gradually and grows more intense with prolonged exposure [45,46]. It is believed that the photochromism in the amorphous films is produced by the high energy radiation which results in a photodecomposition. Another type of electrochromic material also exhibits photochromism. Prussian Blue films, galvanostatically deposited on n-$SrTi_3$ wafers, show photochromic behaviour. The absorptance is induced by light changes in the wavelength region of 400–900 nm [47].

2.3. Electrochromism

This section discusses the electrochromism in organic and inorganic substances. Some electrochemical standard measurement techniques for the characterization of the electrochromism are mentioned and the basis elements of electrochromic systems are given. A key quantity, the colouration efficiency, is defined and used to discriminate between the different materials and preparation conditions. Principal processes in cathodically colouring and anodically colouring films are described. The electrochromism of various oxides of the transition metals is outlined in detail.

Electrochromism is the unique property of a material or a system to change colour reversibly, in response to an applied external potential or current. This reversible change in optical quantities (extinction coefficient k and/or refractive index n) can be evoked by a solid-state effect or by an electrochemical effect (sometimes called electrochemichromism). Numerous materials, inorganic and organic, liquids and solids, exhibit electrochromic behaviour. The changes in the optical properties can be due to the formation of colour centres, creation of a new-type band-to-band transition, defect complexes, or to an electrochemical reaction.

Various configurations exist for electrochromic devices, depending on property requirements. The basic elements are very similar to those of an electrochemical cell or battery. Electrochromic systems consist, in general, of two electrodes, an electrolyte, and a minimum of one electrochromic active layer. At least one of the two electrodes must be transparent in order to make visible the optical effect of the electrochromic materials situated between the two electrodes. A schematic representation of an electrochromic device is shown in Fig. 1. A transparent glass (1), usually used as a substrate, is coated with a transparent, conductive electrode (3) (ITO, standing for indium tin oxide, is mostly used for this purpose), which is covered with the electrochromic active material (2). These layers are part of an electrochemical cell

completed by an electrolyte (4). In all-solid-state devices, an ion conductor is used instead of an electrolyte, and an ion storage medium (counter electrode) is necessary. A second transparent electrode (5) is needed for transparent devices.

Traditionally, current or charge is recorded as a function of applied voltage, and transmittance or reflectance is measured as a function of the potential to characterize electrochromic materials. Most investigations for the electrochromism of single films are done in liquid electrolyte experiments. In principle, only two electrodes are necessary for an electrochromic experiment, but for fundamental research a three-electrode configuration is mostly used to control the potential at the electrochromic film (working electrode), relative to a reference electrode (see Section 3.2.3). Current–voltage graphs (CVGs) and transmittance-voltage graphs (TVGs) are typically recorded, but also the response in the electrical and optical data to a constant voltage is measured to determine the switching speed of an electrochromic film.

An important parameter used to discriminate between electrochromic materials and films is the colouration efficiency (CE), expressed as $cm^2\ C^{-1}$. In order to obtain this value, the total injected/ejected charge, as a function of unit area, and the change in the optical density (δOD) must be known. Both CE and OD are wavelength-dependent quantities. The transmittance of bleached ($T_0(\lambda)$) and coloured films ($T_c(\lambda)$) must be known to determine the optical density. From the measured data, δOD can be calculated by

$$\delta\mathrm{OD}(\lambda) = \log(T_0(\lambda)/T_c(\lambda)). \tag{2.1}$$

The change in optical density is correlated with the transported charge Q (per unit area). From the two quantities, the colouration efficiency can be simply determined by the following equation:

$$\mathrm{CE}(\lambda) = \delta\mathrm{OD}(\lambda)/Q. \tag{2.2}$$

CE is a number which is independent of the film thickness, because δOD and Q depend in the same way on the film thickness. In general, CE is constant in the range of low injected/ejected charges, i.e. the change in optical density is correlated linearly to the incorporated charge.

The various types of electrochromic substances can be divided into two classes: *inorganic oxides* and *organic materials* [48–50]. Another classification is related to the potential where the colouration process occurs. *Cathodically colouring* substances possess a reduced coloured state, i.e. they colour at a negative potential, while *anodically colouring* materials are those with an oxidized, coloured state, i.e. they colour when a positive potential is applied. For example, for an inorganic solid film, the ion insertion reaction might be described by the following, more general equation:

$$\begin{aligned} &\text{bleached} && \text{coloured} \\ \text{cathodic:}\quad &\mathrm{MO}_x + y\mathrm{A}^+ + y\mathrm{e}^- \rightleftharpoons \mathrm{A}_y\mathrm{MO}_x, \\ &\mathrm{A}^+ = \mathrm{H}^+, \mathrm{Li}^+, \mathrm{Na}^+, \mathrm{Ag}^+, \end{aligned} \tag{2.3}$$

$$\begin{aligned} &\text{bleached} && \text{coloured} \\ \text{anodic:}\quad &\mathrm{MO}_x + y\mathrm{A}^- + y\mathrm{h}^+ \rightleftharpoons \mathrm{A}_y\mathrm{MO}_x, \\ &\mathrm{A}^- = \mathrm{F}^-, \mathrm{CN}^-, \mathrm{OH}^-, \mathrm{H}^+; \quad 0 < y < 0.3. \end{aligned} \tag{2.4}$$

It should be mentioned that these are very simplified versions of possible reactions, only useful for explaining the principles of the two classes of processes. A real electrochromic process is more complicated than described in schematic equations (2.3) and (2.4), and the electrochromism of the different materials is strongly related to the method of preparation, i.e. it is affected by structure, stoichiometry, binding condition, and water content in the films. But this type of representation illustrates that good electrochromic materials should possess both, ionic and electronic conductivity.

The following description of electrochromic material is a subjective selection and has been kept deliberately incomplete. For example, ferric ferrocyanide, known as Prussian Blue, or intercalated electrochromic substances will not be discussed. However, all of the selected substances described in the following have a certain relevance from a technological point of view.

An increasing number of *organic materials* exhibiting electrochromism have been found in the past decade. Historically, the viologens are the best-known materials, which have been studied in the past with regard to application in electrochromic display devices. One attraction of the different types of viologens is the possibility of choosing various colours by introducing different substituents into viologen molecules. Viologens (dialkyl derivatives of 4,4′-dipyridinium salts) are colourless compounds which can be reversibly reduced at the cathode in a one-electron step, to form highly coloured radical cations, resulting in a deep-blue colour. A second reaction may take place immediately if the solvent used is water, which results in an insoluble purple solid that precipitates as a film on the cathode surface. Electrochromism is also observed in groups, such as pyrazoline, pyridine, or in organometallics, such as polytungsten anions and phthalocyanines of lanthanides.

The group of organic materials also includes polymers. The first conducting polymer was reported in 1977 [51]. It was discovered that polyacetylene, an organic polymer and electrical insulator, could be converted into an electrical conductor by absorbing small amounts of iodine. The synthesis of highly conductive polyacetylene leads to extensive studies of electronic structure and transport in organic polymers. New conductive polymers had been discovered as, for example, polythiophene, polyphenylene, poly-(phenylenesulfide) and, more recently, polypyrrole and polyaniline [52].

The insulator-to-conductor transformation in conducting polymers is induced by "doping", i.e. by absorption of an iodine into polyacetylene. It was found that there is a chemical oxidation/reduction reaction between the polymer and the dopant [53]. Since this electrochemical oxidation/reduction causes a change of colour, conductive polymers are potentially useful as electrochromic materials.

The optical absorption behaviour of such kind of polymers seems to be a consequence of their unique "one dimensionality" and their geometrical structure. Different studies of polymers of interest to electrochromic properties show that the geometry of the polymer in the neutral state is not identical to that in the charged state, as obtained by doping and removal of holes or electrons. It has been shown that poly(heterocyclic)polymers undergo a geometrical relaxation upon doping. The produced local deformation is distributed over several monomers and creates a new

Table 1
Band gap and colours for some polymers in different states

Polymer	Colour	Band gap (eV)
Polyaniline	Green in oxidized state (blue and purple at higher oxidation potential), transparent in reduced state	3.5
Polypyrrole	Brown in oxidized state, yellow in neutral state	3.2
Polythiophene	Blue in oxidized state, red in neutral state	2.2
Polyisothianaphtene	Transparent in oxidized state, black in neutral	1.1

electronic structure. This effect can be described in terms of solid-state physics, namely states which are part of the valence and conduction band (in chemical terminology, the highest occupied molecular orbital (homo) and the lowest unoccupied molecular orbital (lumo)) are split off the original band, with new states being formed in the band gap. Depending on the molecular system and doping level, these states can be described as polarons or bipolarons. Changes in the optical absorption between the undoped and the doped polymer are then due to a band gap transition in the transparent state and to new optical transitions in the coloured state. Some parameters relevant to electrochromic polymers are given in Table 1.

Compared to other electrochromic materials, polymers have some potentially achievable advantages. The manufacturing cost for polymeric electrochromic material should be lower than for inorganic electrochromic films deposited by a vacuum deposition process, since conducting polymers can be coated on substrates by electro-plating, painting or spraying. Rapid switching capability and good optical quality can be created, because polymers can be made with a very porous, fibrilar morphology leading to a fast ion transport in the electrochromic layer. The sophisticated techniques of synthesis organic polymers offer a rich opportunity for molecular design, which can be used to modify the molecular structure for adjusting electrochromic, chemical and mechanical properties. For example, by molecular structure modifications one can influence the electrochromic colours. Polyaniline exhibits a well-known multiple-colour electrochromic effect. By increasing successively the anodic potential, a transparent film switches to green, to blue, and to purple colour [54].

Electrochromic polymers possess the following disadvantages compared to inorganic electrochromic materials. Organic materials are known to be chemically unstable. More recent conducting polymers are more stable, but the durability of electrochromic devices has not been fully tested so far. Another weakness of organic materials is that they are generally attacked by UV radiation. UV instability is one reason for the short life time of devices used in outdoor applications. The UV light seems to produce an undesired, irreversible side reaction of the weakly bound hydrogen and nitrogen ions. Another, more general problem is that polymers do not adhere well to the surfaces of inorganic transparent electrodes (ITO). To overcome these disadvantages, especially the UV instability, further research and development on such kind of materials is necessary. With the rich opportunity for molecular design, it should be

possible to improve the organic materials, so they can be used for application in technical products.

Inorganic materials are, in general, oxidic films possessing electronic and ionic conductivity. Both are necessary, because the mechanism of colouration in such type of thin films is described with a double injection of electrons and small ions to maintain charge neutrality. Inorganic transition metal oxides exhibit both anodic and cathodic reactions, i.e. some substances possess a reduced coloured state (cathodically coloured) and others an oxidized coloured state (anodically coloured). The various thin-film oxides of the materials of this category can be prepared by very different deposition techniques [55]. Similar to what is described in detail in Section 3 for tungsten oxide, the electrochromic behaviour is strongly related to the depositon conditions of such type of films, i.e. the method of preparation with the corresponding deposition parameter determines the relevant quantities of the layer, such as the structure, the stoichiometry, the bonding conditions, and the water content in the films [55,56]. Therefore, an exact description of the properties of one type of material, has to contain details of the film preparation. But more general trends on the fundamentals of the phenomenon can be obtained also by a comparative discussion of the electrochromism on different oxide materials. Fairly recently, a very informative attempt is described to give an unified view of the electrochromism from the perspective of microstructure and electronic bands [57,58]. It is pointed out that electrochromic thin films are composed of MeO_6 octahedra in various corner- and edge-sharing arrangements, forming nano-clusters with numerous defect perovskites, rutiles and layer structure. The variable optical absorption can be due to intraband effects, interband transitions, and polaron hopping [57,58].

Many hydrous oxide films in group VIII (platinum group) exhibit *anodically colouring* electrochromism [59]. The metals of that group are good electrocatalysts for the oxygen evolution reactions, and the oxide films show a high, reversible charge capacity below the oxygen evolution potential. For oxide films of Ir, Rh, Ni and Co, the reversible charge insertion process also gives rise to optical absorption changes. The electrochromism of the hydrous oxides of these materials has been investigated so far. A different type of an anodic material is V_2O_5.

The electrochromism of hydrated *iridium oxide* films is studied for films prepared by a variety of methods. Both anodically oxidized IrO_2 films (AIROF) [60] and reactive sputtered films (SIROF) [61] have been investigated. The films show a transparent-to-blue-black transition with the injection of ions. Most of the properties of as-deposited films are still unknown. The structure of SIROF is identified as being densely amorphous, while AIROFs are highly porous crystalline or amorphous [62]. Different types of reactions are proposed for the colouration. There is still a controversy on whether a proton extraction or a hydroxyl insertion is the relevant process for a charge compensation. The proposed reaction for the colouration can be interpreted as:

bleached coloured

$$\mathrm{Ir(OH)_3 - H^+ + h^+ \rightleftharpoons IrO_2 \cdot H_2O},$$

$$\mathrm{Ir(OH)_3 + OH^- + h^+ \rightleftharpoons IrO_2 \cdot H_2O + H_2O}. \tag{2.5}$$

The first formula describes the proton extraction, the second one the hydroxyl injection. It is obvious that water in the films plays a dominant role for the colouration and bleaching process. Colouration efficiency of $CE = 15–18\ cm^2\ C^{-1}$ has been reported for these materials, depending on the method of preparation and utilized electrolyte [59].

The electrochromism of hydrous *nickel oxide* films, NiO_xH_y, has been investigated more recently. Various deposition techniques have been used for preparation of that inexpensive film material. Films created by anodic oxidation of nickel electrodes [63], colloidal precipitation [64], cathodic electrodeposition [65] chemical vapour deposition [66], reactive sputtering [67], and reactive evaporation [68–70] are at present subject to numerous studies. During colouration, the film changes from transparent to yellow, dark bronze and black with increasing film thickness, and also as a function of the preparation method. Different types of reactions for the colouration are reported. Two general processes are possible:

$$\begin{aligned} &\text{bleached} \quad \text{coloured} \\ &Ni(OH)_2 \rightleftharpoons NiOOH + H^+ + e^-, \\ &Ni(OH)_2 + OH^- \rightleftharpoons NiOOH \cdot H_2O + e^-. \end{aligned} \tag{2.6}$$

A model was proposed recently, including H^+ ejection for low potentials, as well as OH^- incorporation at higher potentials during colouration of NiO_xH_y films produced by e^--evaporation [69,71].

Usually, the electrochromism of such films is investigated in alkaline electrolyte (KOH). But evaporated films are also studied in all-solid-state devices and acid electrolyte [72]. NiO_xH_y films deposited by e^--evaporation are not pure hydroxide; they consist of NiO, $Ni(OH)_2$, and also of Ni_2O_3. The exact mechanism for the colouration is certainly a function of the initial nickel oxide films, but also depends on the nature of the used electrolyte. A peak colouration efficiency of $CE = 50\ cm^2\ C^{-1}$ has been analyzed between 350 and 500 nm for NiO_xH_y films prepared by cathodic electrodeposition, whereas films produced by reactive evaporation exhibit lower values. Typical for evaporated films are $CE = 30.1\ cm^2\ C^{-1}$ (550 nm) [73], $36\ cm^2\ C^{-1}$ (550 nm) [68]; a spectral CE for evaporated films is given in [74], which shows that colouration efficiency in the UV region is larger than in the IR region. NiO_xH_y films prepared by sputtering possess a $CE = 36\ cm^2\ C^{-1}$ at 640 nm [75]. In that deposition technique, the CE depends on the sputtering atmosphere's total pressure but is independent of its oxygen content. NiO_xH_y films created by reactive sputtering are probably not completely oxidized, because the transmittance in the as-deposited state is generally lower than in the bleached state. Nickel oxide films prepared by chemical vapour deposition exhibit a colouration efficiency of $44\ cm^2\ C^{-1}$ at $\lambda = 550$ nm [69]. Much work is in progress at present on NiO_xH_y films, because this type of material is a possible candidate for large devices because of its low costs.

Iron oxide films deposited by the dip-coating method from an iron-ion-containing sol exhibit electrochromism in the UV-visible region when they are heat-treated in the temperature range of 200–350°C [76]. Colouration is obtained at an anodic potential

(+ 0.6 V) and bleaching occurs at cathodic potential (− 1.4 V) in LiOH, KOH and NaOH electrolytes. The maximum absorption chance appears in the spectral range of 300–390 nm. From the Li^+ intercalated charge is concluded that the films consist of particles of small grain sizes (γ-Fe_2O_3 (maghemite)) with dimensions < 10 nm and well-developed grain boundaries, which contain OH^- and other defective bonds originating from residual acetate groups [76].

Colour changes are observed on anodically *oxidized rhodium* electrodes upon cycling the potential. For thin films, a colour change between yellow and dark green is reported, and for thicker films a transition from yellow to brown purple. The following reaction is suggested:

bleached coloured

$$1/2\ Rh_2O_3(\text{hydr.}) + OH^- + h^+ \rightleftharpoons RhO_2(\text{hydr.}) + 1/2\ H_2O. \quad (2.7)$$

The anodic rhodium oxide films were investigated in 5 M KOH and 1 M KOH. A colouration efficiency of $CE = 20\ cm^2C^{-1}$ is determined at 546 nm [77]. One problem with that material is that the anodic peak, giving rise to colouration, in the cyclic voltamogram overlaps heavily with the onset of O_2 evolution; this means that full colouration could not be achieved without simultaneous O_2 evolution occurring as a side-reaction [59].

Electrochromic behaviour in anodically grown *cobalt oxide* has been reported, too. The material is not well characterized and only few investigations are available for such films. During the anodic colouration, the colour switches from red purple to grey-black [78].

Thin CeO_2 solid films and mixed CeO_2–TiO_2 prepared by the sol–gel route via the dip-coating technique exhibit electrochromism in lithium-containing electrolyte solution [79]. Both types of coatings show variations in the spectral range $500 < \lambda < 330$ nm, but remain nearly unchanged in the visible spectral range and may be used as an optically passive counter electrode [79].

V_2O_5 films exhibit a more complicated colouration behaviour than other materials of inorganic, anodic colouring films. Although the substance is classified here as anodic material, the electrochromism of V_2O_5 films rather is comparable with the type of WO_3. Electrochromism of V_2O_5 films has been mentioned for layers prepared by evaporation [80] and reactive sputtering [81]. V_2O_5 shows a heavy anodic colouration in the UV region (300–500 nm) and a weak cathodic colouration in the NIR range. The colouration is produced by a striking shift to higher energy of the optical band edge, which results in effective bleaching of the yellow contribution to the absorption. V_2O_5 films dissolve in acidic aqueous electrolytes, and, therefore, distilled water or LiCl in methanol has been employed as electrolyte; but also 1 M $LiCl_4$/propylene carbonate has been used. A lithium insertion reaction is indicated to explain the colour change, and a change in the molecular state from V_2O_5 to VO_2 is suggested. In sputtered, polycrystalline V_2O_5 samples, the Li^+ insertion is described by the reaction:

bleached coloured

$$V_2O_5 + xLi^+ + xe^- \rightleftharpoons Li_xV_2O_5 \quad (2.8)$$

The colour changes, during the insertion of lithium, from yellow to green-blue, to dark blue or black. A spectral colouration efficiency for $Li_xV_2O_5$ films is given in [82] for different amounts of injected charge. CE shows a maximum at 400 nm and varies between 60 and 100 $cm^2\ C^{-1}$, depending on the thickness of the sputtered V_2O_5 films. $Li_x\ V_2O_5$ films have been made also by reactive dc magnetron sputtering followed by electrochemical treatment in $LiClO_4$ [83], and the relation of the optical absorption to the microstructure is investigated. Electrochromism (and thermochromism) is also reported for $Li_x\ VO_2$ films made by reactive sputtering and postannealing treatment, followed by electrochemical cycling in an electrolyte containing $LiClO_4$ [84]. The films bleach under Li insertion.

Variations of electrochromic colours are possible by the use of vanadium-containing composite materials. Mixed oxides as V_2O_5–WO_3 and V_2O_5–MoO_3–WO_3 and V_2O_5–TiO_2, are reported [85], and fairly recently composite thin thin films of Au–V_2O_5 have been described which are prepared by alternating thermal deposition of Au and V_2O_5 layers, with thicknesses of 1.5 and 10–40 nm, respectively. The electrochromic properties of such films depend on the Au content and the calcination temperature. The composite film containing 26 at% Au calcined at 400°C exhibits electrochromism and the colour switches between reddish-violet (cathodic polarization) and green (anodic) [85]. The strong optical absorption peak is ascribable to the dispersed Au particles at 615 nm in the cathodic range or 555 nm in the anodic region.

Electrochromism based on *cathodic colouration* has been reported for WO_3, MoO_3, V_2O_5, Nb_2O_5 and TiO_2, i.e. for the highest oxidation state of these transition metals [86]. The mechanism for colouration in this type of thin oxide films is generally described with a double injection of electrons and small charge compensating cation. Incorporated water appears to dictate the electrochromic coloration speed. The bulk of the cathodic electrochromic research has been performed on WO_3. The colouration efficiency for this material seems to vary between $CE = 42\ cm_2\ C^{-1}$ (650 nm) for polycrystalline materials [87] and $CE = 115\ cm^2\ C^{-1}$ (633 nm) for amorphous films [88]. The electrochromic behaviour of tungsten oxide is discussed in larger detail in Section 3.

Electrochromic colouration has been reported for MoO_3 films prepared by evaporation [89], sputtering [90], chemical vapour deposition [91] and plasma-enhanced chemical vapour deposition [92]. The absorption spectra of H_xMoO_3 films are fairly similar to those of H_xWO_3, and their characteristic colour is purplish blue. The colouration phenomena are comparable to those observed in tungsten oxide films; a-MoO_3 films, as well as crystalline materials have been investigated. The heat treatment in the chemical vapour deposition produces films in which the (0 1 0) planes are predominantly oriented in parallel with the subtrate. It is also mentioned that the crystallization behaviour increases with the film thickness. The reported colouration efficiencies are somewhat contradictory. They vary between $CE = 10\ cm^2\ C^{-1}$ for amorphous films deposited by plasma-enhanced chemical vapour deposition [92], and $CE = 45$–$51\ cm^2\ C^{-1}$ ($\lambda = 633$ nm) for polycrystalline material created by chemical vapour deposition [91].

Mixed WO_3/MoO_3 films also exhibit electrochromism. Such composite systems can be produced by co-evaporation [93]. The absorption spectrum of electrochemically

coloured WO_3/MoO_3 films is shifted to an energy higher than that of either amorphous WO_3 or MoO_3 alone, and the absorption band of the mixed film is broader than that of WO_3 or MoO_3. The mixed films change colour to dark-blue or black. In the visible region, the efficiency is improved about twice by addition of small amounts ($< 1\%$) of MoO_3 in WO_3 films prepared by evaporation. For MoO_3/WO_3 ratio of ~ 0.01, a CE $= 95\ cm^2C^{-1}$ at 640 nm is reported [94]. Tungsten oxide films, doped with molybdenum up to a percentage of 2% by a different technique, exhibit also good electrochromic properties [95]. Films, electrochemically prepared from a metal peroxide bath, give a better film-dynamical optical response, because the switching range between the transmittive values is increased. Larger dopant concentration ($> 2\%$) leads to a longer transition time for the reduction in the oxidation process. Additionally, the doping produces a flatter spectrum in the visible and infrared region, which gives a grey colouration [95].

Improved electrochromic properties are found also [96] for mixed WO_3–TiO_2 films produced by sputtering and a sol–gel technique. Since both shape and position of the electrochromic absorption peak are not affected by the coexistence of titania in the film, it is concluded that the absorption mechanism remains unchanged in tungsten oxide with TiO_2 doping. From the decreased colouration efficiency, the conclusion is drawn that only the probability of an absorption process per injected electron/ion couple is decreased. Other electrochromic properties, such as the bleached state absorption, the colour stability and the aging durability, are improved with titania doping. These effects are explained by the annihilation of lithium ion "trapping sites", i.e. W=O or W–O–H bound is reduced and less optically inactive lithium is accumulated in the film [96].

Tungsten oxyfluoride films prepared by dc sputtering show a larger density of charge insertion/extraction and faster colour/bleach dynamics than unfluorinated material [97]. Further, the oxyfluoride can reach a much lower transmittance ($\sim 3\%$) after 20 s of current injection. A CE $\sim 60\ cm^2\ C^{-1}$ is evaluated. From this quantity it is concluded that the obtained low transmittance is a consequence of a large charge insertion. Tungsten oxyfluoride films show a limited durability during cycling, and degradation is noted after ~ 100 colour/bleach events [97]. But the durability can be improved by an electron bombardment of the films [98].

Electrochromism in *Nb_2O_5 films* with reversible optical changes have been reported for anodic oxide films [99], but also for Nb_2O_5 films deposited by sputtering, chemical vapour deposition, and also thermally grown oxide on Nb [86]. An onset of colouration in aprotic electrolyte is observed at 0 V against NHE, but a more cathodic potential (-0.6 V) is required to give a dark blue colouration. For the colouration of Nb_2O_5, the suggested reaction is

$$\begin{aligned} &\text{bleached} \qquad\qquad \text{coloured} \\ &Nb_2O_5 + 2H^+ + 2e^- \rightleftharpoons Nb_2O_3(OH)_2, \\ &\text{or} \quad \rightleftharpoons 2Nb_2O_2 \cdot H_2O. \end{aligned} \tag{2.9}$$

The determined colouration efficiency is fairly low in aqueous acidic electrolyte (CE $= 3.5\ cm^2\ C^{-1}$), but since, at the potentials required for colouration, H_2

evolution is occuring simultaneously with colouration by H insertion, the side reaction has a strong effect on this value. The true CE, if side reactions are avoided, therefore, is slightly above $20\,cm^2\,C^{-1}$, which is a good agreement with a value arrived at by Li insertion [86].

Reversible optical changes in anodic *TiO_2 films* have been studied in acidic aqueous electrolytes. The behaviour of these films is very similar to that of Nb_2O_5 films, where colouration requires potentials at which H_2 evolution occurs simultaneously. The amorphous titanium oxide films undergo electrochromic reaction according to:

bleached coloured

$$TiO_2 + H^+ + e^- \rightleftharpoons TiOOH. \tag{2.10}$$

The colouration efficiency can only be estimated as $CE = 8\,cm^2\,C^{-1}$ (546 nm) [99]. Fairly recently titanium-oxide-based films have been prepared by reactive dc magnetron sputtering in $Ar + O_2 + CF_4$ [100]. The films show pronounced cathodic electrochromism in a Li containing electrolyte. A maximum colouration efficiency of $37\,cm^2\,C^{-1}$ at a wavelength of $\sim 0.7\,\mu m$ is reported, which is achieved through fluorination. A good cycling durability in lithium-conducting electrolyte is obtained and polaron hopping is believed to cause the absorption [100].

Copper oxide films are deposited by various techniques and show reversible electrochromism. Cu_xO films prepared by evaporation exhibit, in a liquid electrolyte consisting of 1 M $LiClO_4$ in propylencarbonate, colouration by polarizing at a low cathodic voltage [101]. Bleaching is realized by reversing the polarization to a low anodic potential. It is suggested that the electrochromic properties depend on the film structure and that the lithium sites in the copper oxide films have an important role in the electrochemical reaction [101].

2.4. System design and applications

This section regards the design of electrochromic systems and applications. All-organic electrochromic devices and systems with organic electrolytes are reviewed briefly and own work on all-solid-state devices for reflective operation is described. Different types of reflective devices, with focus on application as the car mirror, are outlined.

As illustrated in Fig. 1, thermochromic and photochromic devices only consist, in general, of one layer, which makes a discussion of *systems design* highly unnecessary. Questions on the design can be reduced to problems of film thickness and coulors. A large scope of variations is possible in the design of electrochromic devices. The numerous, different materials with respect to the defined, necessary functions allow the design of various types of optically switchable systems [69,102–106]. Therefore, the principles of different system configurations will be introduced in the following. Each of the discussed examples is representative of a class of individual system designs concerning the different materials used, and each of them has its specific merits and shortcomings.

One of the remarkable phenomena of electrochromic devices is the fact that an optical switching process is connected with a transport of charged species in an electric field, i.e. a movement of charged material. Electrochromic devices in two configurations are possible in principle to realize a switching process. These are shown schematically in Figs. 2 and 3. Both have in common that electrodes sandwich the electrochromic material. The arrangements possess some similarity to a battery.

One of the electrodes, which must be conductive and transparent, is in general coated onto a glass substrate. The active electrochromic layer covers the electrode. An insulating dielectric film, sandwiched between the electrochromic film and an ion-storage medium (reservoir), is necessary to avoid short circuit (Fig. 3), i.e. to create an electrical field due to the driving voltage U_c, moving the ionic species from the reservoir to the electrochromic film and vice versa.

In the second configuration (Fig. 2), the electrochromic material is solved in a matrix, which is an electrical insulator. Similar to Fig. 3, substrate glasses are coated with electrodes. A cell is built up with solvent in which the electrochromic material is incorporated. The electric field, due to U_c, transports the electrochromic active ions to the appropriate electrode, where they change their optical characteristics by a charge transfer process.

In any case, electrochromic devices should be thin-film systems, because only thin oxide films are highly transparent to make the optical switching process visible. The necessary charge transport in this type of thin-film devices causes an electric current similar to an electric circuit, which leads to two important demands on the electrodes: low resistivity, to obtain short switching times, and for optical reasons they should

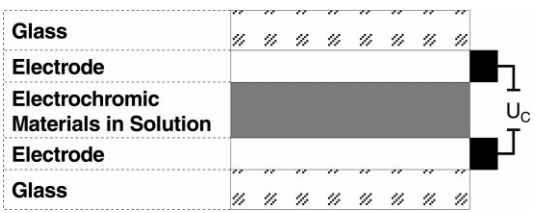

Fig. 2. Basic configuration of an electrochromic device working with solvent material.

Fig. 3. Principal components of a multilayer electrochromic device.

possess high optical transparency. Both requirements are best compromised at present by ITO layers of approximately 200 nm thickness, where a sheet resistance of 8 Ω ($\sigma = 6.250\ (\Omega\,\mathrm{cm})^{-1}$) can be obtained and an absorptance of $k < 0.01$ is achieved in the visible range. In any case, the electrical current and the switching time, respectively, are limited, especially for large areas.

The construction of *all-organic electrochromic devices* is possible by using organic dyes in a polymer matrix [102]. Only the transparent electrodes are inorganic thin-film layers (e.g. ITO). With such systems, depicted in principle in Fig. 2, it is possible to produce rapidly switching optical elements with great changes of transmission and/or reflection as being desirable for many applications. The disadvantages of these systems, for use in technical products, are the limited UV stability, especially in the case of those intended for outdoor operation, and the employment of the solvent PC as liquid electrolyte, so that splinter binding of the system is incomplete. Additionally irreversible side reactions occour upon long-term colouring. However, many other material and system configurations are possible.

Electrochromic systems based on liquid electrolytes or gel-like gelatinous *organic electrolytes*, in connection with inorganic electrochromic materials, e. g. Li_xWO_3, have achieved a high cyclic stability of more than 10^5 cycles when using an unspecified gel-like organic electrolyte. The limited temperature and UV stability of these systems, however, still is a problem. Fig. 3 shows the principle of such a system when, instead of the dielectric layer and the reservoir, $LiClO_4$ in PC is used. By modifying the system with an additional reflector, it is also possible to design devices with good infrared reflection. Recently, solid-state devices consisting of molybdenum-doped tungsten oxide films, amorphous polyethylene oxide electrolyte, and a polyorganodisulphide counterelectrode have been described, which switch rapidly from a pale yellow to a deep blue-green upon application of -1.2 V [107].

A further class of electrochromic systems consists of an entirely all-solid-state construction. As early as 1969, it was proposed to build an electrochromic display with the basic structure electrode/EC materials/inorganic ionic conductor/electrode [108]. Such systems can be designed for reflective operation, as shown in Figs. 4 and 5 [69,102,109,110]. Transmissive operation is also possible by removal of the reflecting layer and the use of two transparent electrodes. But problems can arise out of the utilization of the second transparent electrode. Most systems are prepared by PVD techniques, but fairly recently solid state electrochromic coatings have been produced by using sol–gel techniques [103].

In these systems, the transported charged species required for colouration of the tungsten oxide can be produced by decomposition of water. This can restrict the long-term stability, on account of oxidation or of gassing at the electrode. Oxide formation at the metallic electrodes can have the consequence that the system is no longer able to be bleached completely after prolonged, excessive cycling. This disadvantage can be avoided by systems using the same material for the optical (electrochromic) function as for ionic storage (Fig. 4). In these systems, the colouration producing ions migrates in the electric field from the storage (reservoir) layer to the optically active layer (and back again). Since no side reactions have to be contended with, these systems show extremely high long-term and cycle stability

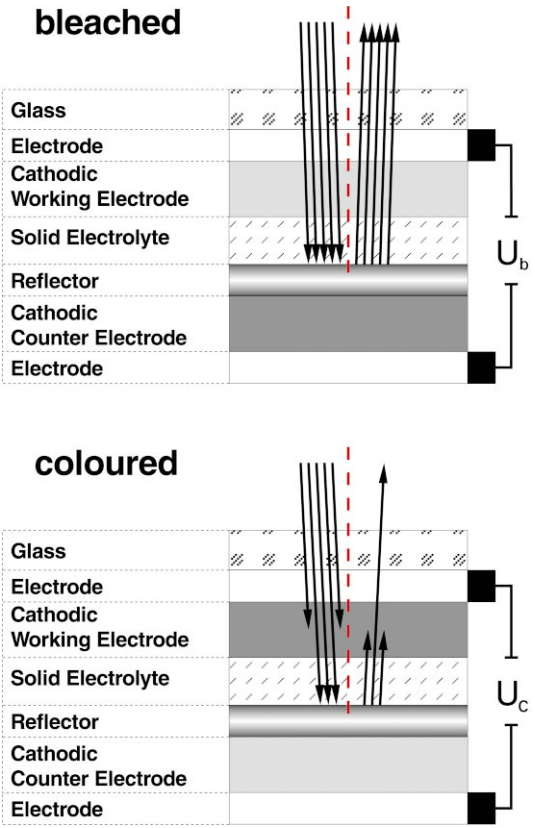

Fig. 4. Scheme of a reflecting all-solid-state-device containing cathodically colouring films (WO_3) as working and counter electrode in bleached and coloured state. The reflector is placed between the active materials.

($\sim 10^6$). In such type of constructions, the second reservoir layer is also electrochromically active. Therefore, the reflector has to be positioned in front of the storage layer, or the storage layer has to be modified to create an optically inactive film (e.g. by doping). Pt metal or dielectric multilayer systems can be used as a reflector.

Instead of using a storage layer of the same electrochromic material, a so-called active counter electrode can be incorporated in the system. The combination of cathodically and anodically colouring material is an innovative choice to realize all solid-state devices with increased colouration efficiency. For example, the combination of WO_3/PB, WO_3/IrO_2 or WO_3/NiO_xH_y can be used. Fig. 5 shows such a system in principle. Colouration efficiency larger than $CE = 90\ cm^2\ C^{-1}$ (633 nm) can be achieved with a system using WO_3 and NiO_xH_y [111]. As a result of these large CE values, systems can be constructed with relatively thin layers, leading to reduced manufacturing costs. A further advantage is that only a low amount of charge transport is necessary to realize the optical switching behaviour in such devices.

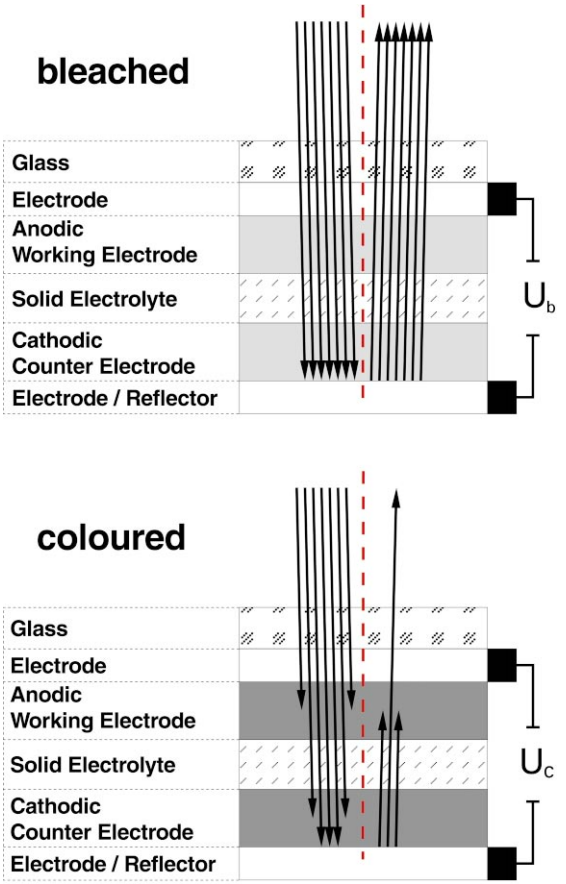

Fig. 5. Scheme of an asymmetric reflecting all-solid-state device containing an anodically colouring layer (e.g. NiO_xH_y) as working electrode and cathodically colouring film (e.g. WO_3) as a counterelectrode in bleached and coloured state. The reflector is used also as a back electrode.

One of the most intensified *applications* concerns large-area *electrochromic displays*. In comparison to the liquid crystal system, the two main important advantages of electrochromic systems are their high optical contrast and the independence of their optical properties in respect of the viewing angle. Although it is possible today to achieve an optical contrast ratio of 1 : 15, for example, by using ferroelectric liquid crystals, the contrast deteriorates to less than 1 : 3 at viewing angles larger than 60°, with the best liquid crystal system known today. Especially for large area displays, electrochromism possesses a general advantage.

The chief objection to the use of electrochromic systems in display devices can be their high current drain. This, in particular, prevents the application of electrochromic layers in fast switching displays, such as wrist-watches. Another shortcoming of electrochromic displays is the difficulty of matrix addressing to the cross-talking effect.

In consequence, the application is restricted to large-area displays with limited pixel density. Taking into account these characteristics and the good stability of electrochromic systems in the face of several environmental conditions, electrochromic layer systems for displays are being developed today, especially for large-area indicators, for example, as changeable-message signs on railway stations and motorways. The memory effect of the electrochromic systems, i.e. their property of retaining the respective optical state without external current and power supply, may lead to additional application advantages in other fields, for the electrochromic systems, as compared with liquid-crystal devices requiring continuous presence of the operating voltage.

Electrochromic car mirror, an automatically dimmed, sensor-driven device uses a property of electrochromic systems which plays little or no role for displays. In electrochromic "smart" mirror systems, it is possible to vary, continuously and without much effort, layer transmission, namely mirror reflection, with high contrast [109,112]. Liquid crystals and devices based on many other electro-optical effects can be switched only between two stable states, high and low transmission.

A lot of research and development work has been in progress for a considerable time to automate the dimming function of automobile rear-view mirrors. The manually operated interior prismatic mirror has been replaced by a sensor control system. Mirrors have been combined with liquid crystal devices for dimming not only the interior, but also the external mirror. However, driving tests with these on/off systems have brought only unsatisfactory results. In comparison with electrochromic mirrors, it was found that the reflection of an automobile rear-view mirror must be adjustable continuously, in a manner matched to the adaption capability of the human eye [114]. Therefore, electrochromic systems found their first application in a technical product as automatically dimmed automobile mirrors, adding a considerable safety and comfort factor.

One of the most desired applications of electrochromic systems is their use in so-called "*smart windows*". Compared with other window/glass constructions, up to 50% of the energy costs for heating and cooling buildings can be saved with "smart windows" [11]. Today, these advantages are still offset by the following unsolved problems.

The charge quantity required for the colour change process has an order of magnitude of $100\ \mathrm{C\ m^{-2}}$, even for the best systems known today. Since the system operating voltage normally must not exceed a voltage of the order of 2 V, a current of several amperes must be applied for a fast-switching system via the surface electrodes at this relatively low-operating voltage. In order to obtain colour-changing times in the minute range for a window having a typical dimension of $2\ \mathrm{m} \times 2\ \mathrm{m}$, a current of approximately 10 A (of 2 V) is necessary [110]. There is the effect of inhomogeneous colouring, too. This leads to partly darkend parts of the window (near the electrodes), which may cause irreversible material detoriations.

A second sigificant problem is the heating-up of the window by use of absorptive materials. In the darkened state, this undesired absorption in the electrochromic substance can create heating of the system, leading to impairment of the long-term stability. For example, amorphous tungsten trioxide, which has so far been

investigated in greater detail, changes to a crystalline state at high temperatures. But also alterations are observed in the modification of water in films. The intolerable slow-down of the colour change processes can be partially explained to be due to decreased water incorporation capability of the layer. For the construction of "smart windows", electrochromic materials are therefore necessary that don't modulate the absorptance, but the reflectance; especially, films with a high variation of the reflectance in the IR region are desireable. The electrolytes known today also have stability problems at temperatures above 80°C.

On the basis of the wide range of known photochromic inorganic and organic compounds, different *photochromic applications* are possible in the future. Photochromic glasses, which are mainly used for self-adjusting sun glasses, are the most commercialized material, due to the eye glass market. Products with photochromic thin films are not available so far. Different applications are discussed which are mainly related to safety aspects. Large-area applications, for instance sun roofs, or windows, or privacy glasses for automobiles, are in the discussion, but no technologies are available for the production of such type of devices.

It is well known that some organic materials are used in *thermochromic applications* as temperature indicator or sensor which change the optical properties in response to the temperature. The use of photochromic thin films for architectural glazings is in the discussion. The most important control function of such smart windows is the control of the intensity of the transmitted solar energy. Heat-sensitive coatings can be selected to respond properly to minimize cooling energy for buildings, but may not provide large lighting savings [113].

3. Optically active tungsten oxide films

Colouration has been studied in large detail in evaporated tungsten oxide films and is considered in this chapter. Results of as-deposited state, i.e. generally the bleached film, are outlined in Section 3.1. Composition, local structure and film density are found to be the main film characteristics, which are influenced by the deposition parameters and which determine the colouration behaviour. Nine different colouration techniques in hydrogen-containing surrounding are described in Section 3.2. Five electrochromic colouration methods used in our experiments exhibit a complete reversibility, while some others are only partially reversible. The coloured state of these highly disordered films is presented in Section 3.3. The main characteristic features affected by colouration are discussed, the influence of the species in the reservoir is described, and different models for material transport across the interface are developed, which satisfy the various experimental results. Reasons for reversible and nonreversible colouration processes are discussed in Section 3.4, and the role of interface potentials in different media for the colourations is outlined.

Various techniques of film deposition have been used to prepare cathodically colouring tungsten oxide layers so far. Beside evaporation, which will be described later in greater detail, other physical vapour deposition (PVD) methods, like sputtering, are applied, but also chemical and electrochemical techniques.

Sputtering in $Ar + O_2$ plasma [115–117] and "chemical" sputtering in $O_2 + CF_4$ plasma [118] have been reported. For sputtering from a metallic tungsten, target oxidation is observed when the oxygen content exceeds $\sim 2\%$. Fairly high sputter rates, up to 4.8 nm s^{-1}, are obtained by chemical sputtering. A very proper adjustment of the sputter parameters is required for producing films with good colouration behaviour. Almost all of the techniques used for the characterization of these films indicate a strong structural and compositional kinship between evaporated and sputtered-deposited tungsten oxide films.

Chemical vapour deposition (CVD) involving pyrolysis of $W(CO)_6$ on hot substrates has been used to prepare tungsten oxide films [119–121]. A variety of this technique is *spray pyrolysis* in which a solution is sprayed against the hot surface under conditions causing the droplets to evaporate before striking the surface. Recently, spray pyrolysis has been carried out with solutions of WCl_6 in organic solvent [122–124], but also data are available for films prepared from an aqueous solution of metatungstic acid ($H_6W_{12}O_{39}$) on substrates with temperatures $T_s = 150$–$200°C$ [125]. Investigations of these film materials exhibit a microstructure that is significantly different from those of PVD films.

Plasma-enhanced chemical vapor deposition (PECVD) is a modern technique capable of yielding high deposition rates onto substrates of low temperature. This technique has been developed for making tungsten oxide films by composition of WF_6, together with O_2 in a rf discharge at a pressure < 100 Pa. The maximum deposition rate is ~ 40 nm s^{-1}, which is much higher than the rates reported for PVD films [126].

Anodic oxidation, i.e. anodization under potentiostatic, potentiodynamic, as well as galvanostatic conditions has been used for making tungsten oxide films [127–134]. Amorphous and crystalline films are obtained, depending on the anodization voltage, and also highly disordered "polymeric" structures are discussed. The results of different investigations indicate that the anodization voltage is the main parameter to produce films with quite different properties [129,131].

Sol–gel-derived films are made from colloidal solution by dip coating, spin coating or spraying. The colloidal oxide can be obtained through polycondensation process, either by acidification of an aqueous salt or by hydrolysis of an organometallic compound. To obtain stable tungsten oxide films, a post-deposition annealing is necessary that leads to a crystalline state. Up to now, very different solutions have been employed successfully for the deposition of tungsten oxide films by dip coating and spin coating [135–143].

Several other techniques are possible for making tungsten oxide films. Among them, one can note decomposition of oxalatotungstate compounds [144], electro-deposition [145], thermal oxidation [146] and hydrothermal treatment [147].

These considerable differences in deposition conditions create differences in structure, in optical and electrical behaviour of the as-deposited tungsten oxide films. But also the colouration behaviour of the respective thin film depends strongly on the original form initially deposited. In order to explain the various colouration processes of tungsten oxide films, the subsequent description is restricted to films produced by *thermal evaporation*, that are best characterized so far. Results from films deposited

by other methods are only used when they are helpful for the understanding of the data of evaporated materials.

3.1. As-deposited (bleached) state of evaporated tungsten oxide films

As-prepared films are considered in this section. An introductory part on tungsten oxide bulk crystals (Section 3.1.1) is followed by a brief description of thermal evaporation of tungsten trioxide and the principal constituents of the vapour (Section 3.1.2). Results on optical properties of our films are reported (Section 3.1.3) and are combined with data available in the literature. The density of films is summarized in Section 3.1.4 as a function of substrate temperature and background pressure. Nanostructures of columns and clusters of our standard films apparent from electron microscopy and Raman spectroscopy are described (Section 3.1.5). As-prepared films are highly disordered, and electron diffraction, XRD and Raman spectroscopy suggest an amorphous state. The crystallization evoked by post-deposition annealing is given. This section is completed by a local cluster model developed from X-ray scattering data by Nanba and Yasui [148]. The final Section 3.1.6 is devoted to elemental composition of as-deposited materials. The oxygen deficiency of WO_{3-z} and the hydrogen content of our films, determined quantitatively by several techniques, are given. The complex composition of as-deposited films can be best described by $WO_{3-z-q}(OH)_q \cdot pH_2O$, whereby the exact variables are very sensitive to the deposition conditions and post-deposition treatment.

Evaporation has been used in the pioneering work by Deb [149] and is today a still convenient and widely used method for the deposition of tungsten oxide films. Various deposition conditions and parameters are reported, e.g. for the deposition rate, the substrate temperature, the oxygen partial pressure, the total pressure, and so on. Despite differences in deposition conditions, a comparable colouration is obtained for evaporated tungsten oxide films. Influences are found, for instance in the values for optical density or colouration rate, but no basic differences in the colouration behaviour is observed. Nevertheless, in the following, the deposition parameters are given for results not referred to any references. These "*standard*" layers are produced in a commercial system (Balzers BAK 760) by thermal evaporation on substrates, with temperatures kept below 100°C, and exhibit an optimized colouration behaviour. The total pressure was 2×10^{-2} Pa. A deposition rate of $1\,nm\,s^{-1}$ is used and the thicknesses of the films varied between 200 nm and 800 nm. Further details are given elsewhere [150]. Most of the results described below are obtained on films prepared under similar conditions.

3.1.1. Tungsten oxide bulk crystals

A large interest in tungsten oxide materials stems in part, from the ability to join basic WO_6 octahedral building blocks together in a number of different ways of preparation, giving a variety of crystal structures. The symmetry of the octahedral WO_6 building blocks may be described by the perovskite structure illustrated in Fig. 6. The tungsten ions occupy the corners of a primitive unit cell and oxygen ions bisect the unit cell edges. The central atom (C) of the unit cell is absent and the

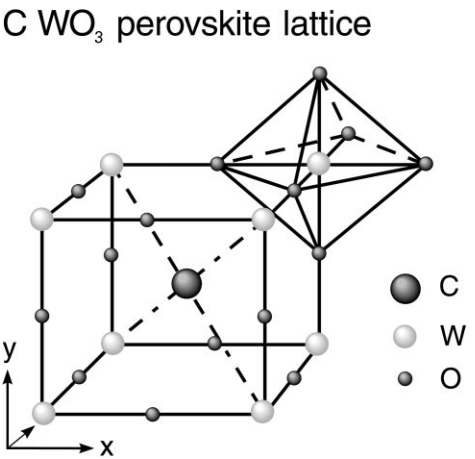

Fig. 6. Unit cell for the perovskite lattice. The octahedral symmetry is emphasized.

corresponding defect perovskite WO_3 configuration is often referred to the rhenium oxide structure.

Tungsten oxide bulk crystals are built up from perovskite-type corner-sharing WO_6 octahedra. The tungsten atom is placed in the centre of the octahedra and possesses the oxidation state of W^{6+}. In an ideal case, the octahedra are connected on the corner, as schematically illustrated in Fig. 7, and the length of the bondings are given in nm for a monoclinic structure. But normally, some atomic displacements and rotations of WO_6 octahedral occur so that, depending on the temperature, tetragonal, orthorhombic, monoclinic or triclinic symmetries are found.

Tungsten oxide bulk crystals have a tendency to form substoichiometric shear phases (Magnéli phases) containing edge-sharing octahedra. The crystalline structures have been clearly displayed by high-resolution electron microscopy. Fig. 8 exhibits four different crystal structures and indicates the positions of the absent central atoms. Open hexagonal phases, depicted in Fig. 8, have sixfold tunnels of particular relevance to the chromogenic behaviour, as will be found later. The spaces between the WO_6 octahedra are large enough to accommodate ions, i.e. the tungsten oxide framework serves an excellent intercalation and deintercalation host. More recently, tungsten oxide has been synthesized with a pyrochlore structure which has a much more open structure (0.068 nm^3 per WO_3) than either the hexagonal (0.060 nm^3) or perovskite (0.054 nm^3) phases [151].

The corresponding simplified band structure for a defect perovskite crystal is shown in Fig. 9 [152,153]. The atomic s, p and d energy levels of the metal are indicated, as well as the 2 s and 2 p levels for oxygen. For WO_3, the pertinent levels are 6 s, 6 p and 6 d. The positions of these levels are governed by the values of the isolated atoms, as well as by the Madelung energies of the atoms when located in different sites of the perovskite lattice. Each tungsten ion is octahedrally surrounded by the six oxygen ions and each oxygen is linearly flanked by two tungsten ions. This arrangement leads

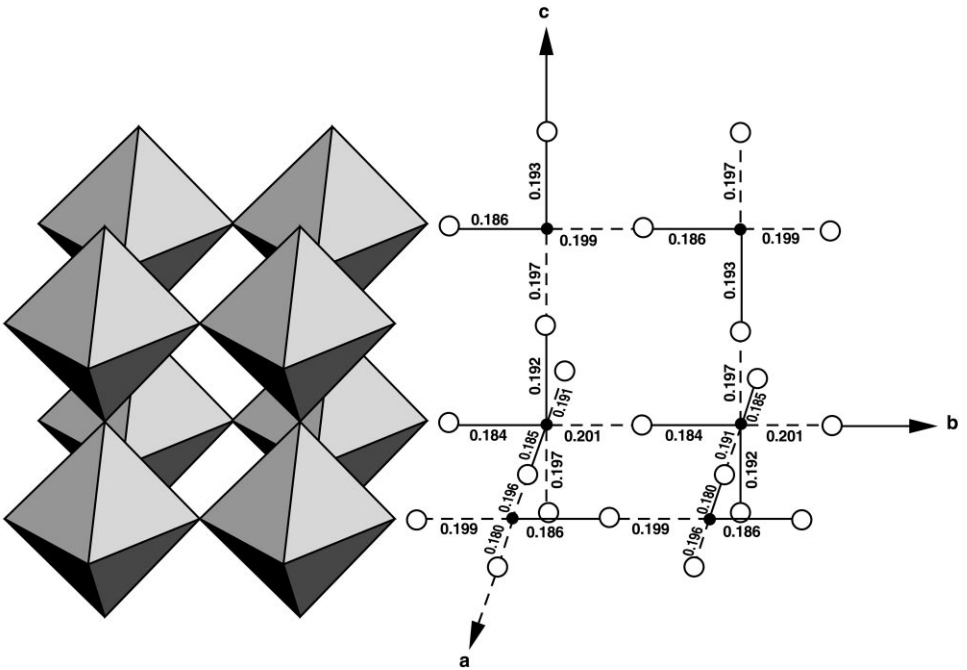

Fig. 7. Structure of crystalline WO_3. Distances are given in nm.

to the split-up of the d level into e_g and t_{2g} [153] level as shown in Fig. 9. The number of states available for electron occupancy is fixed for each band and determines the Fermi level of tungsten oxide which lies in the bandgap indicated in Fig. 9 with an arrow.

3.1.2. Evaporation products and condensation process

WO_3 evaporates in vacuum by sublimation at temperatures > 1200 K. Usually, Knudsen cells are used to study the vapour above WO_3 in thermodynamical equilibrium between the gas phase and the solid state. Most of the investigations are done with ionizing electron energies for the mass spectrometer, higher than 40 eV [154–156]. Under these conditions, the following species are found: WO^+, WO_2^+, WO_3^+, $W_2O_5^+$, $W_2O_6^+$, $W_3O_8^+$, $W_3O_9^+$, $W_4O_{11}^+$, $W_4O_{12}^+$ and $W_5O_{15}^+$. Additionally, a preferential oxygen evaporation is analysed and the influence of the concentration of water in the back pressure is studied [157].

Technical evaporation processes occur under conditions that are far away from the thermodynamical equilibrium. The main differences to Knudsen cell experiments [156] are the open crucibles, the lower evaporation temperature and the composition of total pressure, which is evoked by very different gases. Fig. 10 gives an overview of the tungsten containing species detected at a constant evaporation rate with the mass spectrometer under technical conditions. The used ionizing electron energy of 83 eV

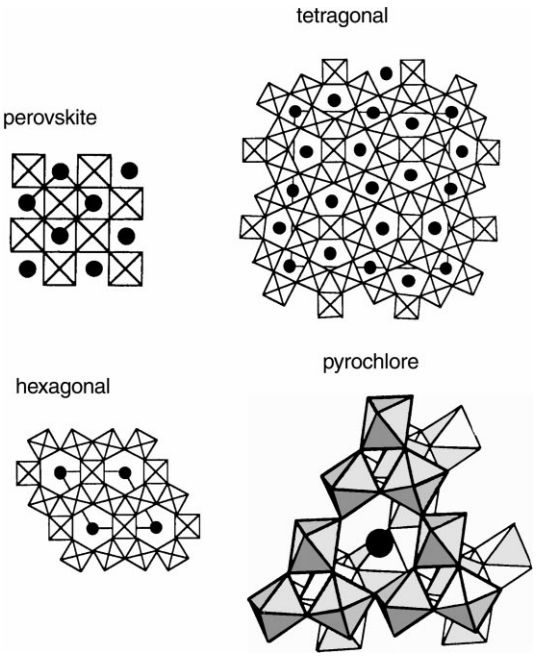

Fig. 8. Atomic arrangement for crystalline tungsten oxide with perovskite (cubic), tetragonal, hexagonal and pyrochlore structure. Dots indicate available sites for ion insertion and the unit cells are marked. From [151].

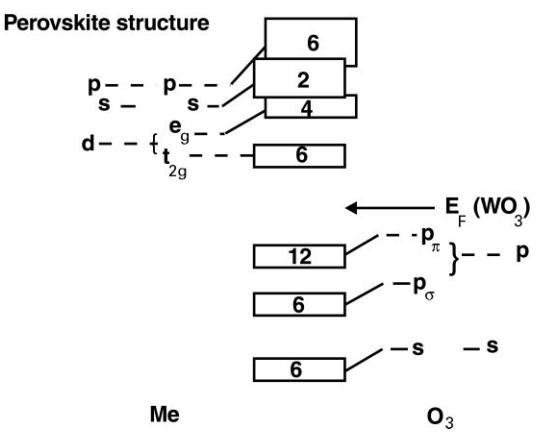

Fig. 9. Schematic bandstructure for WO_3 (ReO_3) defect perovskite structure. From [153].

produces additional ions extensively investigated by Berndt [154]. At 16 eV ionizing electron energy, for instance, the following species are detected and ion current intensities are given:

$$WO_2^+ : WO_3^+ : W_2O_6^+ : W_3O_9^+ : W_4O_{12}^+ = 2 : 7 : 2 : 7 : 1.$$

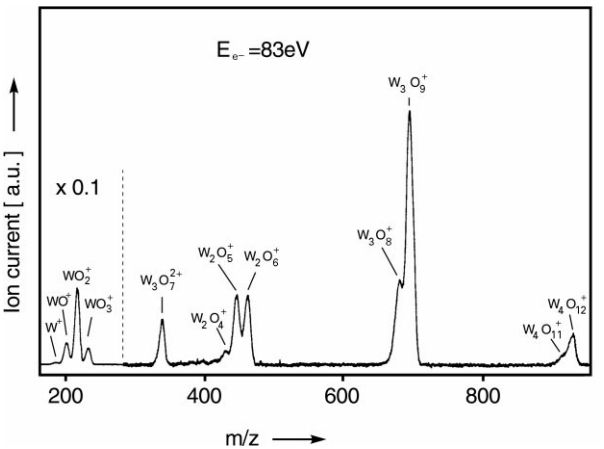

Fig. 10. Mass spectrum of vapour above WO_3 detected with an ionizing electron energy of 83 eV. From [154].

But a variation in the water partial pressure changes drastically the composition of the evaporated species [154].

Fairly recently, the vapour content of evaporated powder tungsten trioxide has been studied by means of mass spectrometry [158]. At a base pressure of 5×1^{-6} Pa, the evaporated particles are ionized by electron impact energies of approximately 40 eV. The observed mass spectrum consists of the lines of WO_2, WO_3, W_2O_5, W_2O_6, W_3O_8 and W_3O_9. A weak signal is also detected for W_4O_2. For ionizing electron energies below 20 eV the lines of WO_3, W_2O_5, W_2O_6 and W_3O_8 are not detectable. From temperature-dependent investigations it is found that the lines of WO_2, WO_3 and W_2O_6 clearly differ in shape and, therefore, may not be created by dissociation of W_3O_9. The line intensities are converted into relative concentrations of the corresponding molecules [158] which are, under the used experimental conditions for WO_2 35%, WO_3 5%, W_2O_6 10%, W_3O_9 50%. For modelling of the growth and the structure of the films, information about the tungsten oxide species arriving the substrate can be useful.

The various data on evaporation products in the literature can be summarized as follows:

- Under good vacuum conditions, W_3O_9 molecules exist preferentially in the vapour, but also WO_3 monomers.
- At high water partial pressure, the number of the polymers and the size of polymers increase.
- At high water pressure, the $W_3O_8^+/W_3O_9^+$ ratio decreases, which suggests that substoichiometric W_3O_8 is a primary particle in the vapour beam.

Different structures are proposed for the various molecules detected with the mass spectrometer. Some are depicted schematically in Fig. 11. On the basis of the

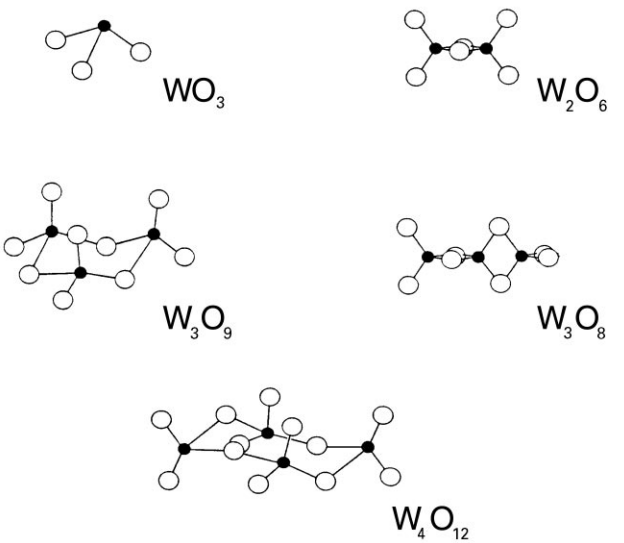

Fig. 11. Configurations of monomers and polymers in the vapour From [154].

concentration of charge at the tungsten atom, an angular molecule is assumed for WO_2, and a pyramidal shape for WO_3. For W_2O_6, a configuration is favoured which contains a double oxygen bridge, and for W_3O_9, a circle-formed polymer is guessed.

It is reported, and we found, that good colouration behaviour is obtained for films deposited at low substrate temperature and high water pressure [159–161]. In connection with these results, the following conclusion can be drawn from the vapour-phase data. Under technical conditions, WO_3 monomers and polymers adsorb preferentially at the substrate. Minor species are substoichiometric fragments. Additionally, water adsorbs in a concurrent process. Since, generally, the substrate temperature is low and the background pressure is high the adsorbed particles are not very mobile on the surface and create a porous film with a low density. With increasing water partial pressure, the number of larger molecules, especially trimers increases. These polymers probably contain their structure and create films which possess molecular, i.e. nearest-neighbour order. These conclusions are consistent with experimental results describing the highly disordered films as "amorphous", i.e. Raman-, X-ray- and electron diffraction-"amorphous", which is discussed in detail in Section 3.1.5.

3.1.3. Optical properties

The optical properties of as-deposited tungsten oxide films depend to some extent on the deposition parameters. Both, the refractive index n and the extinction coefficient k in the ultraviolet (UV), luminous (VIS) and near-infrared (NIR) are influenced by the evaporation conditions and post-deposition processes. This is illustrated in the following.

Fig. 12 shows the spectral transmittance (T) and reflectance (R) in the wavelength range between 300 and 1000 nm for a 730 nm thick tungsten oxide layer deposited under "standard" conditions on glass. The reflectance is depicted as $1 - R$, because the difference between the T and R curvature exhibits additionally the absorptance. On the basis of such type of data, the refractive index n and extinction coefficient k can be calculated [150,162].

The spectral $n(\lambda)$ and $k(\lambda)$ is shown in Fig. 13 for the transmittance and reflectance depicted in Fig. 12. For the refractive index, a dispersion is obtained which is typical for oxides. A refractive index of 1.97 is analysed at a wavelength of 550 nm. The

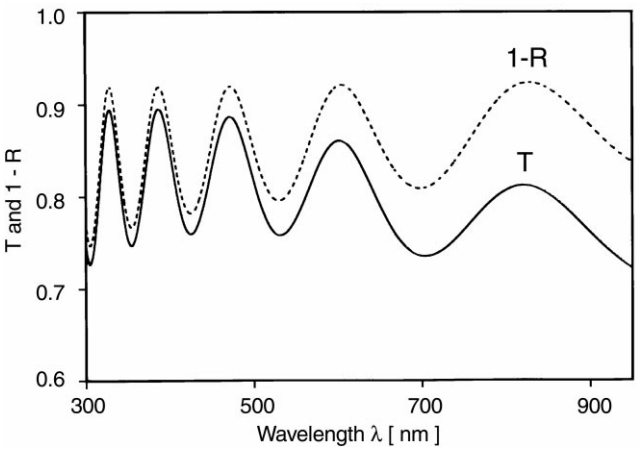

Fig. 12. Transmittance (T) and reflectance (R) of tungsten oxide film on glass substrate.

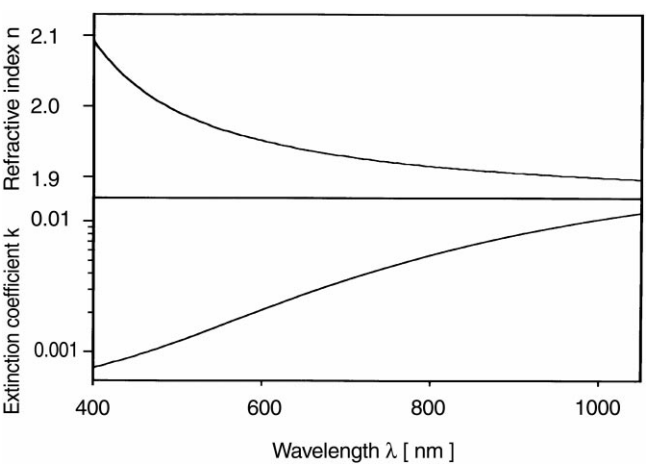

Fig. 13. Spectral refractive index and extinction coefficient for the tungsten oxide film depicted in Fig. 12.

extinction coefficient increases with increasing wavelength indicating that as-deposited films possess a weak absorptance in the NIR after the deposition. This typical absorptance can be reduced by short annealing in air at 150°C or by storaging in air for a certain time [150].

The influence of the vacuum conditions on the absorptance of evaporated films is also reported [163]. High-vacuum evaporation leads to a distinct absorption band centered at approximately 1.2 eV, while evaporation in low vacuum exhibits no absorptance. The pronounced feature at 1.2 eV is ascribed to oxygen deficiency and has a strong resemblance to absorption bands that can be created by the various coloration processes (Section 3.2).

The influence of the substrate temperature T_s is demonstrated in Fig. 14, which presents the spectral refractive indices for layers deposited at room temperature and at $T_s = 150°C$. Higher substrate temperature increases the refractive index at approximately 0.06. A similar tendency is observed for tungsten oxide films deposited by sputtering [164].

The optical absorption in the UV is dominated by the bandgap E_g of the semiconductor, as illustrated in Fig. 9. The bandgap is wide enough to render the material transparent. E_g can be derived by applying the relation

$$\alpha h\omega \sim (h\omega - E_g)^{\eta}, \tag{3.1}$$

where α is the absorption coefficient, ω the angle frequency, h is Planck's constant divided by 2π, and η depends on the kind of optical transitions that prevail. Specifically, η is 1/2, 3/2, 2 and 3 for transitions being direct allowed, direct forbidden, indirect allowed and indirect forbidden, respectively.

Fig. 15 shows experimental data for an evaporated tungsten oxide film. It appears that the relation 3.1 is well obeyed, provided that $\eta = 2$, assuming indirect allowed

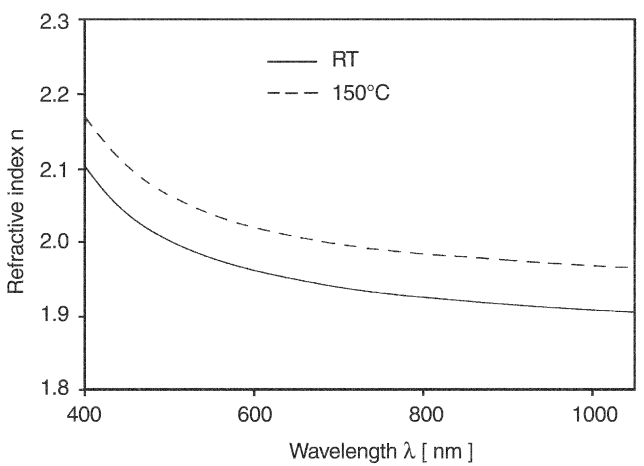

Fig. 14. Refractive indices for tungsten oxide films deposited at room temperature (RT) and at 150°C (dashed line).

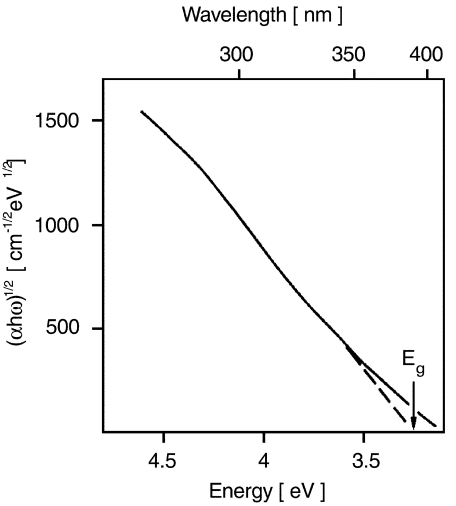

Fig. 15. $(\alpha h\omega)^{1/2}$ versus energy for an evaporated tungsten oxide film. From [149].

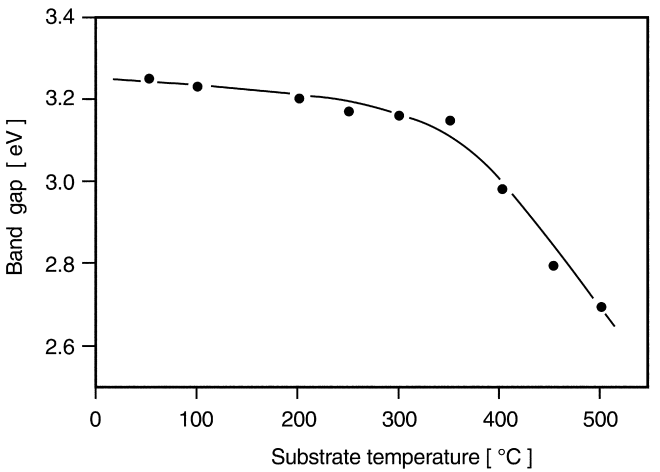

Fig. 16. Bandgaps for tungsten oxide films evaporated onto substrates of different temperatures. From [165].

transitions [149]. The indicated linear extrapolation yields $E_g \sim 3.25$ eV, which is typical of a highly disordered tungsten oxide film [149].

Similar to the refractive index or the absorptance in the NIR, E_g also depends on the film preparation conditions. Fig. 16 shows results for evaporation onto various substrate temperatures T_s. A monotonic drop is noted for E_g with increasing substrate temperatures [165]. The strong decrease at $T_s > 300°C$ indicates that crystallization causes a narrowing of the bandgap. This effect is probably associated with changes in

the structure of the nanocrystals from an extremely fine-grained hexagonal configuration to a large-grained monoclinic atomic arrangement. Another interpretation is that quantum confinement in semiconductor clusters causes a bandgap widening in the "amorphous" films [166].

3.1.4. Density

The density of tungsten oxide films possesses a strong influence on the rate of the colouration reactions, especially in electrochromic, but also photochromic processes [167]. For electrochromic colouration, this is usually explained with the fact that low density films are good ion conductors, and the density controlling the ion intercalation/deintercalation rate. But low density films may cause problems regarding long-term durability [150,168].

In general, the density of thin-oxide films depends strongly on the actual deposition conditions [169]. The main parameters in the evaporation process, which influence the density, are the background pressure (p) of the vacuum chamber, the substrate temperature during the deposition (T_s); but also post-deposition annealing temperature (T_a) can change the density [168,170]. A weak influence on the film density is also reported for the water partial pressure p_{H_2O}, which is varied between $p_{H_2O} = 6.1 \times 10^{-4}$ and $p_{H_2O} = 4.0 \times 10^{-3}$ Pa in a vacuum chamber back-filled to 4×10^{-2} Pa by introducing oxygen [161]. Fig. 17 illustrates the dependence of the relative packing density of films on various parameters. Here, the packing density is defined as the relative density to ideally packed bulk WO_3 with $\rho_{bulk} = 7.16\ g\ cm^{-3}$ [171]. Evaporation in high vacuum onto an unheated substrate yields a relative density of ≈ 0.8. An increase in the partial pressure of nitrogen p_{N_2} or oxygen p_{O_2}, which is indicative of an increase in the total pressure, decreases the density. Densities

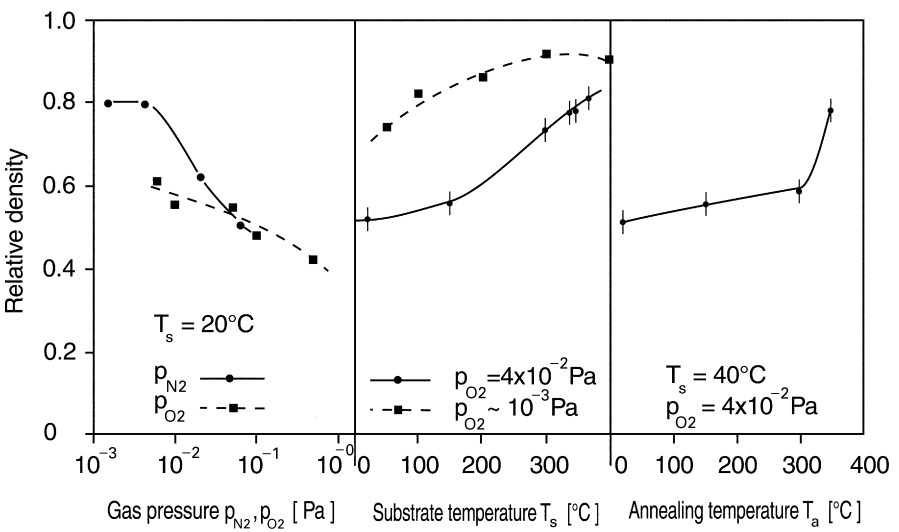

Fig. 17. Relative packing density for tungsten oxide films prepared by evaporation. From [168,170].

as low as ≈ 0.4 are obtained [168,170]. The opposite effect can be realized by an increase in substrate temperature or annealing temperature. With increasing temperature, densities between ≈ 0.5 and 0.9 are readily obtained. It should be mentioned that for temperature $T > 300^{\circ}C$ an increased crystal growth is observed (Section 3.1.5).

The film density can be manipulated also by different post-deposition approaches. For example, ions in the energy range of MeV can be used for this purposes (Section 3.2.2.2). Compaction of evaporated tungsten oxide films up to nearly bulk density is observed for various types of irradiated ions of different energies up to 30 MeV and fluences up to $10^{18}\,cm^{-2}$. No changes in stoichiometry are detectable. Raman investigations show that the ion beam modified films are not crystalline, but have a nanostructure different from as-deposited material [172].

3.1.5. Structure

Investigations of tungsten oxide films by electronmicroscopy give various types of structural information. Studies on "standard" film cross sections prepared by ultramicrotomy [173] exhibit a *columnar structure* for evaporated material [150]. A diameter for the column of approximately 20 nm is found for a 500 nm thick film, and the columns appear to be very homogeneous, i.e. no grain boundaries can be recognized. The nanostructural features occur at all dimensions, up to those comparable with film thickness [174]. It is known that columnar structures occur spontaneously in films grown by a directional vapour flux. The phenomenon can be explained by models based on ballistic aggregation of structural units and ensuing reaccomodation of these, as well as originating from growth instabilities in continuum theories. It is possible to increase the columnar character and to enhance the porosity of films by depositing at an oblique angle [175,176].

The *topography* of our film surfaces is examined on C/Pt replicas. A strong correlation between the used substrate and the topography for tungsten oxide is found for films with thicknesses < 250 nm [150]. For thicker films, the dependence in the surface topography on tungsten oxide disappears. This finding has a certain relevance for the chromogenic behaviour, because tungsten oxide films, for instance, used in electrochromic cells are usually deposited on ITO. The surface topography of ITO, and especially the surface roughness, is strongly related to the used deposition conditions. These differences are also to be found in tungsten oxide layers [150].

For the investigations of film growth and film structure, 40-nm-thick tungsten oxide films are prepared on Formvar, different C-substrates and different types of glasses with our "standard" deposition conditions. Films with such thicknesses produce no homogeneous contrast in the TEM micrographs. *Clusters* with sizes between 2 and 10 nm are observed. The clusters size depends on the type of substrates used [150]. Electron diffraction produces a strong diffuse halo suggesting a certain short-range order, but this appearance is usually interpreted as *amorphous* state for films. A temperature treatment at $T_a = 100^{\circ}C$ for 110 h in air does not change the electron diffraction halos, but the cluster size is increased by about 10–20%. Similar changes are observed by storaging tungsten oxide layers for 550 h at room temperature and 80% of relative humidity [150].

Higher T_a increases the cluster size, but the electron diffraction pattern is still fairly diffuse. Temperature treatment to 450°C for 20 min leads to crystallization. The diffraction pattern indicates monoclinic WO_3 but additional features are present, suggesting also different crystal phases. The sizes of the crystals are larger than 50 nm [150].

High-resolution transmission electron microscopy using axial beam illumination has been carried out on tungsten oxide films deposited on glass substrates at room temperature. Films with a thickness of 10 nm are floated on distilled water for thinning to less than 5 nm [177]. As-deposited films heated at 350°C for 2–5 h give rise to amorphous halos in electron diffraction, and crossed fringe-like structure images of the order of 1–2 nm are observed. It is suggested that the amorphous films consist of nanocrystallites in which WO_6 octahedral is arrayed like crystalline tungsten oxide. When the thin films are heated at 350°C for 10 h, they grow to crystals of WO_3 as large as 10 nm. In films thicker than about 20 nm, crystals of a few microns grow after shorter heat treatment [177]. For films with a thickness of 40 nm, the structure changes in tungsten oxide films are different during heat treatment. Crystals of a few microns in size grow after heat treatment at 350°C for 2 h, or at 400°C for 10 min, and films are almost full of crystals after 5 or 2 h, although the very thin films heated at 350°C for 5 h still give more amorphous halos in their electron diffraction patterns [177].

Additional observation and analysis of the amorphous halos in electron diffraction have been carried out on tungsten oxide films of a thickness of 8 nm, which are deposited onto clean NaCl substrates at room temperature [178]. Crossed fringes forming a region of about 1 nm in size are frequently seen in the micrographs, and each of their spacings corresponds to the lattice spacing of WO_3 crystals. From the behaviour of the lattice fringes by tilting the films is concluded that the nanocrystallites are distributed at random in the film. The experimentally obtained electron diffraction intensity is explained by a nanocrystal model in which nanocrystallites are distributed randomly with sizes of 0.8, 1.0 and 1.2 nm [178].

The *local order* structure of amorphous tungsten oxide layers has been studied by analysis of the atomic density from radial distribution functions (RDF) obtained by means of Fourier transformation of the intensity curves of coherent scattering electrons [179,180]. Five different radii of coordination spheres are obtained [179]. The first and the second neighbour distances, as well as the number of first and the second neighbours, are very similar in these investigations for amorphous and crystalline structures, and W maintains, six neighbours in the amorphous state. The first maximum of RDF for as-deposited material corresponds to the mean tungsten oxygen distance of 0.192 nm and is symmetric, which seems to indicate the absence of statistical distortion of WO_6 octahedra [180]. But also an average nearest-neighbour bond length of 0.189 nm is reported, with a deviation of which is likewise 0.016 nm [179]. Such large deviations cannot be explained by thermal vibration alone, but sizable distortions of local configurations are needed. The existence of deformed octahedra in the amorphous structure of tungsten oxide film is consistent with Raman scattering data suggesting a terminal oxygen in the structure of thin films [181]. A crystalline structure of WO_3 is proposed which consists of a deformed

corner sharing WO_6 octahedra array in three interconnected, perpendicular directions [179].

Since the distance between the adjacent tungsten atoms of 0.373 nm is less than twice the W–O distance, the W–O–W band is nonlinear with the angle of about 150°. The maxima at 0.46 and 0.54 nm correspond to the overlap of the mean W–O, O–O distances from the next coordination spheres, where the W–O distances give the main contribution. A maximum at 0.69 nm is attributed to the W–W distance of the next coordination spheres. All observed maxima are interpreted assuming ordered chains of top coupled WO_6 octahedra distributed in a less ordered octahedral network [180].

But investigations on the structure by electron microscopy can be misleading, because different types of artifacts can be created. It is known that especially thin film materials having a tendency to crystallize (WO_3, TiO_2) can produce different types of problems [150,173]. Two main mechanisms can be responsible for the artifacts. It is observed that preparation by argon ions can change the morphology of the films, and microcrystals are created at high doses. But also the electron beam used during the investigation can produce crystals [150,173]. This has been observed for tungsten oxide films prepared under different conditions, and, therefore, all experimental data obtained by electromicroscopy have to be handled with caution.

For that reasons, Raman spectroscopy is also very useful for elucidating the nanostructural features of thin oxide layers. Fig. 18 shows Raman spectra of our tungsten oxide films with a thickness of 700 nm on Si wafer in the as-deposited state and after annealing to a temperature of $T_a = 400°C$. The annealed film exhibits two pronounced features at about 710 and 805 cm^{-1} (the relative sharp peak at 520 cm^{-1} is due to the one-phonon line of the Si substrate).

Various Raman spectroscopy investigations on tungsten oxide-containing materials are reported [154,170,179,181–183], which can be helpful as reference data.

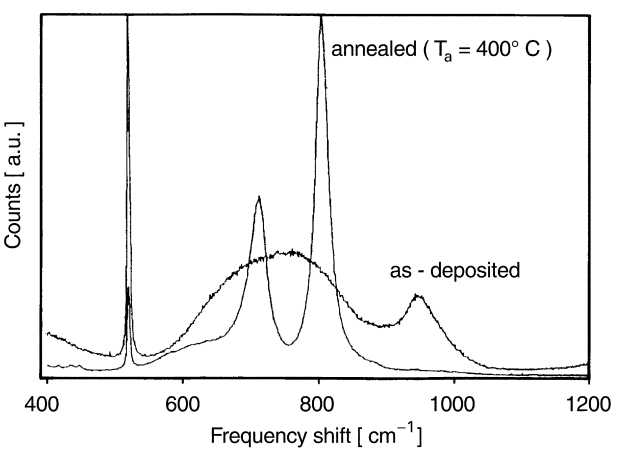

Fig. 18. Raman spectra of as-deposited and crystalline (annealed) tungsten oxide on Si substrate. The intensity scale of spectrum of the as-deposited film is enlarged.

Raman spectra are measured for bulk substances consisting of crystalline $WO_3 \cdot H_2O$, crystalline $WO_3 \cdot 2H_2O$, amorphous bulk $WO_3 \cdot 1.74H_2O$, and different phases of tungsten single crystals [181]. But also results are given for thin films prepared under very different conditions and post-deposition treatments [154,161,184–191]. For crystalline thin films, monoclinic and also orthorhombic and hexagonal phases predominate. A comparison of our results with data in the literature exhibits that the Raman features of the annealed sample in Fig. 18 are probably created by a hexagonal crystal phase [154,185].

For the as-deposited film, a broad peak can be recognized, centred at a wave number $\approx 750\,cm^{-1}$ and a more narrow peak at $\approx 950\,cm^{-1}$. In the wave number region at $950\,cm^{-1}$, in which the small peak appears, no Raman lines are found for crystalline thin films and also not for single crystals [181,192,193]. Only for water-containing material, in crystalline as well as amorphous state, a corresponding vibration mode is analysed [181]. Films deposited under different water partial pressure ($p_{H_2O} = 6.2 \times 10^{-6}$ Torr and $p_{H_2O} = 4 \times 10^{-5}$ Torr) exhibit an increased Raman intensity at $\sim 950\,cm^{-1}$ for film prepared, with higher p_{H_2O} [161]. With increasing annealing temperature, this feature vanishes [170] and can be unambiguously assigned to stretching vibration modes of *terminal W=O bonds* [194].

A detailed analysis of Raman spectra of as-deposited films, which involves a deconvolution into a set of three Gaussian peaks, favours the view that the W=O modes are located at internal surfaces rather than inside dense clusters [170,195]. Infrared absorption spectroscopy capable to give information, that is complementary to the one obtained from Raman spectroscopy, also found a clear evidence for hydroxylation or hydrolysis upon treatment of tungsten oxide films in humid air [196]. It seems that as-deposited tungsten oxide films consist of very small clusters which may be linked by hydrogen bonds through water molecules or by W–O bonds [197]. Within increasing crystallization, the W=O state changes to a W–O–W binding state.

The broad W–O stretching peak centered at $\approx 750\,cm^{-1}$ can be deconvoluted into two Gaussian components peaking at ≈ 710 and $805\,cm^{-1}$, where also the two pronounced features of the crystalline film are located [161]. On the basis of various Raman results on tungsten oxide films with different deposition conditions, it may be guessed that the substrate temperature T_s and also the water partial pressure p_{H_2O} possess a certain influence on the cluster size [161]. The size of the cluster increases with increasing T_s and decreasing p_{H_2O}. Incorporation of water in as-deposited films changes additionally the internal bonding structure between the cluster [154]. This may be concluded from the behaviour of the full-width at the half-maximum (FWHM) at $805\,cm^{-1}$, which is sensitive to the crystallinity. The FWHM at $805\,cm^{-1}$ exhibits a steady decrease by 35%, as T_s is raised from 40°C to 145°C. Subsequent annealing in air at 150°C gave no appreciable changes in the FWHM, and only small changes are observed for a short-time annealing at $T_a < 300$°C [141].

But post-deposition annealing can influence also the cluster size of tungsten oxide layers. Annealing at 300°C in air results in a continuous change of the Raman spectra. One result is depicted in Fig. 19. The Raman intensity at $805\,cm^{-1}$ is shown as

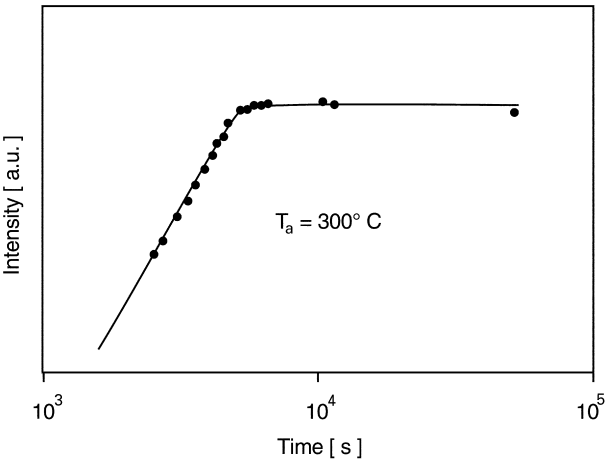

Fig. 19. Raman intensity at 805 cm^{-1} during annealing at $T_a = 300°C$ in air.

a function of annealing time ($T_a = 300°C$) for 400-nm-thick tungsten oxide layer. A continuous increase for the Raman intensity is observed and a saturation value is reached after approximately 3 h [150]. As these changes are consistent with an integrated intensity ratio of W=O/W–O stretching mode, they seem to be caused by the growth of clusters constituting the framework structure [161].

Structural information on evaporated tungsten oxide film has been obtained further from X-ray investigations, for instance X-ray extinction, specifically small-angle X-ray scattering (SAXS) [125,148], extended X-ray absorption fine structure spectroscopy (EXAFS) [198], X-ray absorption near-edge spectroscopy (XANES) [199], and X-ray diffraction (XRD) [170].

As reported above, high substrate temperature during the deposition and post-deposition annealing change the degree of crystallinity, but also the film composition (Section 3.1.6). On the basis of XRD data, evaporated tungsten oxide films are "X-ray amorphous" for $T_s < 340°C$ and $T_a < 350°C$. For this temperature region, only a broad diffraction peak is present in Fig. 20, which is characteristic for the amorphous phase. For $T_s > 350°C$, two broad peaks appear to be corresponding to crystalline Bragg diffraction peak from (200), (020), (001) and from (021) (201) planes [170,179]. In post-deposition annealing experiments, crystallization takes place in the same temperature range, i.e. for $T_a > 350°C$ [170], and similar diffraction features are observed.

For annealing of tungsten oxide films, which are stored in high relative humidity, different diffraction patterns at other T_a are obtained. For relative humidity of 95% and annealing temperature $T_a = 40°C$, a polycrystallization in films is reported [196]. Peaks in the XRD spectrum are observed also for our tungsten oxide films on ITO-coated glass at relative humidity of 95% and $T_a = 80°C$ [150]. The d spacings of X-ray analysis can be assigned closely to d spacings of the (010) planes of $H_2WO_4 \cdot H_2O$ and the intensity ratios agree exactly. These results are attributed to

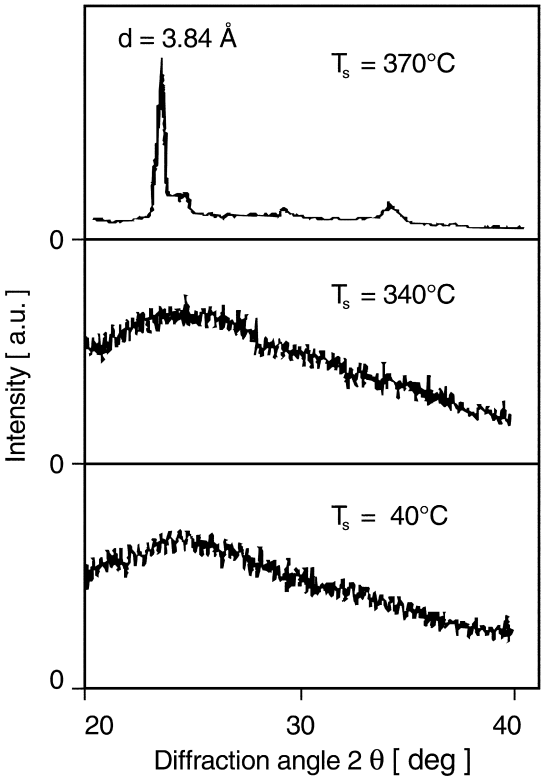

Fig. 20. X-ray diffraction pattern of tungsten oxide films prepared at different substrate temperatures. From [170].

the presence of monoclinic $H_2WO_4 \cdot H_2O$ which is crystallized with a preferred orientation of the (010) plane parallel to the substrate. An additional peak indicates the presence of a small amount of $WO_3 \cdot H_2O$ [196].

Detailed structural information, especially on nanocomposites with grain sizes in the range of 1–1000 nm, can be obtained from SAXS by detecting the scattering angles 2θ between 20″ and 2°. The features responsible for this scattering are electron density fluctuations associated with nanocrystallites and voids. Scattering intensity versus scattering angle (reciprocal space) are sampled in general, and from the Fourier transformation [125,148] it is possible to extract a radial distribution function (RDF),

$$N(r) = 4\pi r^2 \rho(r) \tag{3.2}$$

that includes information on the density correlation $\rho(r)$ in the analysed material. Fig. 19 illustrates RDF's for films prepared at three different substrate temperatures T_s (RT, 150°C, 300°C).

To analyse such type of RDF data, various structural models have been proposed [125,148]. From Nanba and Yasui [148], eight different crystallographic structures are employed as starting point and corresponding RDF's are computed. The first group tested consists of monoclinic and tetragonal stoichiometric WO_3, which is described as a distorted cubic structure of the ReO_3 type. In the second group, substoichiometric tungsten oxide, $W_{18}O_{49}$ ($WO_{2.72}$) and $W_{20}O_{58}$ ($WO_{2.9}$) are employed as starting points for the computation of the RDFs. In this structure, the shortage of oxygen is compensated by formation of the edge-sharing octahedral, and a channel structure stabilizes this cluster. The third group contains the hydrated oxides. Since the accurate structural parameters of $WO_3 \cdot 2H_2O$ have not been given, the structure of molybdenum oxide hydrates is used, which is thought to have a very similar structure. The last group use six-membered rings with structures of hexagonal WO_3 and $WO_3 \cdot 1/3\ H_2O$, which have been reported by Gerand [147,200]. The hexagonal type is a new form of WO_3, and WO_6 octahedral are arranged in the manner of not only four-membered rings, but also three- and six-membered rings sharing the corners.

The position of the first and the second peaks in the observed RDFs are consistent with all of the calculated RDFs for the compared structures, i.e. all of them yielded peaks at ~ 0.2 nm due to W–O nearest neighbours, and at 0.37–0.40 nm due to W–W nearest neighbours, and to a smaller extent W–O nearest neighbours. All of these features stem from the *basic octahedra* WO_6 building blocks. The peak positions in the region > 0.4 nm are somewhat different among the examined crystals, which is due to the difference in the configuration of the network formed by WO_6 octahedral. Peaks observed around 0.5–0.6 nm are mainly attributed to the W–W pairs located at the opposite corners in the four-membered rings and the second neighbours of the six-membered ones, i.e. the peaks at radii > 0.5 nm are of more decisive importance for the structural model. In particular, a large characteristic peak at ≈ 0.73 nm, commonly presented in the observed RDF, can be reconciled only with a hexagonal structure. In addition to this, even the small peaks in the observed RDFs are consistent with the peaks of the hexagonal WO_3 and $WO_3 \cdot 1/3\ H_2O$. For these reasons, a structural model of evaporated tungsten oxide film, a framework structure, is proposed by Nanba and Yasui, which is similar to that of hexagonal WO_3 and $WO_3 \cdot 1/3\ H_2O$.

The upper left-hand panel in Fig. 21 shows a structure model based on a *hexagonal* WO_3, and $WO_3 \cdot 1/3\ H_2O$, in which *three- and six-membered* rings are displayed in the projected X–Y plane and *four-member rings* are parallel to the vertical Z direction. The cluster size of the model is 1.6 nm in diameter and is consistent with high-resolution electron microscopic evidence [150,177]. The three-membered rings can be ascribed to the W_3O_9 molecules produced during evaporation as described in Section 3.1.2 [154,156], and such molecules can be tied together to form six-membered rings. The models satisfy also the observed O_{tot}/W ratio. Finally, the clusters are arranged in space with consideration to their hexagonal plate configuration, and the cluster models are therefore placed in positions similar to a hexagonal close packing. The distance between the clusters is calculated to be 2.46 nm to satisfy the observed film density of 4.09 g cm^{-3}, so that they constituted a model film, and

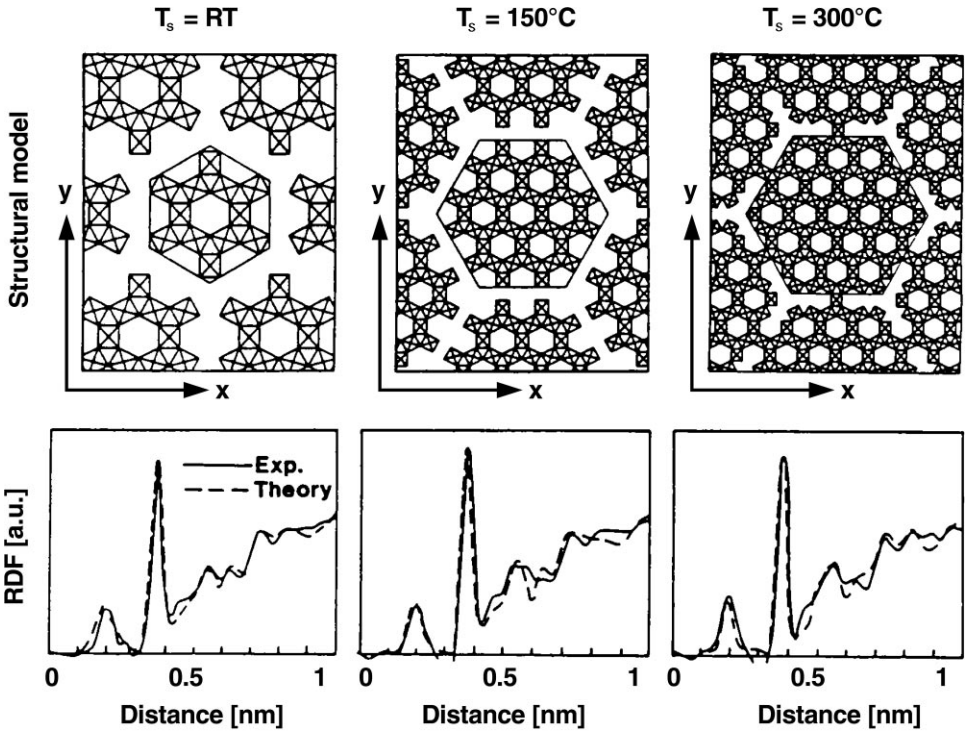

Fig. 21. Radial distribution functions (lower parts) determined from SAXS (solid curves) and as computed from the shown structural models (upper parts) are based on connected WO_6 octahedra. From [148].

RDFs are computed. It is seen from the lower left-hand panel in Fig. 21 that theory and experiment are in good agreement, which gives some credibility to the shown structural model.

An extension of this model to films evaporated at elevated substrate temperature T_s is also shown in Fig. 21. Cluster growth, as well as cluster–cluster linking, are apparent. At substrate temperature $T_s = 150°C$, the diameter of the cluster is 3 nm, which is greater than that at room temperature. The arrangement of the cluster is similar to the room temperature model, which has no direct bonds as W–O–W between the cluster. The results suggest that the three- and six-membered rings are fairly stable at $T_s = 150°C$. Increase in substrate temperature to $T_s = 300°C$ leads to a film density of 5.4 g cm^{-3}. The diameter of the calculated cluster grows up to 3.9 nm. The calculated RDFs from this model are consistent with the observed value. Below $T_s < 300°C$, the clusters are isolated, but they are connected to each other at $T_s = 300°C$. This result seems to reflect the structural change from the isolated cluster to a continuous structure.

3.1.6. Composition

As described in Section 3.1.2, tungsten oxide is not stable thermodynamically at evaporation temperatures of 1000–1300°C [155]. The thermodynamical equilibrium

varies as a function of the oxygen partial pressure to a smaller oxygen content and is additionally influenced by the water partial pressure. Non-stoichiometric evaporation material and technical evaporation conditions, which are far away from a thermodynamical equilibrium, can produce a further decrease in the O/W-ratio in thin films [160]. For evaporation temperature $> 1300°C$, the tungsten oxide layer exhibits a light blue colour. The reported literature data can be summarized as follows: vacuum-evaporated layers are substoichiometric, i.e they can be described as WO_{3-z} with $z > 0$. For that reason, the O/W-ratio, which is of large interest for the colouration behaviour, has been determined with different methods by different authors.

Fairly low *oxygen concentrations* are reported from AES and ESCA measurements [201–203]. Most of the given values are not correct, because they are taken from depth profile measurements which possess a principal error evoked by the preferential sputtering effect [201–203]. For these surface-sensitive methods, only such data are reliable which are taken from the film surface without pretreatment, and not from depth profiles. With that, limitation values of 2.5 and 2.7 are obtained, but with large uncertainty [154,160].

From the ESCA spectrum in Fig. 67, it can be concluded that our as-deposited standard tungsten oxide films are not completely oxidized. Beside the dominating W 4f doublet, with a W $4f_{7/2}$ peak at binding energy of 35.85 eV, a weak feature is observed at lower binding energies, which indicates that the surface region of tungsten oxide also contains W with an oxidation state W^{5+}. An estimation of the O/W peak ratio leads to a composition of $WO_{2.85}$ for the surface region [204].

For high-precision determination of the bulk stoichiometry of tungsten oxide films, RBS is an appropriate tool. O/W-values between 2.96 and 3.28 are analysed for oxygen partial pressures between 10^{-3} and 10^{-1} Pa [205]. These values also contain the water content in the layers. For transparent evaporated films, an oxide/W-value of about 2.7 is found by RBS [206,207].

To increase the accuracy of analysis films, we deposited tungsten oxide film on carbon substrate. Fig. 22 shows RBS data of a 500-nm-thick "standard" tungsten oxide film in as-deposited state and stored for 6 months in air. The contribution of W, O and C are very well separated, increasing the precision of the analysis. A stoichiometry of $WO_{3.4}H_{1.1}$ is obtained [207].

The *hydrogen content* in the layers, which is of high relevance for the colouration process, cannot be analysed with RBS, but can be measured with a high precision by the ^{15}N method [150]. Some hydrogen depth profiles of our standard tungsten oxide layers deposited on ITO, coated glass are depicted in Fig. 23. The increase in the H/W content can be seen for storaging at RT in a relative humidity of 80%.

The surface of the film is located in the energy scale at 6.4 MeV, and the tungsten oxide/ITO interface at approximately 8 MeV. As-deposited films exhibit a H/W-ratio of about 0.3 in the layer. Changes in the hydrogen concentration versus the time are depicted in Fig. 24 on the basis of such data. It can be recognized that a saturation value of $H/W > 1$ can be obtained. But such layers tend to delimitation, and other defects are observed [207,208].

Additional information can be obtained by a careful analysis of the NRA data depicted in Fig. 23. Beside the increase in hydrogen content with the storage time, also

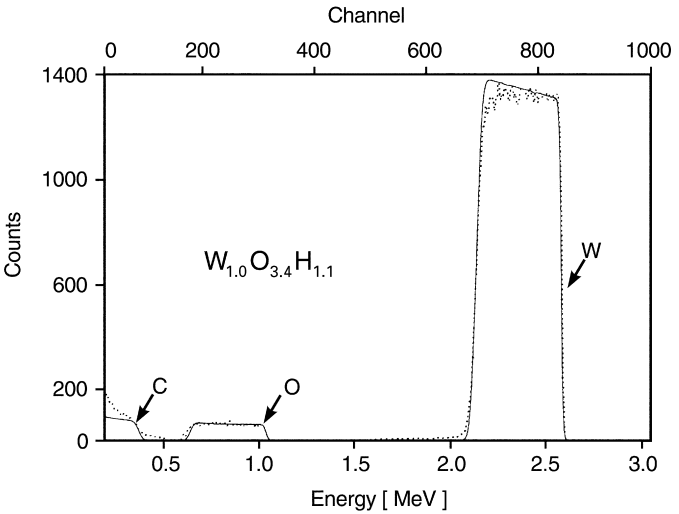

Fig. 22. RBS spectrum of tungsten oxide film on carbon.

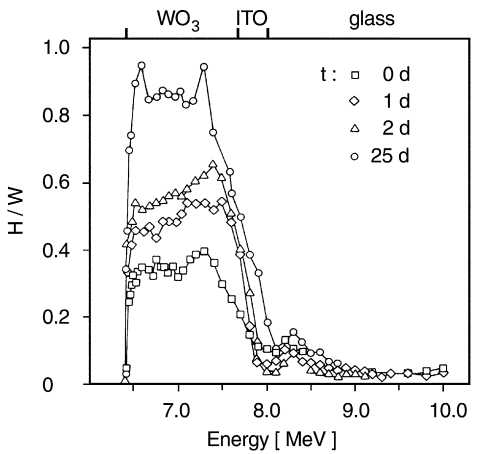

Fig. 23. NRA H-depth profile of tungsten oxide film on ITO. Different storage times t (in days) are shown.

a broadening of the profiles can be analysed, i.e. the interface WO_3/ITO seems to shift to higher energy. This can be explained by the assumption that beside hydrogen also oxygen is incorporated in the layer. The shift in energy can be explained with a $\delta H/\delta O$ ratio of 2 [209,210], which is a strong indicator for water uptake of the WO_3 film.

NRA exhibits that a significant amount of hydrogen is incorporated in the films, but the method is not sensitive to the chemical state of the elements, i.e. NRA cannot distinguish between molecularely adsorbed *water* or dissociatively adsorbed water.

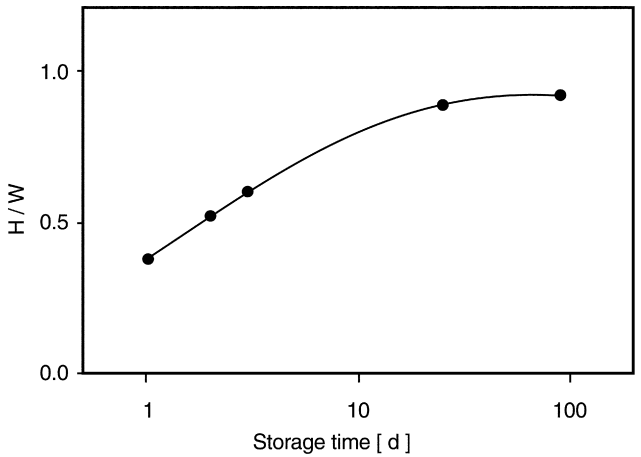

Fig. 24. H/W ratio versus storage time.

But IR investigations, which are sensitive to molecular species, show two vibration modes. A broad absorption band is centred at approximately 3400 cm^{-1}, and a sharp band at 1600 cm^{-1}. These IR data are interpreted as O–H stretching mode of water, which can also be adsorbed in the form of hydroxyl groups on internal surfaces and as H–O–H scissore mode, which interacts only very weakly with the environment [196].

Water adsorption is also investigated as a function of storage time in air at 25°C and 50% relative humidity. The peak at 1600 cm^{-1} increases remarkably by about 25%, with a storage of 24 h, but scarcely changes upon longer storage. On the other hand, the peak at 3400 cm^{-1} increases continuously with the time after a remarkable increase of about 23% for 24 h storage. From this result it is concluded that the amount of chemisorbed OH groups is continuous, increasing gradually with time, while the physisorbed water content in the film comes to equilibrium within 24 h [196].

Two different adsorption sites are postulated for water molecules. It is proposed that one place is between single WO_6 octahedra, i.e. inside the small clusters [196]. This place will be occupied during the film deposition, and the water uptake is finished after 24 h [196,211]. The second mechanism for the water uptake is the adsorption of water at internal surfaces of the films. This process happens within a period of a few weeks.

The O–H stretching mode is also analysed for films deposited at different substrate, T_s and annealing temperatures, T_a in the range of $T = 40$–290°C [167]. The total water content of the tungsten oxide films is estimated by integration of the O–H stretching mode (2800–3600 cm^{-1}) in the infrared spectra. The results are shown in Fig. 25 as a function of the substrate and annealing temperature (annealing time of 1 h) [147]. A decrease is observed in the O–H stretching mode with increasing temperatures.

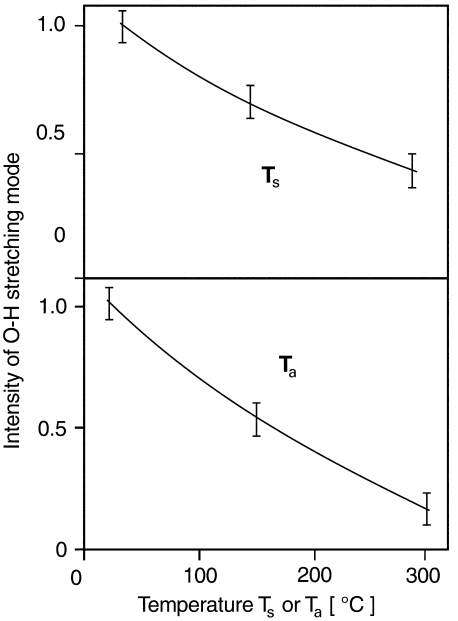

Fig. 25. Integrated intensity of O–H stretching mode as a function of substrate (T_s) and annealing temperature (T_a). From [167].

Relative to films deposited at $T_s = 40°C$, a decrease of 47% in the integrated intensity of the O–H stretching mode is observed at $T_a = 150°C$ for 1 h and of 85% at $T_a = 300°C$ for 1 h. The changes in the OH content in the tungsten oxide films with the substrate temperature can be interpreted by an increase in the packing density of the films, i.e. the films deposited at low temperature are very porous, while the films deposited at higher temperature possess a less porous structure.

Differences in the O–H stretching mode of FTIR spectra are found for post-annealed films deposited at low and high p_{H_2O} [161]. It is suggested that water molecules are present in forms of physical adsorption, chemisorption (known as Brönsted acid site) and structurally involved water [125,196,212]. The water which survived the annealing procedure is thought to be structural water. For high p_{H_2O} films, it is found that more structural water exists, and three distinguished peaks at 3050, 3200 and 3530 cm^{-1}, which appear after annealing, indicate the very well-defined existence of this kind of water [161,170].

The presence of water in the film suggests that the stoichiometry obtained by RBS contains also the oxygen of water, i.e. by the subtraction of the amount of oxygen; due to the water, there is a large oxygen deficiency to stoichiometric WO_3, which can be described as WO_{3-z} with $z > 0$. This oxygen deficiency is inherent in the structural models described in Section 3.1.5.

As mentioned above, annealing can change the degree of crystallinity, but also the film composition. Fig. 26 displays results from thermal gravimetric analysis (TGA)

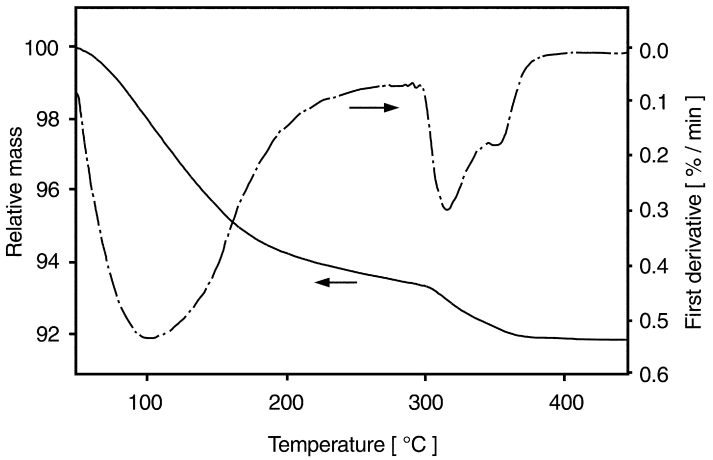

Fig. 26. Mass loss spectrum during thermal gravimetric analysis. From [208].

[208]. Heating of films at a rate of 10 K min^{-1}, which are stored 30 h under ambient conditions, exhibit a substantial mass loss, starting at about 50°C. Molecular water is evolved in a broad temperature range between 50°C and 270°C. The sample loses 4.5% of its mass. At 290°C, most of the hydroxyl groups are condensed, and the water formed during this reaction is expelled. From the derivative of the TGA analysis results, it can clearly be recognized that at approximately 295°C a second desorption process occurs and a mass loss of 1.1% is obtained between 295 and 395°C.

Differential scanning calorimetry (DSC) experiments are conducted to evaluate whether any other changes occur during heating. The endothermic reaction between 50 and 250°C is due to the evaporation of water as confirmed by TGA [208]. At higher temperature, an exothermic reaction takes place at 300°C, which is followed by an endotherm at 304°C and an exotherm at 331°C. The temperature behaviour above 300°C is interpreted as a condensation of W-OH groups (Brönsted sites). While the first water loss, observed in TGA, seems to occur as a result of the removal of molecular water, in the second temperature region, i.e. above 300°C, water expelled is a reaction product of W–OH condensation. The exothermic reaction at 331°C is due to the start of the crystallization of the material. From this type of experiments for evaporated tungsten oxide film, the chemical formula is given by $WO_x\,(OH)_q \times pH_2O$ with $x = 2.82$, $q = 0.36$ and $p = 0.6$, respectively [208]. Endothermic and exothermic effects in evaporated films are also reported by other authors [125]. $0.5H_2O$ per W is lost in the temperature range between 100 and 200°C in a similar study [125]. For films prepared by reactive sputtering and spraying of metatungstic acid, different quantities are given [125,181].

The composition of evaporated tungsten oxide films is also analysed by a combination of different methods for different preparation conditions [148]. The oxide-oxygen to tungsten atomic ratio, O_{ox}/W, is estimated from the peak area of O 1s and W 4f

signals in ESCA measurements. Crystalline tungsten oxide is used as standard with $O_{ox}/W = 3$. The quantity of involved water is estimated by the hydrate-oxygen to tungsten atomic ratio, O_{hy}/W with the combination of TGA and FTIR. Two steps of weight loss in TGA are observed at about 150 and 300°C and are assigned to the dehydration of water involved in the film. For films deposited at room temperature, the following quantities are reported: $O_{ox}/W = 2.8$, $O_{hy}/W = 1$, i.e. $O_{tot}/W = 3.8$. Increase of T_s and also post-annealing raise the O_{ox}/W ratio, while decreasing the two other quantities [148].

3.2. Colouration of tungsten oxide films

In the literature, there is a lot of information available concerning the colouration of tungsten oxide films. Different types of techniques, processes and mechanisms can be used to change the optical characteristics of the material. These are described in this section.

Thermochromic colouration, as a result of heating in vacuum, is reported (Section 3.2.1) followed by the colouration of different types of irradiation (Section 3.2.2). While UV illumination (Section 3.2.2.1) allows reversible switching from bleached to coloured state and vice versa, interaction with ions (Section 3.2.2.2) or electrons (Section 3.2.2.3) creates nonreversible colour. For photochromism, the influence of the surrounding atmosphere, i.e. vacuum, gas vapour, liquid, is given in detail, the dependency on the wavelength and on the film composition, especially on hydrogen and oxygen concentration, is described.

Colouration by electrochromic reactions is presented in a manifold way (Section 3.2.3). Most of the fundamental research on the electrochromism of tungsten oxide films is realized in liquid electrolyte experiments on the basis of electrochemical measurement techniques (Section 3.2.3.1). These established methods allow the control of the experimental conditions, e.g. potential or current, and the measuring of time-dependent quantities. For "standard" films, the changes in spectral refractive index and extinction coefficient are analysed for different states of colouration, and a spectral colouration efficiency is given. Diffusion constants and electromotive forces, as a function of the injected charge, are reported. Other techniques to obtain colouration in liquid electrolyte without applying an external voltage are described.

In the presence of catalyzing material, hydrogen-containing gases colour and oxygen-containing atmosphere bleaches tungsten oxide layers (Section 3.2.3.2). Tungsten oxide films, produced under our standard conditions and coated with thin rhodium films, are investigated in detail. Variation in hydrogen content determines the changes in optical density and colouration rate. Also the relative humidity exhibits a pronounced effect on the colouration behaviour of the tungsten oxide/Rh system. Electrocolouration, i.e. colouration by applying a high electrical field, is presented (Section 3.2.3.3). Reversible electrocolouration is obtained, and the influence of the relative humidity on the process is studied. Colouration of "standard" tungsten oxide films in the presence of a solid-state electrolyte is described also (Section 3.2.3.4). The influence of the different environments on the colouration of

tungsten oxide is compared, and the role of water at the film interface and in the film is discussed.

The different types of processes and mechanisms, which can be used for the colouration of tungsten oxide films, will be exemplified on films deposited by evaporation, with an "amorphous" state, i.e. on nanocomposite materials described in Section 3.1. For photochromism and thermochromism, no injection of external chemical species seems to be necessary for the colouration. Only the surrounding atmosphere, which is air in general, has a certain influence on the processes. Therefore, the electrochromism is restricted to experiments based on hydrogen-containing electrolytes, i.e. techniques involving Li^+, Na^+, etc., containing electrolytes are only used when the respective data of H^+ experiments are not available. A characterization of the coloured state is given in Section 3.3.

3.2.1. Thermochromic colouration

Since variation of temperature is experimentally one of the simplest methods to change the state of a film, i.e. to obtain a coloured tungsten oxide film, it is convenient to use the thermochromic process for investigations of the coloured state of tungsten oxide layers [115,163,205,213]. But only a few detailed analyses of the thermochromism of evaporated tungsten oxide films are reported.

Thermochromic colouration is investigated on tungsten oxide films prepared by thermal evaporation in a vacuum of approximately 10^{-4} Pa and substrate temperatures of $T_s \sim 80°C$ [163]. In addition to optical density measurements, a capacitance-voltage technique is employed to study the involved charge transfer between the coloured and bleached state. The films are subjected to heat treatment in vacuum at a $T_a \sim 300°C$ for 15 min, and in air at a $T_a \sim 450°C$ for 1.5 h, to vary the chemical composition and the optical density. Thermochromic colouration of the tungsten oxide films occurs as a result of heating in vacuum, while bleaching is obtained when the films are annealed in air [163].

During this thermochromic colouration process, the degree of structural ordering in the films remains unchanged according to high-energy electron diffraction data [163], i.e. the films appear to be amorphous during heating in vacuum. Transparent tungsten oxide films possess a composition of $WO_{2.9}$. It is postulated that, during the heating, the oxygen deficit is increased by desorption of oxygen in the form of O^+ [214], and an increased negative surface charge of the density of surface state is obtained. An oxidizing annealing of coloured films reduces the surface charge to zero [163]. The change in the absorption coefficient, which is produced by a thermal colouration T_a, is depicted in Fig. 27. The absorption band is centred at approximately 1.2 eV, reaching a maximum absorption coefficient of 1.2×10^4 cm^{-1}.

Thermochromic colouration is also reported at lower temperatures [213]. Colouration occurs simply by annealing of films in vacuum at temperatures $T_a > 80°C$, which exceed the substrate temperature $T_s \sim 30°C$ used during the preparation. Heat treatment at consecutively higher temperatures increases the intensity of the colouration induced in the films. In addition to the colour change, irreversible changes of electrical conductivity and thermoelectric power are observed [205,213]. The tungsten oxide films are annealed in vacuum at temperatures between 80°C and 230°C,

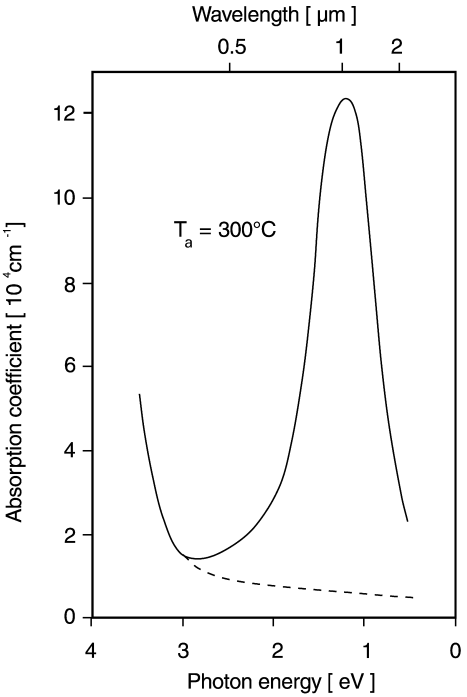

Fig. 27. Change in spectral absorption after annealing at $T_a = 300°C$. From [163].

and oxygen loss from the films occurred during the annealing. This is illustrated in Fig. 28 which shows the variation of the oxygen content detected by a quadrupol mass spectrometer positioned directly beneath the uncoated and coated substrates. The results suggest that annealing of tungsten oxide films in vacuum introduces reduction of the oxygen content of the films.

When such coloured films are annealed in an oxygen environment, a partial bleaching occurrs for the temperature range from 80°C to 230°C. Typically, the colouration decreases by approximately 10%. Total reversibility of thermochromically coloured films to the transparent state is achieved by annealing in an oxygen environment for long periods of time. To obtain the transmission of the transparent state (7%), for example, an annealing of 120°C is necessary for 40 h [213].

The release of oxygen, during annealing in vacuum, suggests that the colouration process, arising in the heat treatment of tungsten oxide films is associated with the oxygen loss. This behaviour can be described by the relation of

$$WO_{3-z} \cdot pH_2O \xrightarrow{Ta} WO_{3-z-r} \cdot pH_2O + \frac{r}{2} O_{2^+}\uparrow, \tag{3.3}$$

with p also probably changing (Section 3.1.6).

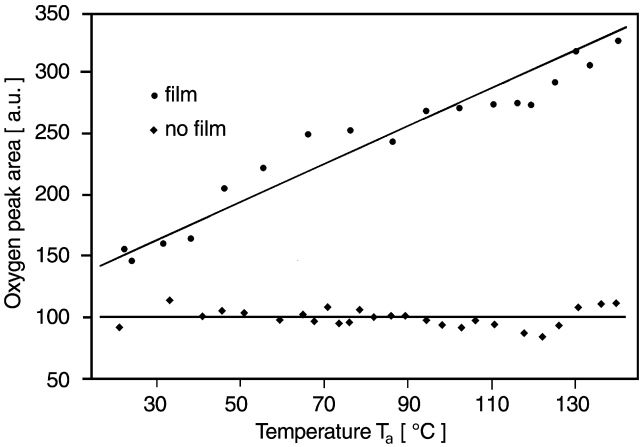

Fig. 28. Oxygen desorption during annealing of a substrate before and after deposition of a tungsten oxide film (heating rate 1 K min^{-1}). From [213].

But also contradictory results are reported for well-characterized films with thicknesses in the 300–800 nm range [115]. Transparent layers are deposited by thermal evaporation of tungsten oxide powder in a vacuum between 10^{-4} and 10^{-5} Pa. In the temperature range from 1000 to 1300°C, for the evaporation material, an indistinguishable O/W ratio is obtained. Higher temperatures ($T > 1300$°C) give virgin blue films. Variation of the substrate temperature T_s between LN_2 and RT does not induce obvious effects, but virgin blue films are obtained for $T_s > 270$°C [115].

The variation of the O/W ratio, measured by RBS versus the annealing temperature T_a under vacuum, is given by the dotted line in Fig. 29. Within the experimental uncertainty of 3%, the O/W ratio does not change even for annealing temperatures in vacuum as high as 550°C [115]. The continuous line gives the variation of the O/W ratio versus the annealing in oxygen-containing atmosphere and shows that O/W ratio increases monotonically from 2.7 to 3 between 30°C and 250°C.

Under annealing in vacuum, the absorption coefficient changes as a function of T_a. The variation of absorption versus the photon energy curves have growth only up to $T_a = 200$°C, then keep approximately the same shape, and the intensity increases up to 350°C. For higher a, the intensity still increases further until 450°C and then decreases, but with a maximum of the absorptance curve centred around 0.7 eV instead of 1.3 eV [115]. This appears more clearly in Fig. 30, where a normalized absorption is depicted in a linear scale. The shift between 1.3 and 0.72 eV occurs abruptly between 350°C and 400°C, i.e. in the temperature range where crystallization takes place (Section 3.1). These results in vacuum suggest that colouration can be induced by temperature without injection of any foreign species in the tungsten oxide layer. But it should be remembered that a substantial mass loss is observed by TGA in that temperature range (Section 3.1.6)

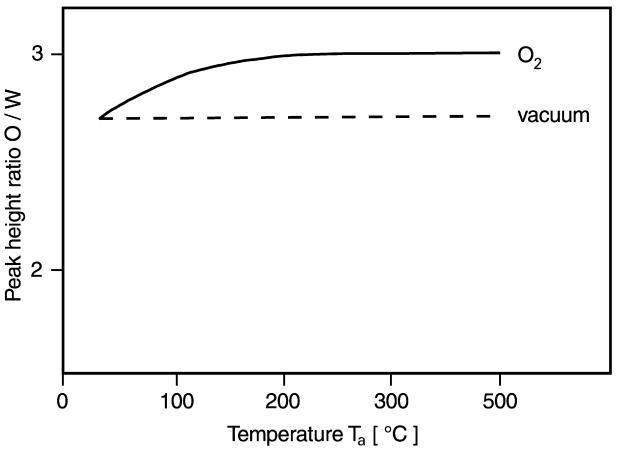

Fig. 29. O/W ratio versus the annealing temperature T_a under vacuum (dotted line) and oxygen atmosphere (continuous line). From [115].

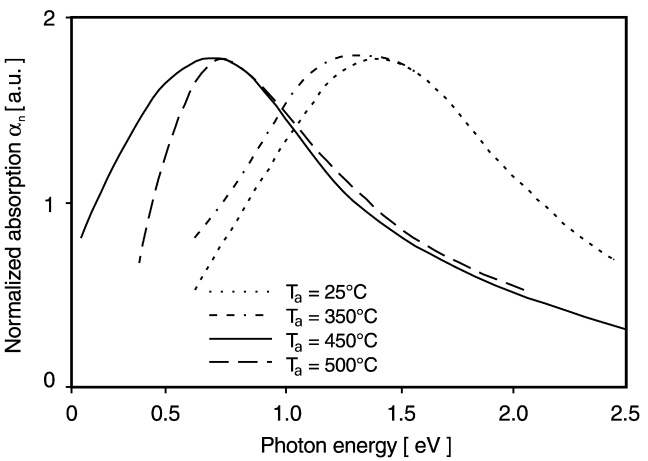

Fig. 30. Normalized absorption curves versus photon energy after annealing under vacuum. From [115].

3.2.2. Colouration by irradiation

Switching from the bleached state to the coloured state can be induced by different types of irradiation. While the interaction of tungsten oxide films with charged particles, i.e. electrons or ions, creates non-reversible colouration, UV illumination allows a reversible switching from bleached to coloured state and vice versa. Some relevant results are summarized in the following for colouration of tungsten oxide films by the three different processes.

3.2.2.1. Photochromism. Various investigations are reported of the colouration of tungsten oxide films by UV illumination [149,167,180,206,213,215–217]. The

obtained fast and short-time changes in the optical absorption are small for tungsten oxide films with thicknesses > 300 nm, compared to the change in optical absorption of the electrochromic process. Usually, light exposure times ranging from hours to days are required in order to observe differences in the transmittance spectrum [167]. To overcome this lack of experimental data dealing with small photochromic colouration changes, in fairly recent time, the attenuated total reflection (ATR) technique has been used which allows the detection of even very small changes in the optical constants of thin film [215–217]. This technique is employed especially to observe the dynamics of the photochromic effect in a scale of seconds.

In the interface between a metal and a dielectric film, the excitation of surface plasma (sp) can take place. Under proper experimental arrangement, there exists at the interface a trapped surface mode which has an electric field normal to the boundary, decaying exponentially into both media, but which, tied to the oscillating surface charge density, propagates along the interface. Because of its confinement to the interface, the surface plasma parameters, such as amplitude, velocity and damping, are sensitive functions of the properties of the boundary between the two media.

The applied ATR technique uses optically excited surface plasmons in a silver film to determine the real and the imaginary part of the dielectric function of the tungsten oxide films. The light of the p-polarized HeNe laser is reflected from the base of the prism coated with the silver film and a thin tungsten oxide layer on top. The angle of incidence Θ of light determines the light wave vector component $k_{\|}$ parallel to the Ag/tungsten oxide interface. Surface plasmons with a frequency of the laser light w will be excited if their wave vector k_{sp} is matched by $k_{\|}$ of the incident light ($k_{\|} = k_{sp}$). In the experimental data, this gives rise to a tip in the reflected light intensity at an angle where the resonance occurs (Θ_R). From the value of Θ_R, information about the real part of the dielectric function is obtained, while the depth of the minimum is most pronounced if radiation damping of the surface plasmons, caused by their decay into photons, equals the internal damping due to dissipation within the layer system. Details concerning the ATR method are given in the work of Sambles et al. [218].

Fig. 31 shows an example of the effect of UV radiation on a 10-nm-thick tungsten oxide layer deposited on a 53-nm-thick silver film by thermal evaporation – before and directly after 5 min. UV illumination with a 150 W xenon high-pressure lamp ($\lambda < 450$ nm). Both, a shift of Θ_R to smaller angle and a simultaneous increase in the minimum of the reflectivity R_{res}, are observed. This corresponds to the changes in the real and the imaginary part of the dielectric function with the colouration, which have been found also in investigations of the electrochromic effect [219].

The dynamics of the bleaching process is depicted in Fig. 32. A typical result is shown of the photochromic behaviour of a 10-nm-thick WO_3 film. During the exposure to UV light in oxygen atmosphere, for 20 s the layer absorption increases rapidly. Immediately after the irradiation is stopped, the absorption decreases strongly and reaches its initial value after about 1000 s. The bleaching behavior is described by a fast and a slow process with two time constants, which does not depend on the light exposure time [216,217]

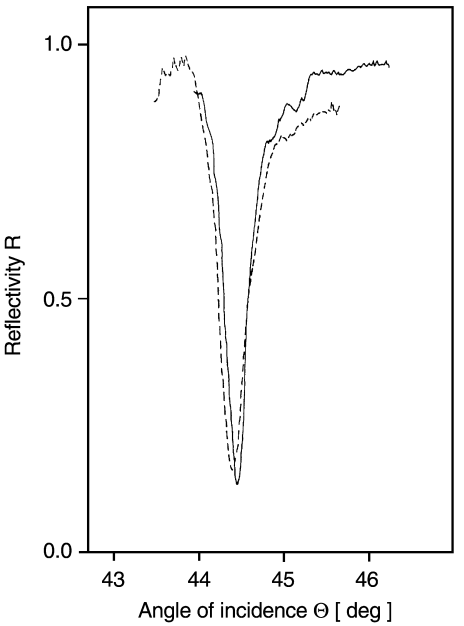

Fig. 31. Reflectivity R versus the angle of incidence Θ for a 10-nm-thick WO_3 film before and directly after (dashed line) UV irradiation. From [217].

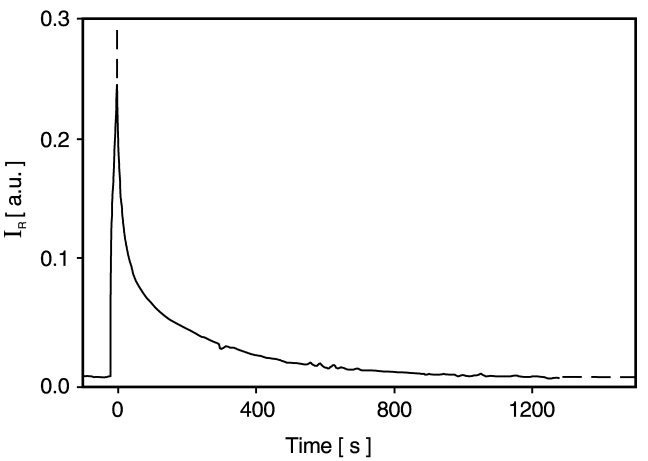

Fig. 32. Reflected light intensity, I_R (which is proportional to the absorption) as a function of time after 20 s UV irradiation in oxygen atmosphere. From [217].

The photochromic behaviour of tungsten oxide is strongly influenced by various film properties, for instance the film density and film thickness, the wavelength of the irradiated light and, also by the surrounding *atmosphere*. It has been found that the photochromic response is increased considerably by the presence of *vapour* containing

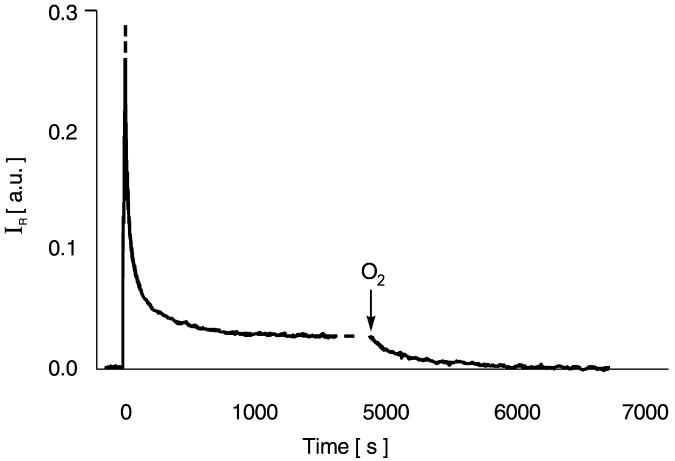

Fig. 33. Dynamics of the reflected light intensity, I_R, during a colouration and bleaching experiment in nitrogen atmosphere. The arrow indicates the change of the gas atmosphere from nitrogen to oxygen. From [217].

hydrogen compounds [220–224]. It is also reported that the bleaching behavior is strongly influenced by oxidizing agents, like ozone or H_2O_2 [149]. Fig. 33 shows a typical result of the photochromic effect in nitrogen atmosphere of 150 Pa, with a light exposure of 20 s. The UV light causes a strong increase in absorption. After exposure, bleaching starts in a qualitatively similar way, as shown in Fig. 32 for oxygen atmosphere. At longer bleaching times, however, a difference is observed: a stable absorption level which is distinctly higher than the value at the beginning of the measurement is obtained. This indicates that the photochromic effect in nitrogen atmosphere is not completely reversible, which is in contrast to the results obtained in oxygen atmosphere. A careful analysis of the experimental data exhibits that the slow and the fast relaxation times are greater by 40% and 3%, respectively, in nitrogen than in oxygen atmosphere [216,219].

The arrow in Fig. 33 indicates an exchange between N_2 and O_2. Obviously, the oxygen atmosphere creates a complete reversibility in the absorption behavior. This behavior suggests that there are at least two different decay channels for the colouration in tungsten oxide. Only one of them is affected by the ambient atmosphere, whereas the other one is independent of it [216,217]. A more detailed analysis of the data depicted in Figs. 32 and 33 shows that, for the same irradiation time, the efficiency of the photochromic colouration in nitrogen is slightly enhanced compared to that in oxygen. This suggests that the creation and decay of colour occur simultaneously during light exposure. The later effect is partially surpressed in the case of the nitrogen atmosphere, and the net colouration is larger [216].

The influence of oxygen on the bleaching process of UV-coloured films is also confirmed by experiments in vacuum [213]. The colouration is stable with respect to the time over which the films were retained in vacuum. However, upon exposure to

dry oxygen under atmospheric pressure the colouration begins to decrease immediately. The UV-induced colouration process and also the instability in oxygen ambients may be described as [213].

$$WO_{3-z} \cdot pH_2O \overset{h\nu}{\leftrightarrow} H_{2p}WO_{3-z} + \frac{p}{2}O_2\uparrow \tag{3.4}$$

This relation also includes the reaction of UV photodissociation of water adsorbed into the amorphous films [213].

The influence of various vapours of hydrogen compounds on the photochromism is investigated in larger detail [220,223,224]. Fig. 34 illustrates the dependence of the photochromic properties of tungsten oxide films on the composition of the surrounding atmosphere during the illumination. The UV-induced changes in the optical density at a wavelength of $\lambda = 1$ μm versus the illumination time is depicted for a film with a thickness of 1.8 μm. While under "normal condition" only a slow increase in the optical density is obtained, irradiation in a vapour of hydrogen compounds leads to a sharp increase in the photochromic sensitivity.

The effect of different alcohol vapours on the photochromism of tungsten oxide films is also discussed. In general, the photochromism is enhanced in the presence of alcohols at the surface, and the mechanism of the enhancement is interpreted by analogy with the mechanism of current-doubling effect [223]. But the value of the obtained changes in the absorption strongly depends on the type of alcohol used: it

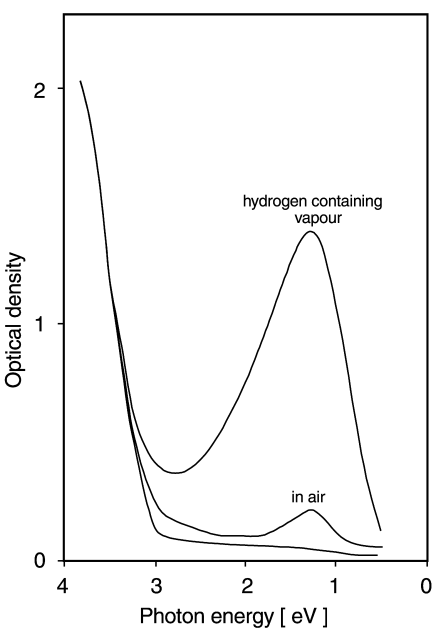

Fig. 34. Change in optical density with the illumination time ($\lambda = 1.0$ μm) under normal conditions and in the presence of hydrogen compounds. From [220].

decreases in accordance with the following order: methanol, ethanol, 2-propanol, 2-methyl-2-propanol, and the colouration saturates at concentrations greater than 1 vol%. The nonlinear relation between the alcohol concentration and the changes in optical absorption is interpreted by considering the adsorption of alcohol onto the surface of the tungsten oxide films, and the experimental results can be explained by using Langmuir's adsorption isotherms [223]. But also the number of adsorbed molecules necessary for monolayer coverage (which is determined by their size) have to be considered to explain the saturation adsorption for different alcohols. The changes in the absorptance, even when no alcohol is present, is related to the inevitable presence of water in the film. A different response for alcohol vapours on the photochromism is noted for MoO_3 films [224].

The photo-induced changes in the optical properties of tungsten oxide films have been studied also for films in contact with *liquids*. A cell of the form of quartz glass/semitransparent Au/ethanol/WO_3/ito-coated glass is illuminated with near-UV light through the quartz window, under open-circuit and short-circuit conditions [225]. The changes in the optical transmittance with the time, under continuous illumination, is depicted in Fig. 35. The film thickness and the intensity of the incident light are shown also. In both cases, open and short circuit, the illuminated part of the film shows a blue colouration. Correspondingly, the transmitted light intensity significantly decreases with time and tends to reach a constant value. The stored colouration was retained for several days.

A qualitative explanation of the effect at the tungsten oxide/ethanol interface is provided as follows. In contact with the ethanol, a space-charge region is produced in the film surface of the n-type semiconductor. The UV light photo-generates electrons and holes, which are separated in the space-charge layer in the film by a built-in field. They drift towards the bulk and surface, respectively. The holes interact with the

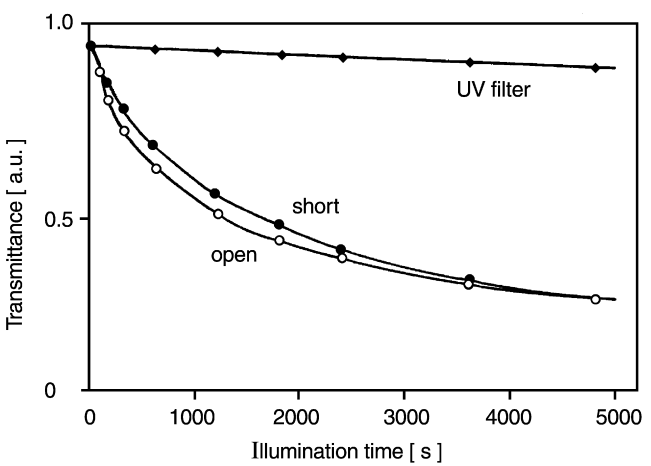

Fig. 35. Change in transmittance of a cell containing liquid C_2H_2OH (see text). From [225].

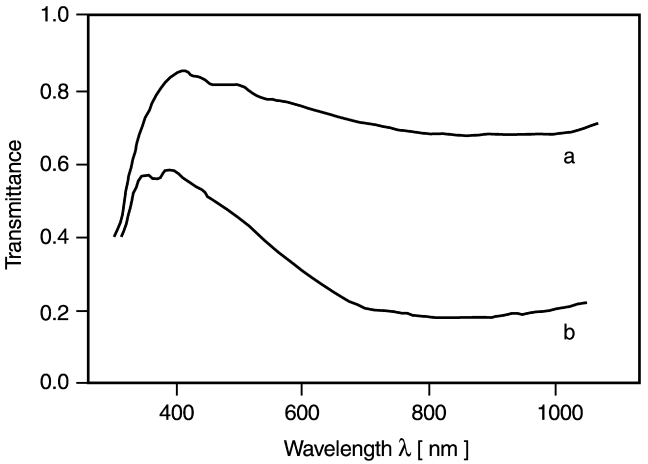

Fig. 36. Spectral transmittance of tungsten oxide film before (a) and after (b) UV illumination in contact with formic acid solution ($d = 800$ nm). From [226].

ethanol molecules at the surface, and charge compensating particles are formed, which may be diffuse in and out of the film [225].

Tungsten oxide films with thicknesses ranging from 500 to 800 nm are investigated also in a quartz basin filled with a solution of 24.3 M formic acid or 1 M dehydrated lithium perchlorid in propylene carbonate $LiClO_4 + C_4H_6O_3$ [226]. As shown in Fig. 36, a saturation value of the optical density is reached within an illumination time of 90 min., and the transmittance value is decreased to a value as low as 20%. A considerable difference is observed for the decolouration rate when the illuminated films are left in air. The films coloured in formic acid were bleached in 24 h, whereas, after 29 days, a blue colour is still observed in the other liquid.

Beside the atmosphere, other quantities influence the colouration process. Fig. 37 exhibits the *wavelength dependence* of the colouration rate of a 340 nm-thick WO_3 film. The samples are irradiated with monochromatic UV light for several seconds, and the resulting increase of the absorption is recorded as a function of time [216,217]. For wavelengths down to 380 nm, no photochromic colouration could be detected; however, there is a strong increase in the colouration rate towards shorter wavelengths. The onset of the photochromic effect is in good agreement with the bandgap energy E_g of 3.25 eV (as indicated by the arrow in Fig. 37) of thermally evaporated tungsten oxide films [149]. This implies that in the wavelength range where electron–hole pairs are created in the tungsten oxide films colour is also formed. Both processes are apparently closely connected to each other, as shown by the following comparison: The creation rate of electron–hole pairs by photons depends strongly on the incident photon wavelength. At energies near the band edge, the relation (3.1) is a good approximation, when instead of the absorption coefficient a the creation rate of electron–hole pairs η is written. A plot in analogy of Fig. 36

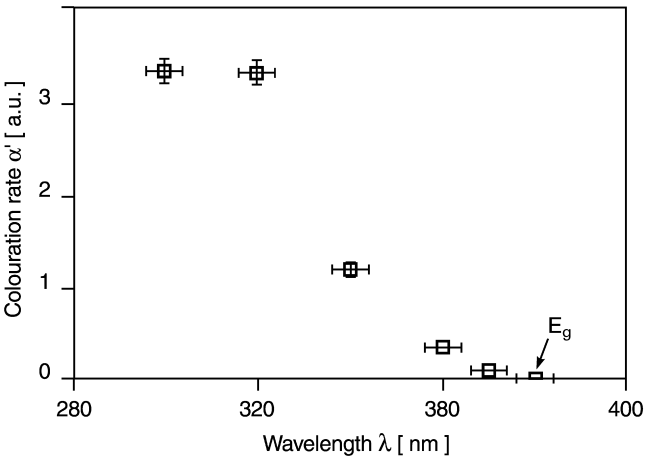

Fig. 37. Wavelength dependence of the colouration rate α' of a 340 nm-thick WO_3 film. From [217].

shows that the optical absorption rate follows the same functional dependence on $(h\omega - E_g)^n$ as the electron-hole pair generation rate. This result strongly suggests that the photochromic colouration proceeds via the generation of charge carrier [216,217].

This explanation is supported also by the transmittance behaviour in the UV-filtered light illumination case (cut-off wavelength of the filter is 420 nm) shown in Fig. 35 for films in contact with a liquid. No significant optical effects are obtained from the VIS illumination. It is evident that the near-UV component with energy above the bandgap causes the optical effect. This is a reasonable result, since tungsten oxide films can be described as a semiconductor with a bandgap of about 3.2 eV (Section 3.1.3) [225].

The photochromic colouration of tungsten oxide films exhibits a different time scale for thick and very thin films. Evaporated tungsten oxide films have been studied in the 400–700 nm thickness range [167]. A typical optical absorption spectrum of a tungsten oxide film before and after UV irradiation for 164 h is shown in Fig. 38. A broad absorption band having a maximum at 900–1000 nm is clearly observed, which exhibits almost the same optical profile as those coloured by other techniques. The subtraction of the absorptance at 900 nm of as-deposited films from the photochromic coloured films is shown in Fig. 39 as a function of exposure time. The influence of the substrate temperature is also depicted. What is recognized is that after an irradiation of approximately 200 d a saturation of absorptance is observed for all different films. Only a weak influence of post-annealing treatment is reported [167]

The colouration and colour capacity of tungsten oxide films with thicknesses between 300 and 1000 nm depends strongly on the composition of the films produced by various deposition conditions. Especially the *hydrogen* and *oxygen contents* in the film possess a strong influence on the photochromic properties under UV

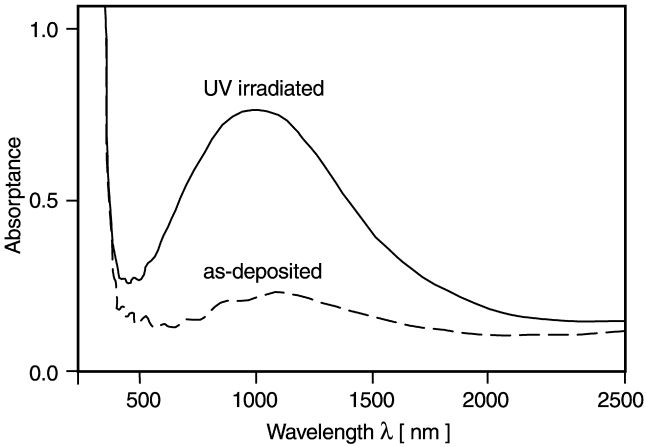

Fig. 38. Absorptance before and after 164 h UV irradiation. From [167].

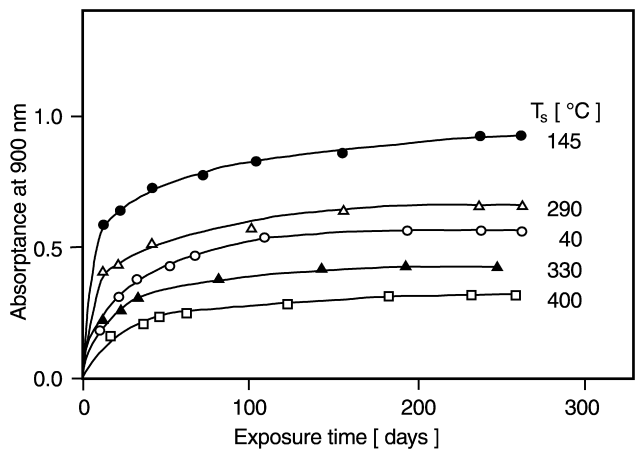

Fig. 39. Absorptance ($\lambda = 900$ nm) of film irradiation with 366 nm light as a function of exposure time. The influence of the substrate temperature, T_s, used during the deposition, is also depicted. From [167].

illumination. Gerard et al. [206] distinguish five ranges for the H_xWO_y films deposited by evaporation and rf sputtering.

1. In the region of high oxygen deficiency ($y < 2.5$ when $x = 0$, increasing to $y = 2.8$ when $x = 1.5$), the films have a metallic aspect and do not change their properties after UV irradiation.
2. The virgin films are deep blue ($y \sim 2.5$ for $x = 0$ increases to $y \sim 2.8$ when $x = 1.5$) and do not change their properties under UV illumination.
3. In this range, as-deposited films are transparent and highly resistive ($y > 2.65$ for $x > 0.2$, $y \sim 2.8$ up to $x = 1.5$). UV illumination induces a strong blue colour and

also changes the electrical conductivity. The depth of the colouration obtained after identical illumination depends on the composition. Higher values of x correspond to higher efficiency for UV colouration. For $x \sim 0.2$, the UV efficiency is very poor. Films prepared by evaporation generally fall in this range.

4. The virgin films are transparent and highly resistive, but UV illumination does not change the colouration. Only the conductivity exhibits some influence ($y \sim 2.55$–2.65 for $x = 0$, up to $y \sim 2.9$–2.98 for $x \sim 1$).
5. The films are highly transparent and resistive and remain unchanged under UV irradiation ($y \sim 2.65$ for $x = 0$ to $y \sim 3$ for $x = 1$).

It is described further that the hydrogen and the oxygen contents are not independent quantities [3.91]. Additionally, it is suggested that especially films prepared by evaporation exhibit a high colouration efficiency by UV radiation. But not only the stoichiometry influences the photochromic effect, it is also the film density that exhibits a certain effect on the photochromic properties. Higher densities showed lower saturated photochromic colouration [167]. Since the density of the film is a direct measure of porosity, i.e. the packing density of the tungsten oxide clusters, an increasing density (Section 3.1.4) decreases the number of adsorption sites of water at the internal surfaces. In other words, a denser tungsten oxide film can keep a smaller amount of adsorbed species available for the UV photodissociation which might decrease the photochromic colouration.

3.2.2.2. Colouration by ion beam. The effect of nonreversible colouration by ion-beam irradiation on amorphous tungsten oxide films is studied for various types of ions (^{1}H, ^{2}He, ^{15}N, ^{16}O, ^{23}Na, ^{40}Ar, ^{70}Ga) with different energies [172,227–236]. Thermionic Na^+ ions with an accelerating voltage of 4–12 keV are used for detailed investigations [227]. At ion doses beyond a certain threshold value D_0 ($D_0 \sim 5 \times 10^{-4}$ C cm^{-2} at 5 keV), the behaviour of the optical absorption spectra and the ion-induced secondary electron emission yield of the irradiated film suggests the formation of sodium tungsten bronze by ion implantation. The threshold value, which is almost independent of the film thickness, decreases gradually with increasing accelerating voltage. Irradiated films exhibit near D_0, an insulator–metal transition, and the blue-coloured tungsten oxide is insoluble in alkaline solution, which is caused by the change in chemical potential at the transition as threshold dose [227].

Fig. 40 exhibits the optical absorption spectra of a tungsten oxide film before and after ion irradiation. After irradiation with a sufficient dose (2×10^{-3} C cm^{-2}) beyond D_0, the film shows the blue colouration and the characteristic absorption becomes apparent. This broad spectrum is very similar to that obtained from the colouration by other processes [227].

Irradiation effects are also obtained by hydrogen bombardment. So, for instance, the use of tungsten oxide layers is reported to record the position for H_2^+ beams in the energy range of 5–15 keV. The ion beam irradiation produces colour centers within the material. An ion dose of 2×10^{16} ions cm^{-2} is noted to produce easily detected colouration [228].

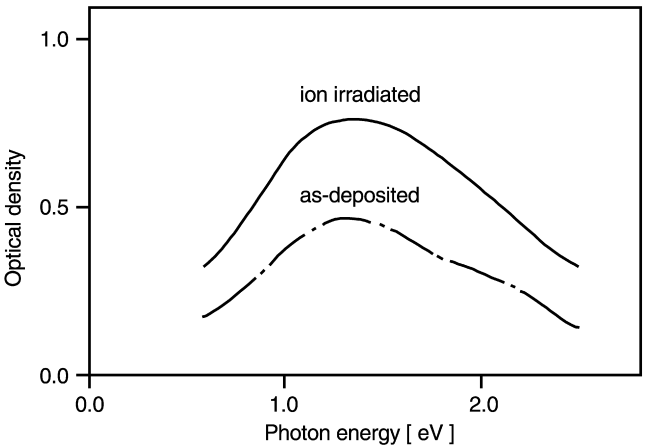

Fig. 40. Optical absoprtion spectra of a WO_3 film before and after ion irradiation From [227].

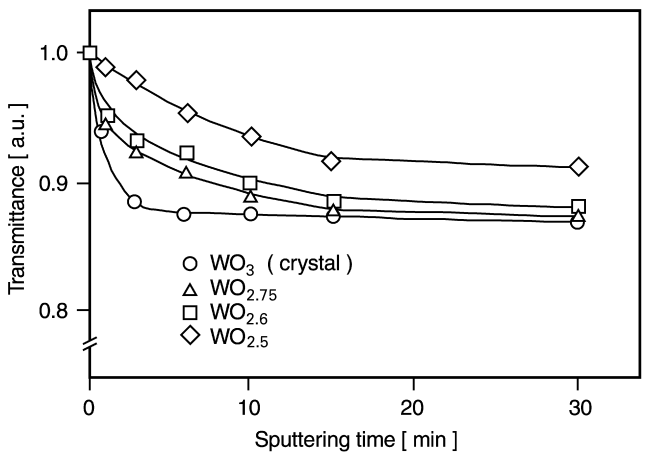

Fig. 41. Variation of transmittance with Ar exposure time. From [229].

Colouration is also induced by the irradiation of Ar ions within an energy of 2 keV [229]. A variation in the transmittance with sputtering time is observed which is depicted in Fig. 41. A simultaneous AES analysis exhibits changes in the peak height ratio (O/W) with argon sputtering time. It is concluded that the light absorption of the films increases with oxygen deficiency. This is supported by the fact that the oxygen-deficient substoichiometric films show a bluish colour. The results indicate that oxygen atoms are removed at a ratio of about twice the amount of that of tungsten atoms from the surface [229].

Also high-energy ion beam irradiation has been reported to be an excellent means for modifying tungsten oxide films [172,230]. Our amorphous "standard" tungsten

oxide films with low density are deposited on different substrates and have been irradiated with various types of ions (^{1}H, ^{4}He, ^{15}N, ^{40}Ar) of different energies, up to 30 MeV and with fluxes of up to 10^{18} cm^{-2} [172]. Compaction of the films up to nearly the bulk density is observed. No changes of the stoichiometry are detectable. Raman measurements show that ion-beam-modified films are also "amorphous", but possess another nanostructure than the as-deposited material. The irradiated films have a higher refractive index than the as-deposited ones but show the typical blue colour. The low threshold found for the compaction effect (few time 10^{12} ions cm^{-2}) leading to the conclusion that one beam ion displaces more than 10^{5} tungsten molecules [172].

A series of experiments is also done on tungsten oxide films with thicknesses between 100 and 10 000 nm, which use the films to monitor and to adjust the beam position and to study ion-beam profiles in charged-particle accelerators. The following ions have been applied: H^{+} from a few keV to 6.3 MeV, He^{2+} from a few keV to 24 MeV, O^{2-} from a few keV to 5.8 MeV, and Ar^{+} from a few keV to 10 MeV [230]. A minimum dose detectable by the eye on the basis of the colouring of the film is found at about 10^{13} ions cm^{-2}. But this minimum is affected by several factors, like ion energy, mass, and charge, irradiation intensity, etc. When the dose is varied from 10^{13} to 10^{15} ions cm^{-2}, no saturation is observed in the colouring of the tungsten oxide films. It is argued that, therefore, in that range the material is useful to monitor ion beams. Further, it is suggested that the oxygen vacancy is a primary defect reduced in the transition metal oxide by ion bombardment [230]. This vacancy is due to the extremely high mobility of oxygen ions. In other words, the ion beam reduces the oxide and produces an absorption band in the visible region, which is manifested by colouring of the film.

3.2.2.3. Colouration by electron beam. The reaction of electron beams with surfaces of inorganic materials is a complex process which depends on many experimental parameters. Under that aspect, tungsten oxide films have been exposed by electrons in a wide range of energy, to investigate the lithographic properties of amorphous films [231], the outgassing characteristics of coatings [232], the electron-stimulated desorption of oxygen [214,229,233], or the changes during electron microscope observation [233,234]. But only a few investigations are made which describe the colouration during the electron beam bombardment.

The blue colouration obtained by electron beam irradiation is studied for tungsten oxide layers with thicknesses between 200 and 1000 nm [235]. The electron current density is about 5 $\mu A\ cm^{-2}$, and electron energies of 3, 6, 10 keV are used. Fig. 42 shows the optical absorption spectra before and after electron beam irradiation. The coloured tungsten oxide films also become insoluble in 0.04 N NaOH solution, and the exposure characteristics show that threshold doses required for this effect increase with increasing incident electron energy and film thickness [235].

The blue colouration simultaneously obtained by electron-beam irradiation of the amorphous tungsten oxide films is not directly responsible for the drastic change in solubility in alkali solutions. While the colouration is explained by the formation of hydrogen bronze, H_xWO_3, their changes in regard to solubility may be produced from

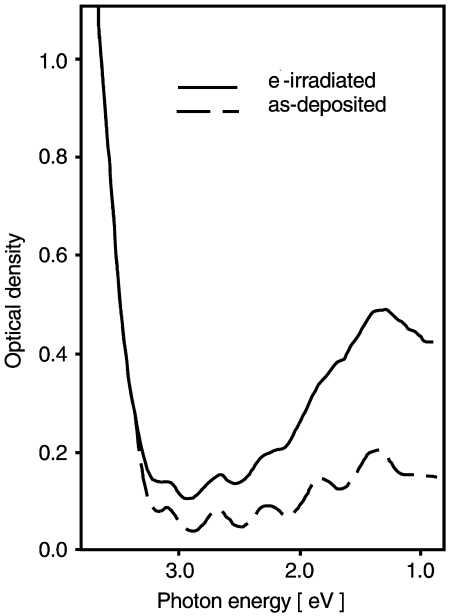

Fig. 42. Optical absorption of tungsten oxide films before and after electron exposure. From [235].

structural changes likely to decrease the degree of the lattice disorder in "amorphous" films [235]. Additionally, it is suggested that an irradiation-enhanced out-diffusion of oxygen would result in a visible darkening and in a change of the solubility in alkaline solution [236].

The colouration of tungsten oxide films induced by low electron energy (1.9 keV) has been investigated, using an AES electron gun at a current of 50 μA and a 0.1 mm beam diameter [229]. The films turned to a bluish colour and show the so-called "cathodechromism". The variation of O/W ratio is measured with the electron beam irradiating time. The results, indicated in Fig. 43, also show a decreasing tendency of oxygen atoms, i.e. the energetic electron beams not only excite the electron to the excitation level in the tungsten oxide film for the Auger process, but also increase the oxygen vacancy. It is suggested that the colouration is induced with the extraction of oxygen, rather similar to the coloured state of substoichiometric oxygen-deficient WO_{3-z} ($z > 0$) films [229].

The influence of the bombardment of electrons with energies of 3, 7 or 25 keV on the electrochromic behaviour of tungsten oxide films will be described in the next section [237].

3.2.3. Electrochromic colouration

Electrochromic reactions for tungsten oxide films are obtained in very different surroundings. Best characterized and most investigated so far are tungsten oxide films in contact with liquid electrolytes. Some experimental data of such type of studies are

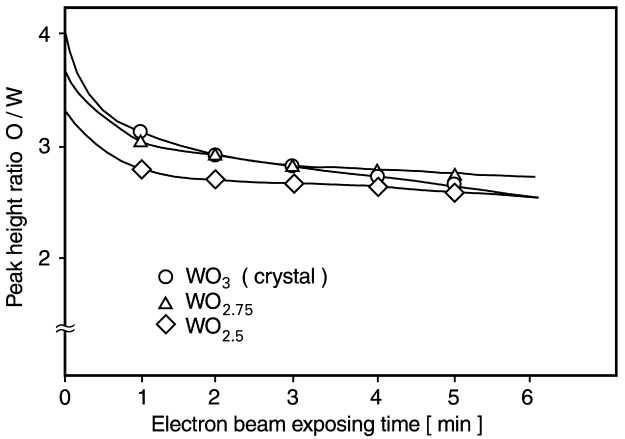

Fig. 43. Change of the AES peak height ratio O/W with electron beam irradiating time. From [229].

summarized in Section 3.2.3.1. In general, results are described from aqueous, i.e. protic electrolytes. A different situation is given by the electrochromism evoked by gases. A controlled gas atmosphere is necessary which contains hydrogen for colouration or oxygen for bleaching. Some results are reported in Section 3.2.3.2 for this type of electrochromism. For electrocolouration, the surrounding atmosphere also has a certain influence on the colouration, but additionally high electrical fields parallel to the film plane have to be applied. This technique, which is fairly old, was first reported by Deb [149] and is described in Section 3.2.3.3. From a technological point of view, colouration of tungsten oxide in the presence of solid-state electrolyte is most important, as mentioned in Section 2.4. The properties of some solid-state electrolytes and the interaction with the electrochromic layer are given in Section 3.2.3.4.

3.2.3.1. Electrochemical colouration. Most of the fundamental research on electrochromic tungsten oxide films is realized in liquid electrolyte experiments. A three-electrode configuration is used usually to obtain controlled, defined potential conditions at the electrochromic substances. In such three-electrode arrangements, the potential difference between the non-polarizable reference electrode and the working electrode (electrochromic film) is measured, and the counterelectrode is connected to the working electrode via a polarizing circuit, through which a controllable current is made to pass and produce alterations of the potential at the working electrode.

In cyclic voltammetry, a voltage between the tungsten oxide film and the counterelectrode is swept forth and back between two extreme values, and the electrical currents associated with the intercalation/deintercalation of the charged species are measured. The technique can be used qualitatively to give a "fingerprint" for the electrochemical processes, to trace reversible and irreversible effects, and to ascertain voltage levels that yield stable operation, as well as quantitatively to measure charge densities involved in the ion exchange processes.

To obtain a satisfactory cycle stability, acid solution is applied for the investigations. For the reported results on the "standard" films in Figs. 44–48, 2 M HCl is used and a Ag/AgCl electrode is the reference electrode; the samples consist of glass/ITO/tungsten oxide (working electrode), and platinum sheet is taken as counter electrode [238]. Data obtained with different experimental conditions are marked.

Fig. 44 represents a typical data set to characterize the electrochromism of a film. The shown results are obtained with films with a thickness of 200 nm and having a sweep rate of 50 mV s^{-1}. The response of the *transmittance T* and *current i* to the potential *U* on the working electrode can be recognized. Data are shown during colouration (C) and bleaching (B) process. Increasing the cathodic potential generates an increasing current and a decreasing transmittance. The shown transmittance data are recorded at a wavelength of $\lambda = 543$ nm.

Such types of measurements are extensively reported [150,185,239–249]. Various experimental conditions have to be considered for comparing data of different references. So, for example, an increase in the active area of the investigated sample or in the sweep rate increases the measured current. Usually, acid electrolytes (H_2SO_4, HCl) are used. Difference in the concentration of the used electrolyte produces a shift in the potential scale, because the "Fermi" level of the electrolyte is influenced via the Nernst equation [238]. To obtain the same change in optical density OD, it is therefore necessary to apply a more negative potential in experiments with lower

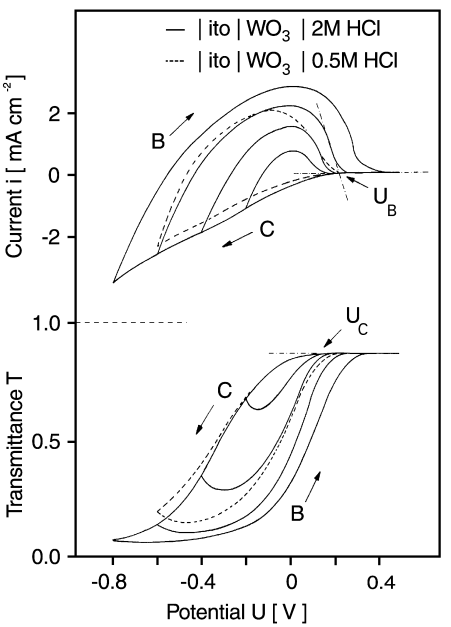

Fig. 44. Current, *i*, and transmittance, *T*, as a function of the applied potential during the electrochromic colouration (C) and bleaching (B) of tungsten oxide in 2 M HCl.

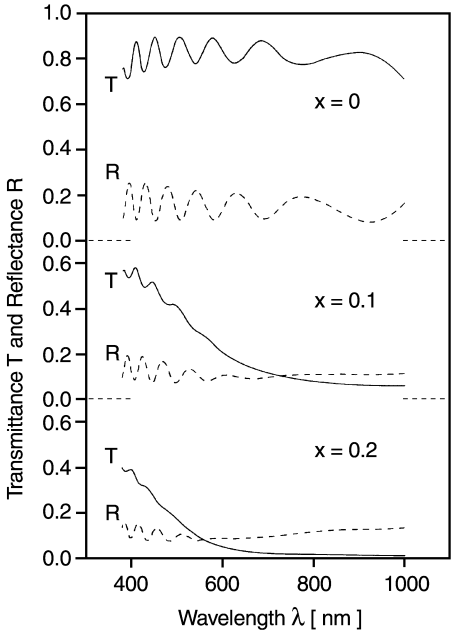

Fig. 45. Spectral transmittance of tungsten oxide film ($d = 755$ nm) on ITO-coated glass for an as-deposited film ($x = 0$) and in two different colouration states ($x = 0.1$ and 0.2).

H concentration, i.e. for a given colouration voltage, a smaller amount of charge is injected in the case of lower electrolyte concentration.

Our "standard" films exhibit a strong light absorption, not only in the visible region, but also in the near infrared range. This can be concluded from transmittance and reflectance measurements shown in Fig. 45. The depicted data represent the transmittance in the wavelength range between 400 and 1000 nm, for films in three different colouration states indicated by the x-values ($x = e^-/W$). They are measured on films with a thickness of 755 nm. While as-deposited films ($x = 0$) possess high transmittance in the whole wavelength region, small amounts of injected charge ($x > 0$) decrease the transmittance in the VIS range, but particularly in the NIR. This spectral dependence creates the typical blue colour of tungsten bronzes. Absorptance increases with increasing wavelengths and x-values. The interference structure in Fig. 45 is caused by a superposition of the interference produced by the ITO and tungsten oxide layers on glass.

From the measured transmittance and reflectance of the two layer system (glass/ITO/tungsten oxide), the *refractive index n* and the *extinction coefficient k* can be calculated under the assumption that the layers are homogeneous and that the refractive index n and extinction coefficient k do not possess discontinuities in the investigated wavelength range [162]. The determined spectral dependence of n and k is depicted in Fig. 46. A continuous variation in n is obtained with increasing injected charge, with a minimum at $\lambda \sim 550$ nm. The extinction coefficient exhibits

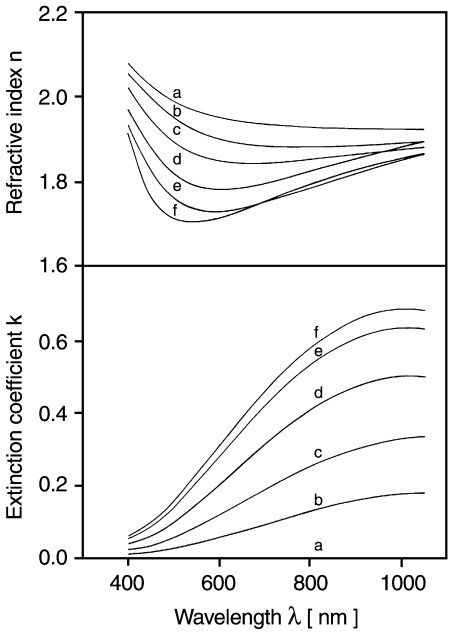

Fig. 46. Spectral refractive index n and extinction coefficient k for tungsten oxide films as a function of injected charge for $x = 0$ (a), $x = 0.058$ (b), $x = 0.1$ (c), $x = 0.19$ (d), $x = 0.29$ (e) and $x = 0.38$ (f).

a different spectral behaviour. While for $x = 0$ the tungsten oxide layer shows very small absorption, k increases strongly with injected charge. A maximum is observed at approximately 950 nm. Similar results are reported for the spectral absorption coefficient, when charge densities δQ between 190 and 1800 C cm^{-3} are inserted in a tungsten oxide film from H_2SO_4 electrolyte [250]. An absorption band centred at ~ 1.3 eV increases monotonically upon increased δQ and reaches a maximum absorption coefficient of $\sim 10^5$ cm^{-1}. Comparable data have been obtained for the intercalation of H^+, Li^+ and Na^+ in many investigations [250,251].

To enlighten the absorption behaviour as a function of the injected charge, the data from Fig. 45 are depicted in a different representation in Fig. 46. It is obvious that the extinction coefficient exhibits a saturation. A linear dependence exists between k and x for $x < 0.2$, and for $x > 0.3$ the absorption saturates (Fig. 47).

By correlation of electrical and optical data, another important parameter to describe electrochromism can be determined. This quantity, the *colouration efficiency* *CE* (Eq. (2.2)), is a useful number to discriminate between different electrochromic materials. Typically, colouration efficiency is given only for one wavelength, because most of the optical data are recorded by a laser. Since interference effects cannot be simply eliminated with such experimental equipment, the change in the optical density necessary to determine the colouration efficiency may contain a certain error. To overcome that problem, the colouration efficiency can be calculated as a function of the wavelength from the measured spectral data. The result is shown in Fig. 48.

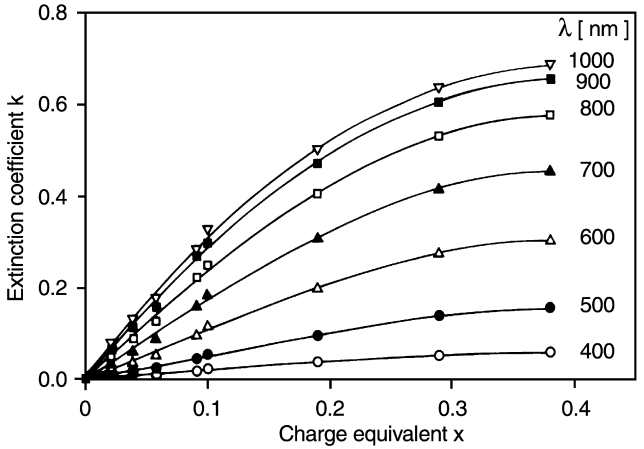

Fig. 47. Extinction coefficient k of tungsten oxide films in different colouration state, as a function of injected charge for several wavelengths.

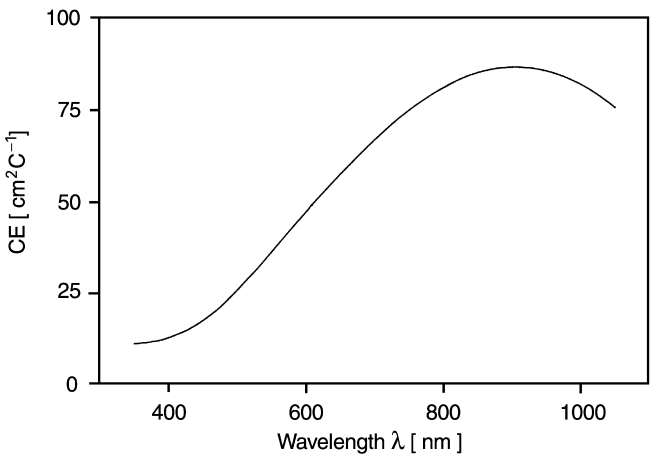

Fig. 48. Spectral colouration efficiency (CE) of tungsten oxide.

A maximum appears at about 900 nm. In the visible range ($\lambda = 550$ nm), our standard film possess a CE $= 37 \pm 2$ cm^2 C^{-1}.

A fairly similar spectral colouration efficiency CE (λ) is reported for amorphous tungsten oxide films deposited by evaporation [252]. It is postulated that the colouration is obtained in electrochemical environment by H^+ insertion. The amorphous films have CEs peaked at ~ 1.3 eV, and CE is ~ 40 cm^2 C^{-1} at 550 nm. Crystalline films annealed at $T_a = 400°C$ have lower CEs in the luminous range and higher CEs in the infrared; the peak lies at about 0.7 eV and the CE depends on the deposition conditions [252]. For example, high CEs have been given for the infrared in films

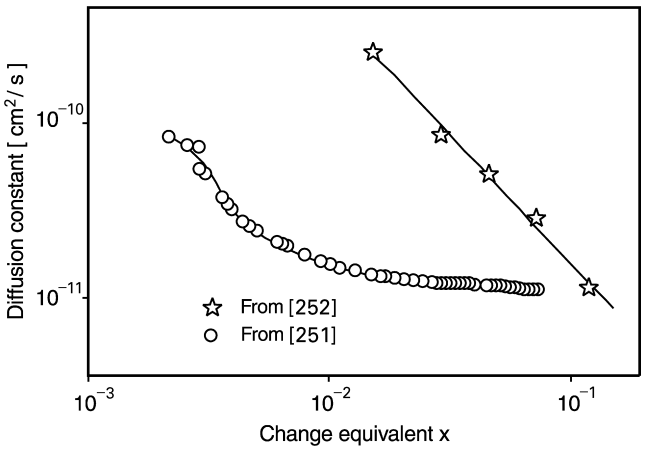

Fig. 49. Chemical diffusion constants D versus the amount of injected charge. From [253,254].

made by sputtering under carefully selected conditions [252]. But also some anodized films have been reported to exhibit a remarkable CE $\sim 260\ \mathrm{cm^2\ C^{-1}}$ at 633 nm [185].

Many other convenient and established techniques are employed for electrochemical characterization of electrochromic tungsten oxide. They are often an immediate link to potantial device performance. *Diffusion constants D* (Fig. 49) for various charged species can be derived from several different electrochemical techniques for films made by evaporation [253,254], and D's have been evaluated in many works. It is seen that D seems to vary with the colouration level, but the results depend also on the used electrolyte and on the blocking of the diffusion path. Additionally, D is influenced by many deposition parameters and is increased at elevated temperature and for films with enhanced porosity, i.e. low density [255].

Diffusion constants are obtained from impedance measurements on 1 μm thick tungsten oxide films coloured in 0.1 M H_2SO_4 [254]. The results are based on the assumption that all the charge going through a cell consisting of In_2O_3/H_xWO_3/electrolyte/H_xWO_3/In_2O_3 is consumed for proton injection into the electrochromic electrode. The diffusion coefficient for protons in tungsten oxide films is determined from the Warburg constant W_F, which is the constant of diffusion impedance of the carriers. The Warburg constant W_F is related to D as

$$W_F = R_g T_e (F^2 c (2D)^{1/2})^{-1}, \tag{3.5}$$

where R_g is the gas constant, T_e the temperature (K), F is the Faraday constant and c the concentration of the ions. A decrease in the diffusion coefficient with the injected charge is obtained. This is explained in terms of a two-step colouring mechanism. At the initial stage of colouring ($x = 0.01$–0.02), large values $\mathrm{D} > 10^{-10}\ \mathrm{cm^2\ s^{-1}}$ are analysed which are described as a fast step, while at $x > 0.04$ typical values for $D < 5 \times 10^{-11}\ \mathrm{cm^2\ s^{-1}}$ for the slow step are obtained. It is mentioned that these are typical values for tungsten oxide films with a density of $5.5\ \mathrm{g\ cm^{-3}}$ [254].

Diffusion coefficients in tungsten oxide films are measured also by using a chronoamperometric technique. Tungsten oxide films are deposited on ITO-coated glasses with thicknesses in the range of 570–1030 nm [256]. For the electrochemical measurements, a 1.8 M H_2SO_4 electrolyte is used. From polarograms, obtained by using anodic single-sweep voltammetry with sweep rates in the range of 5–50 mV s^{-1}, the diffusion coefficient is analysed by

$$\ln i(t) = -\frac{\pi^2 Dt}{2d^2} + \text{const}, \tag{3.6}$$

where d is the film thickness. From the obtained results, for the diffusion coefficient from films of different thicknesses and different degrees of colouration, it is concluded that an average value D exists, which is nearly independent of the colouration state of the film. For amorphous tungsten oxide films, a value is given by $D = 5.5 \times 10^{-10}$ cm^2 s^{-1}. Additionally, it is found that $D = 2.1 \times 10^{-11}$ cm^2 s^{-1}, after the films are stored in air for a period of about 12 months [256].

An estimate of the diffusion coefficient for species, which governs the current in the diffusion-controlled region, can be obtained by assuming a negligible contribution of migration and noting at what time the current begins to deviate from $t^{-1/2}$ behaviour [257]. This occurs roughly when the diffusing species reaches the solid wall side of the film and is approximately given by a time, τ, of 0.3 d^2/D, where d is the thickness of the film and D is the diffusion coefficient. On the basis of current versus time data, a diffusion coefficient of $D = 1 \times 10^{-9}$ cm^2 s^{-1} is obtained from this estimation [257]. The time required to complete colouration of the film is about 10τ. For films prepared by anodic oxidation of tungsten, values of $D = 3 \times 10^{-7}$ cm^2 s^{-1} are reported.

Comparable results are obtained from a digital simulation model for electrochromic processes at tungsten oxide electrodes [258]. Current-potential curves of the electrochromic processes at the tungsten oxide films are calculated with that model, which assigns the rate of charge transfer in the oxide/solution interface and the rate of diffusion of hydrogen in the bulk of the film as major variables. For evaporated films, best fits are obtained for $D = 1 \times 10^{-9}$ to 2×10^{-10} cm^2 s^{-1} [258].

The diffusion parallel to the layer surface is measured by detecting the spread out of the optical absorption of tungsten oxide layers of 500 nm thickness on ITO-coated glass [253]. Tungsten oxide layers are partially covered by an insulating film which prevents the colouration. Such structures are immersed in 0.01 N H_2SO_4 solution, and the unprotected part of the tungsten oxide layer is coloured under potentiostatic conditions. The boundary line between the coloured and the virgin part of the layer is approximated by a step function, and the spread out of the optical absorption is detected with the time. The data are evaluated by Boltzmann's method which could account for an eventual concentration dependence of the diffusion coefficient. Highest D values are observed for $x = 5 \times 10^{-3}$, $D = 8 \times 10^{-11}$ cm^2 s^{-1}, which decrease to $D = 1 \times 10^{-11}$ cm^2 s^{-1} for $x = 3 \times 10^{-2}$. This behaviour is quantitatively explained by the assumption of a fast and a slow channel [253].

For microcrystalline or amorphous films, the diffusion constants normally lie within the brackets $10^{-10} < 2.5 \times 10^{-7}$ cm^2 s^{-1}. Crystalline tungsten oxide films have

lower D's. Also experiments using Li or Na-containing electrolytes exhibit lower diffusion constants. But it should be mentioned again that the reported D values strongly depend on various other quantities. So, diffusion coefficients are given in the range of 1.5×10^{-9}–3×10^{-12} cm^2 s^{-1} for approximately 500-nm-thick tungsten oxide films deposited by evaporation with densities between 3.38–5.84 g cm^{-3} [255]. Additionally, a strong dependence of D on the water content in the electrolyte solution, which is prepared from propylenecarbonate and $LiClO_4$, is described. For comparison, the diffusion constants of electrons in this material are $\sim 2.5\times10^{-3}$ cm^2 s^{-1}, i.e. much larger than D [259].

Even when a constant voltage is applied externally, the effective applied potential on the tungsten oxide films varies during electrochemical colouration, because of the change in *electromotive force* (EMF). Consequently, the response characteristics change. The changes in EMF can be explained as the result of a change in the concentration of redox species shown as C^+ and C in Nernst's equation,

$$\mathrm{EMF} = E_0 + R_g T_e/(n\mathrm{F}) \times \ln(C^+/C), \tag{3.7}$$

where E_0 is the standard electrode potential, n the number of electrons involved in the reaction, C^+ is the ion concentration in the electrolyte, and C is the amount of reduced species in tungsten oxide.

EMF has been measured many times [254,255,260–264]. The variation of the chemical potential in 7.2 N H_2SO_4 electrolyte of tungsten oxide films in different colouration states is measured in the range of $x < 0.5$ [261], and impedance spectroscopy is applied in 0.1 M H_2SO_4 [254]. It is discussed that the observed EMF arises from the chemical potential of hydrogen in coloured tungsten oxide, which changes with x [261]. Fig. 50 shows the EMF values plotted versus the charge equivalent x, which is interpreted as hydrogen composition variable in films and bulk samples [254,261]. What is found is that the EMF decreases monotonously with injected

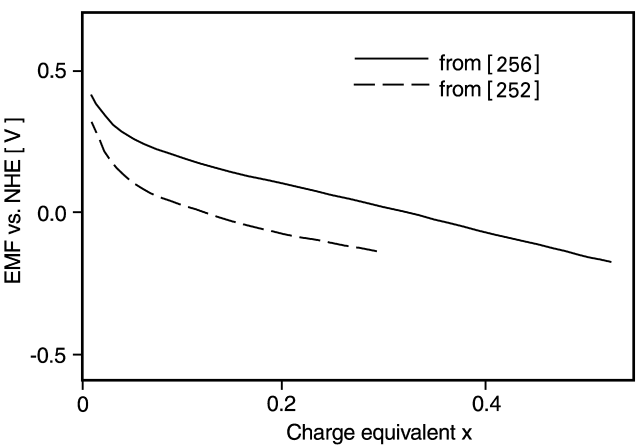

Fig. 50. Normalized EMF versus the charge equivalent x. From [254,261].

charge. Monotonous EMF variation suggests that charge injection takes place without major structural rearrangement [261]. The EMF is given by the fundamental equation [261]

$$\mathrm{EMF} = -\Delta G/F, \tag{3.8}$$

where ΔG is the free energy of transfer of one equivalent to charged species from the electrolyte of the tungsten oxide composite. It is argued that the composition dependence on the free energy is evoked by several contributions. First are those terms which are independent of x. These comprise the free energy of formation of one mole of pure amorphous tungsten oxide. The second set of terms are those linear in x. These arise from the free energy of the reduction of x moles of W^{6+} ions to W^{5+}, the changes in the interactions of those tungsten ions with their neighbouring oxygens when some have been reduced, and the possible bonding of protons to the oxygens. Next come those which are quadratic in x. These terms result from interaction between pairs of those centers that are created upon introduction of charge: W^{5+}–W^{5+}, W^{5+}–OH^-, OH^-–OH^-, etc. [261].

For studying the *kinetics* of the colouration/decolouration process, different electrochemical techniques are used. Chronoamperometric current–time ($i-t$) measurements were carried out to investigate the three principal processes which may control the kinetics of colouration:

(i) charge transport across the electrode/electrolyte interface,
(ii) diffusion in the electrolyte, and
(iii) diffusion in the tungsten oxide film.

Diffusion in the electrolyte can be ruled out as a dominating process, since the values for the current density calculated with the known diffusion constants are two orders of magnitude higher than observed in electrochromic experiments [265]. The diffusion dependence in the tungsten oxide films for the colouration process can be eliminated for similar reasons [265]. For tungsten oxide films in liquid electrolyte, the barrier at the charge-injecting interface is usually dominating and can be viewed as a Helmholtz double layer. The colouration current at that interface can be described by the Butler–Volmer equation, based on the electrode-potential limiting current. The time dependence of the current $i(t)$ for this barrier-controlled colouration process is expected to be [243,244,265,258] as

$$i \propto t^{-1/2} \exp(U/R_g T_e). \tag{3.9}$$

The decolouration kinetics is easier to treat. It is generally expected that the bleaching of tungsten oxide films is governed by a space–charge-limited current of charged ionic species and electrons [265]. It is argued that the space charge builds up because of the enormous difference between electron and cation mobilities ($D_{e^-} \gg D$). The voltage dependence normally observed rules out simple diffusion-limited bleaching. The space–charge-limited current is expressed as [260]

$$i \propto t^{-3/4} U^{1/2} \mu^{1/4}, \tag{3.10}$$

where μ is the mobility of the slower charged particle.

Fig. 51 represents an $i(t)$ plot for the bleaching of tungsten oxide in 10 N H_2SO_4. The results indicate that electrochromic colouration in tungsten oxide films is governed by charge transport across the tungsten oxide/electrolyte interface, and the bleaching response of the coloured film is governed by a space-charge-limited current flow. Similar results are obtained for Li-containing electrolyte [251,255,265].

The optical response of a "standard" tungsten oxide film is depicted in Fig. 52. The transmittance ($\lambda = 542$ nm) versus the time is depicted for a 400 nm thick tungsten oxide layer in 2 M HCl. For colouration, a potential of -0.8 V is applied, and for the

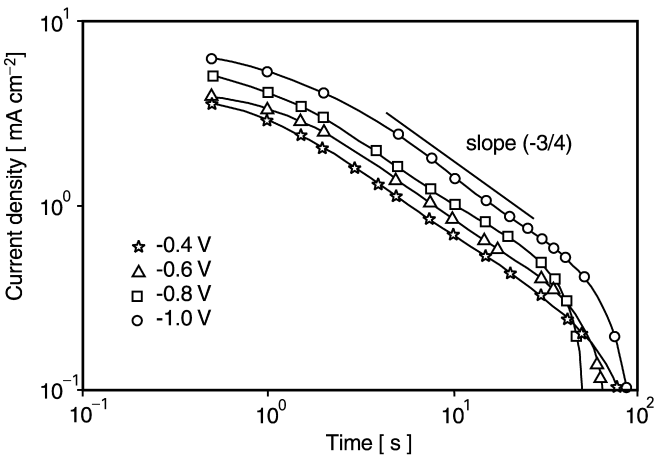

Fig. 51. Bleaching characteristics of tungsten oxide films in symmetric and asymmetric cells in the presence of 10 N H_2SO_4. From [265].

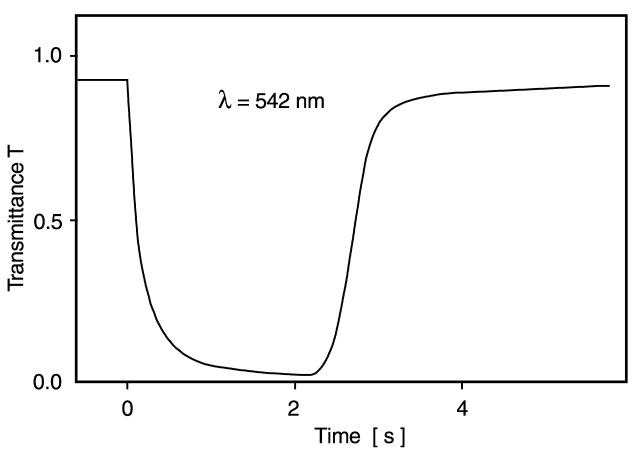

Fig. 52. Transmittance versus time for tungsten oxide film. Potentials of -0.8 and $+0.4$ V versus Ag/AgCl reference electrode are used for colouration and bleaching, respectively.

bleaching process + 0.4 V versus the reference electrode Ag/AgCl [150]. Immediately after applying the potential for colouration ($t = 0$), a fast decrease in the transmittance is measured and after one second the transmittance is reduced to $T \sim 0.05$. Small differences can be seen in the bleaching behaviour. After applying the potential, first a slow increase in the transmittance is obtained. This indicates that in this period of time, charge, which is not optically active, is removed out of the layer [150]. When this charged species is ejected out of the tungsten oxide layer, a linear increase in the transmittance is measured. This "constant-voltage" behaviour is of great interest for practical electrochromic devices.

The response time of the electrochromic effect is strongly determined by the morphology of the films, which is created by the used deposition conditons. The influence of the background pressure and constitution on the response time are reported [266]. Best results are obtained with oxygen at a partial pressure of 2×10^{-2} Pa. A further reduction of the response time has been achieved by oblique deposition technique. It is concluded that obliquely deposited films have a more porous nature, leading to a larger degree of hydration and to a faster electrochromic response [175].

The electrochromic properties of amorphous tungsten oxide films can also be manipulated by electron bombardment of as-deposited films. This effect has been studied for electrons in the energy range between 3 and 25 keV [237] on amorphous tungsten oxide film. The colouring rate and the maximally achievable contrast is nearly unchanged for electron doses $Q < 4 \times 10^{-2}$ C cm^{-2}. For larger irradiation doses, the colouring rate in the contrast drops.

Various other powerful analytical techniques have been used so far to characterize the colouration and bleaching process in electrochemical environment. The beam deflection technique, or mirage effect [267] and quartz crystal microbalance and stress experiments [268], are presently used to investigate the electrochromic reaction of tungsten oxide films prepared by electrochemical deposition, but to our knowledge have not been done so for evaporated thin films so far. This makes it difficult to relate the data to those obtained for evaporated materials.

Different other techniques are reported to obtain electrochromic colouration in electrochemical environment without applying an external voltage. It is described that 1 μm-thick tungsten oxide films on glass can be coloured when the surface is partially covered by an electrolyte (20% H_2SO_4) and in the centre of the electrolyte the film is touched by an indium wire. Colouration occurs around the tip and growth until the electrolyte boundary is reached. It is assumed that electrons are diffusing radially in outward direction from the indium source [150,197,259].

Colouration of tungsten oxide films is also achieved by using sulphuric acid (0.1 N) and a tin foil, which is postulated as a source for electrons. Also this colouration occurs without applying an external potential [270]. Colouration occurs also when tungsten oxide films are in contact with the mixture of HCl and Zn [269]. It is proposed that the film is exposed by atomic hydrogen (H^0), which is obtained from the mixture. For comparison, Fig. 53 shows the colouration that occurs when a tungsten oxide film is exposed by atomic hydrogen (H^0) involved from a HCl + Zn mixture. It

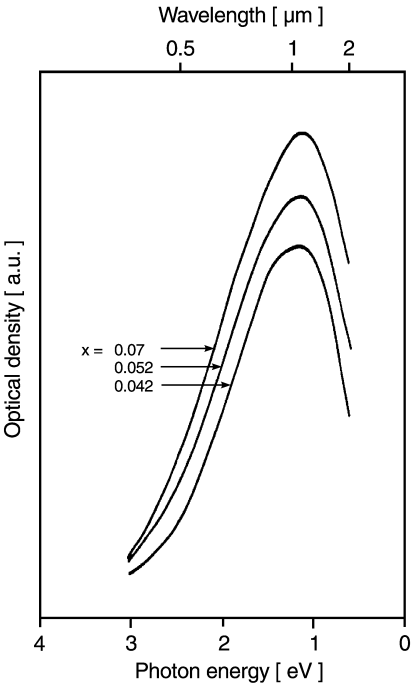

Fig. 53. Change in optical density during the colouration with a HCl + Zn mixture (for sputtered films). From [269].

can be seen that the absorption band is centred at approximately the same energy as for the other colouration processes.

For certain types of experiments, in which non-conductive substrates are necessary, this colouration procedure can be very useful. But the colouration state of this type of material is not well defined since the amount of transported charge cannot be measured in general. Therefore, electrochemical colouration with an applied external potential and the recording of the transported charge should be used for experiments in basic research.

3.2.3.2. Colouration by gases. Beside the electrochromism, which needs an external driving force as, for instance, in liquid electrolyte experiments (Section 3.2.3.1), in high electrical fields investigations (Section 3.2.3.3), or with solid electrolyte studies (Section 3.2.3.4), tungsten oxide films can also be coloured and bleached by a different procedure – with gases – without applying an external voltage. A catalyzing material must be present. Then hydrogen-containing gases colour and oxygen-containing atmosphere bleaches the tungsten oxide layer. The colouration rate of this process is influenced by the density of the tungsten oxide film, the hydrogen concentration in the gas, the amount of catalyzing material (film thickness), and the relative humidity. For fundamental investigations, a closed gas cell is necessary in which a defined gas

atmosphere can be realized. Our subsequently described results are obtained on samples consisting of glass/tungsten oxide/Rh, with film thicknesses of 680 nm for tungsten oxide, and 3–20 nm for Rh. A constant gas flux is used at normal pressure and room temperature. The relative humidity (r.h.) of the gas varies between 0% and 90%, and the hydrogen content in argon between 0.001% and 1%. 20% O_2 in Ar is used for bleaching.

Fig. 54 exhibits a typical time-dependent transmittance and reflectance obtained with 1% H_2/99% Ar-gas for colouration, 20% O_2/80% Ar-gas for bleaching, and an Rh film with a thickness of 3 nm. The reflectance and transmittance of the tungsten oxide/Rh systems during the exposure of the gases is measured with an HeNe laser ($\lambda = 632.8$ nm). The incidence of light proceeds from the side where the Rh is placed, as shown in the inset in Fig. 54. What is recognized that the hydrogen-containing gas colours and the oxygen-containing gas bleachs the layer. At the beginning of the experiments, the cell is filled with Argon. After the exchange of gases, which takes approximately 2 min, a change in the optical data starts. After a small onset, a linear change in the transmittance is observed, and then a saturation value is reached. The data of the reflectance look more complicated, but it can be figured out that the maxima are produced by interferences caused by the change in the refractive index during the electrochromic effect (Section 3.3.2). The transmittance changes between approximately 50% and 5% for this gas concentration and the layer systems.

The partial pressure of hydrogen possesses a strong influence on the minimum transmittance. Fig. 55 shows the influence of the gas partial pressure on the optical data. The dependence of the change in optical density δOD on the ambient gas, log p_{H_2}, is displayed. A linear relationship between the log p_{H_2} and the OD is observed. The H_2O concentration of the gases is constant (60% r.h.).

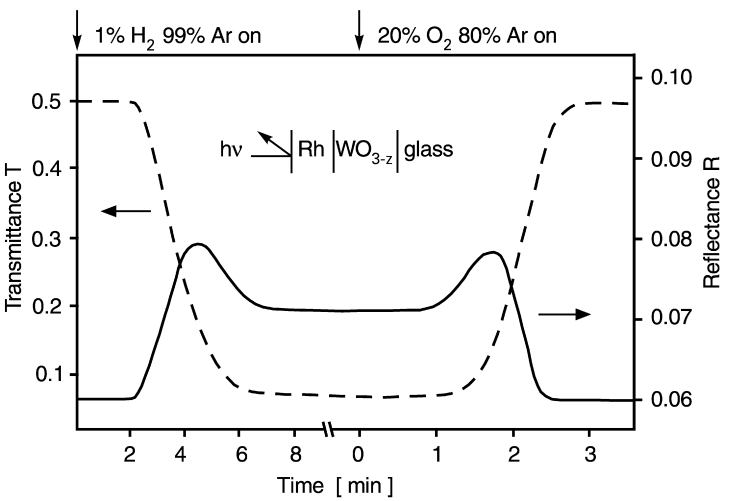

Fig. 54. Transmittance T and reflectance R ($\lambda = 633$ nm) versus the time of the tungsten oxide/Rh system during the exposure of H_2- and O_2-containing gases.

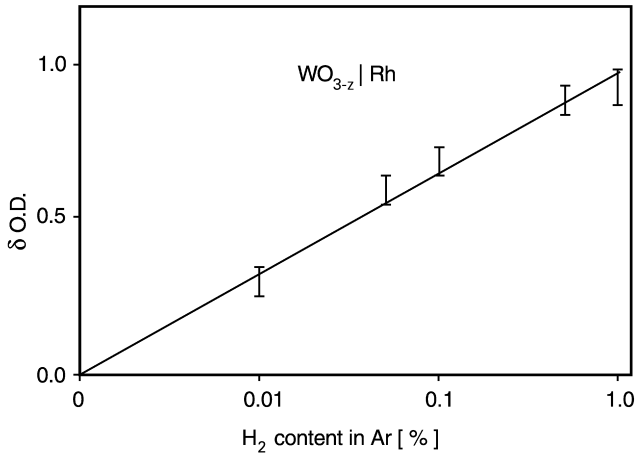

Fig. 55. Change in optical density δOD as a function of the hydrogen content of the ambient gas of a tungsten oxide/Rh system.

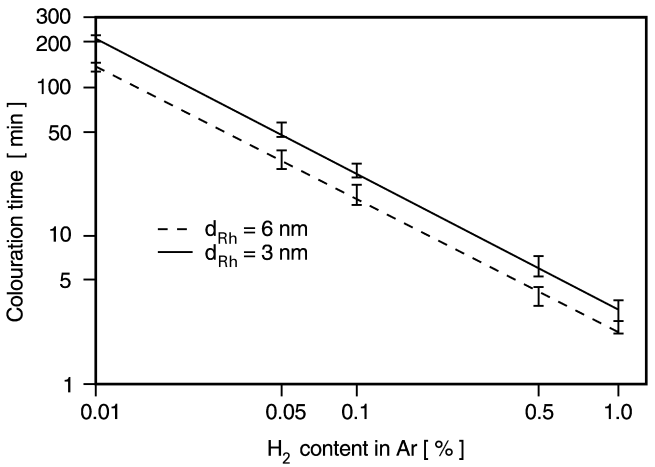

Fig. 56. Influence of the hydrogen content of the ambient gas on the colouration rate for two different thicknesses, d, of the Rh layers.

The rate of the colouration process is also influenced by varying the hydrogen partial pressure p_{H_2}. The colouration time is defined from the linear part of the change in the transmittance during the colouration in Fig. 54 [219,271]. In Fig. 56, the dependence of the colouration time on the partial pressure of hydrogen is depicted. It is seen that a linear relationship exists between the logarithm of the hydrogen concentration and the colouration time. It is also shown in Fig. 56 that an increase in the thickness of Rh layer decreases the colouration time, but decreases the

transmittance, too. It seems that thicker catalyzer films accelerate the colouration process in gases. An increase in speed is observed for film thicknesses up to 20 nm.

The thickness of the Rh film influences obviously the rate of the colouration process, but also the transmittance data. By varying the film thickness, one can change continuously the reflectance and transmittance of an Rh/tungsten oxide system. Fig. 57 shows the transmittance and the reflectance of the bleached and coloured system, as a function of the thickness of the Rh film. One can recognize that for thin Rh films the change in the transmittance is large, while for films with thicknesses of approximately 20 nm a relevant optical change can only be observed in the reflectance. Reflectance and transmittance are measured at $\lambda = 632.8$ nm from the glass side.

All data depicted above are obtained with a constant relative humidity (r.h.) of the gas (60%). But the water content of the used gases possesses a characteristic influence on the colouration time. Fig. 58 exibiths the speed of colouration versus the relative humidity for 1% H_2/99 % Ar-gas. The dependence of the colouration process on that parameter can be divided in three parts. In the range between 0 and 30% r.h., the speed of the colouration process increases linearly with increasing humidity. At

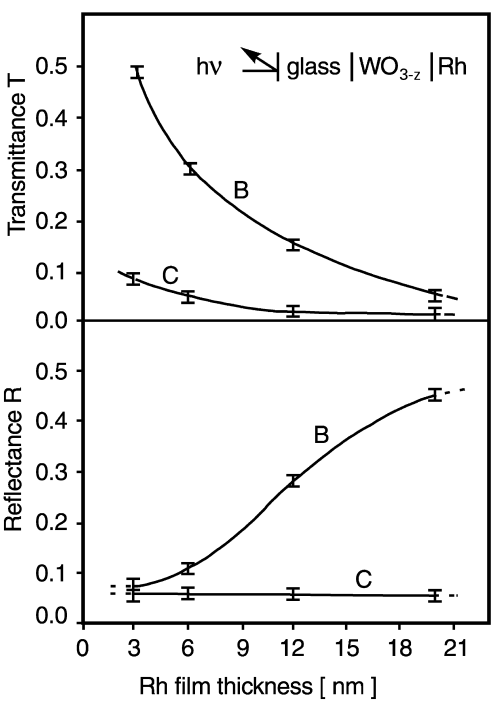

Fig. 57. Transmittance and reflectance of a tungsten oxide/Rh system with different thicknesses of the Rh films in the bleached (B) and coloured (C) state.

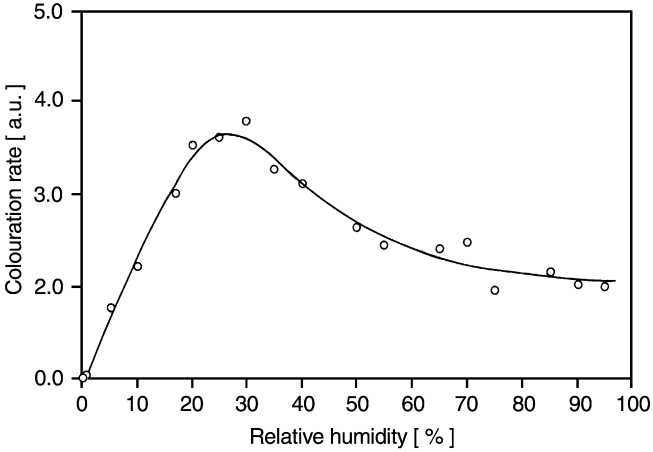

Fig. 58. Colouration rate as a function of relative humidity.

approximately 30% r.h., the shortest colouration time, namely the maximum, in the speed of the process is observed. A further increase in r.h. decreases the rate, and for r.h. $> 45\%$ the colouration time is fairly independent of r.h.

Gas-phase electrochromism of "standard" tungsten oxide/Rh systems are also investigated by NRA measurements [271]. Small changes in the hydrogen content could be observed during the colouration, and a small decrease during the bleaching. It seems that in such kind of experiments the electrochromism is partially connected with a change in the hydrogen concentration of the tungsten oxide layer. The observed increase, however, is very small ($\delta H/W \sim 0.05$) and cannot explain the observed variation in the optical properties of the tungsten oxide films [271].

Similar gas phase experiments have been carried out on sputtered tungsten oxide films [206]. Thin films of palladium, with thicknesses between 7.5 and 17.5 nm, are deposited on top of the tungsten oxide layers, and the devices are transferred to a chamber which could be evacuated to approximately 1 Pa or filled with various gases (oxygen, hydrogen) at pressures up to 10 000 Pa. Values for the relative humidity are not given for this type of experiments. Reversible colouration and bleaching are obtained by direct contact of the film with the reducing or oxidizing gasses, i.e. hydrogen or air. It is described that the kinetics of the colouration depends on the oxygen deficiency of the tungsten oxide film and also the temperature. For the same time of exposure to hydrogen (H_2), the optical absorption coefficient is approximately 10^3 cm^{-1}, when the exposure is carried out at 30°C and increases to 3.5×10^3, 6×10^3, and 8.5×10^3 cm^{-1} when the exposures are carried out at 50, 60 and 90°C, respectively. It is further noted, that the same exposure duration of H_2 at the same temperature (60°C), induces a more intense absorption band for $WO_{2.98}$ (7.5×10^4 cm^{-1}) than for $WO_{2.8}$ (8.5×10^3 cm^{-1}) [206]. Additionally, it is mentioned that the colouration rate is higher on evaporated than on sputtered layers, but no experimental details are given.

Comparable systems consisting of platinum metal on tungsten oxide films have been investigated. Especially, various hydrogen sensor systems are described as having the general configuration: catalytic metal/insertion compound/insulator/semiconductor. Solid-state chemical sensors based on metal–oxide semiconductor (MOS) technology have been studied [272]. The concept is demonstrated for Si/Si2 MOS structures incorporating tungsten oxide, a so called H-insertion compound, and Pd as the gate layers. The description is that, when H_2 comes in contact with Pd, it decomposes to H atoms, which dissolve in the metal. These atoms give rise to dipoles at the Pd/oxide interface, which have the effect of adding a voltage in series across the diode. The magnitude of the voltage is proportional to the H_2 concentration in the gas and is read out as a shift in the capacitance–voltage (C–V) response of the MOS diode [212]. Derivation in the C–V curves gives rise to a maximum at the flat band voltage. The obtained shifts in the flat band voltages are approximately 0.7 V in dry air and 0.1% H_2 in Ar for a $Si/SiO_2/WO_3/Pd$ structure [272]. Also a qualitative effect on the humidity of the C–V curves is reported.

Also a hydrogen detector has been described consisting of tungsten oxide thin film on glass substrate and optically semitransparent Pd film on the former film [273]. Amorphous and polycrystalline tungsten oxide films are investigated which are produced by different heat treatment. The device works at a temperature up to 500°C. Increasing temperature raises the sensitivity of the device. Fig. 59 shows the dependence of the optical density on the hydrogen concentration in air at 71°C. The peak value of the optical density increases with increasing hydrogen concentration in air [273].

Also platinized bulk tungsten oxide reacts with H_2 at room temperature to form the blue colour. This was first recognized by Khoobar [274] in studies of oxide-supported catalysts. In mechanical mixtures of Pt and tungsten oxide, i.e. in a mixture between a metal that can dissociatively adsorb a diatomic molecule and a nonmetal which itself cannot dissociate the molecule, the metal can act as a source of atoms migrating to the nonmetal and participating in various processes. Such a transport of atoms from a dissociating to a nondissociating surface has been called "spill-over" [275]. The rate of reduction of tungsten oxide by hydrogen has been studied in the presence of a cocatalyst with varying proton affinity [276]. As proton affinity increases the rate of reduction decreases in the order: H_2O, CH_3OH, C_2H_7OH, C_2H_5OH, etc. The correlation between the rate of reduction and the proton affinity of the cocatalyst suggests the formation of a solvated proton on the metal, followed by a proton transport in the adsorbed phase of the cocatalyst to the reduction site on the oxide. It seems that the cocatalyst acts as a proton acceptor and the transported species is the solvated proton. It is revealed that beside platinum water is required and necessary as a cocatalyst to observe the reduction at room temperature. If no water is admitted to the system or formed on the platinum surface, no reduction is observed [276].

All the results obtained in the different gas-phase experiments suggest that charge transfer across the tungsten oxide/catalyzer interface is necessary to realize this type of electrochromism in tungsten oxide. In electrochemical experiments at the solid electroylte interface, a potential drop is caused by the applied external potential at the

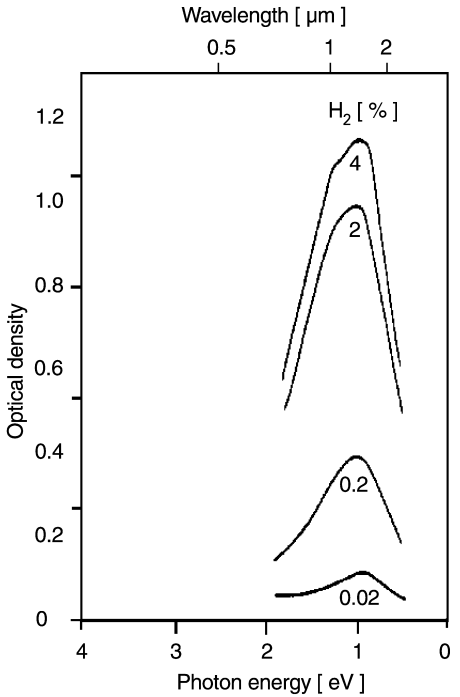

Fig. 59. Optical density for an amorphous tungsten oxide/Pd film system at various hydrogen concentrations in air. From [273].

Helmholtz layer and in the space charge region. Equilibrium is achieved as soon as a Fermi level is equal throughout the whole system. A corresponding mechanism occurs probably at the tungsten oxide/catalyzer system. A schematic representation of the potentials at a metal/tungsten oxide interface is given in [271]. The barrier height of the Schottky contact is determined by the conduction band of the tungsten oxide and the Fermi level of the metal (Rh, Pd), and the barrier height is reduced by exposure to diluted hydrogen ambients.

For an Rh/tungsten oxide system to respond to the presence of H_2, there must be at least a three-step process involving adsorption on the Rh surface, transfer to the Rh film, adsorption at the Rh/tungsten oxide interface. Such a mechanism may be described

$$H_2(\text{gas}) \xrightarrow{1} 2H(\text{chemi.}) \xrightarrow{2} 2H(\text{bulk}) \xrightarrow{3} 2H(\text{inter.}), \tag{3.11}$$

where gas, chemi., bulk and inter. denote gas phase, chemisorbed (at the Rh surface), Rh bulk and Rh/tungsten oxide interfacial hydrogen, respectively. Such a mechanistic sequence involving a direct transfer through the chemisorbed state is the usual treatment of processes involving transfer of H to or through bulk catalyzer [277].

Under the used experimental conditions (thin Rh films and high p_{H_2}), the assumption can be made that Rh-bulk diffusion is too rapid to be involved in the response kinetics and that adsorption at the Rh surface is not the rate-limiting step. A general kinetic rate expression for the tungsten oxide/Rh interface coverage θ_i (defined as H/Rh ratio) can be written as [277].

$$\frac{d\theta_i}{dt} = k_3 X_b(1-\theta_i) - k_{-3}(1-X_b)\theta_i \tag{3.12}$$

where X_b is the Rh bulk coverage and k_3 is the rate constant for the transfer of H between the bulk and the interface, and k_{-3} is the reverse process.

The steady-state interface hydrogen coverage is a thermodynamic quantity and is independent of the kinetic mechanism, depending only on the hydrogen pressure and the potential depth of the interface state. At steady state, the coverage may be described by

$$\frac{\theta_i}{1-\theta_i} \sim \exp(\Delta H_i/R_g T_e), \tag{3.13}$$

where ΔH_i is the enthalpy of formation of interfacial hydrogen for the reaction of $1/2H_2(gas) \rightarrow H$ (inter.). Thus, the potential of the hydrogen well at the interface depends only on the steady-state coverage of hydrogen at the interface, and is independent of the binding energy of hydrogen at the surface or in Rh bulk.

In sum, the H_2 molecule dissociates at room temperature at the catalytic surface. This process is followed by a rapid diffusion of hydrogen to the metal/tungsten oxide interface, where a dipol layer is created, which results in a field across the interface, producing a sharp drop [277]. This potential drop lowers the energy of the conduction band edge relative to the Fermi level, similar to an applied external potential in aqueous electrolyte experiments. Thus, the barrier height is reduced in the presence of hydrogen. The observed dependence of the optical density on the hydrogen concentration indicates that the potential drop of the Schottky barrier is determined by the Nernst equation. It seems that the effect produced in liquid electrolyte experiments by an applied external voltage is created in the gas-phase experiments by the gas itself.

The electrochromism of tungsten oxide/catalyzer systems is not being very extensively studied. Thus, it is not clear whether the hydrogen is incorporated in the tungsten oxide layer or is only necessary as a potential modifier in such a process. Another open question is the influence of the co-catalyzer (H_2O), which is necessary and exhibits a very characeristic, determinant behaviour. However, the exact reaction mechanism is not known so far. Finally, it should be mentioned that it seems possible to colour tungsten oxide films with gases without the use of a catalyzer. It is reported that atomic hydrogen, which is produced in a microwave- induced gas discharge, also colours tungsten oxide. But under the described experimental condition it is not clear whether the light (photochromism) or the atomic hydrogen creates the colour [270].

3.2.3.3. Electrocolouration. As first reported by Deb [149], colouration of transparent tungsten oxide films can be obtained by applying an electrical field parallel to the film plane. On the surface of approximately 1 μm-thick tungsten oxide films deposited on glass, a pair of gold electrodes is evaporated. On applying a d.c. electric field of $\sim 10^4$ Vcm^{-1} across the sample at room temperature, the colouration originates at the cathode and propagates slowly towards the anode. With the time, the colour cloud fills the entire inter-electrode spacing, except for a small region near the positive electrode. It is described that the colouration front is fairly uniform, except for few localized spots where more intense colouration occurs, which is probably evoked by irregular shapes of the electrodes. Under the cathode, a more intense colouration is observed. A rate of migration is analysed to be 3.0×10^{-7} cmV^{-1}s^{-1}. On reversing the polarity of the applied field, the colour cloud migrates towards the anode and finally disappeares in it. By continued application of the field, the colouration appears again at the newly formed cathode and the process of colouration and bleaching can be repeated many times [149].

It is suggested that moisture appears to play a dominant role in such type of colouration phenomena, since no electrocolouration is observed in vacuum [149]. However, most experiments are not carried out under controlled humidity conditions. Only data for two well-defined humidities, which are achieved by placing the sample in exsiccators containing saturated salt solutions, are reported [125]. Typical experimental conditions are at 20°C, and 59% and 32% relative humidity. For applied electrical fields of ~ 300 Vcm^{-1}, the front of the colour cloud propagates at 3 mm h^{-1} and has an optical absorption for white light $I_O/I \sim 4$ in relative humidity of 59%. The corresponding numbers for 32% humidity are 0.1 mmh^{-1} and 1.7, respectively.

Reversible electrocolouration and the influence of the H_2O content is also investigated on tungsten oxide films evaporated on Mo electrodes spaced 1 mm apart from one another. Direct and pulsed current/voltage measurements are carried out in air at room temperature. Electrocolouration is observed at fields < 1 kV mm^{-1} for all samples prepared below 300°C [122]. A uniform colouration front is assumed, and the rate of propagation is given by [122]

$$\frac{dy}{dt} = \mu\left(\frac{U}{L - y + yi_0/i_L}\right), \tag{3.14}$$

where i_0 is the initial current and i_L the final current, μ the mobility of ions, L is the electrode gap (see Fig. 60), and y the distance of the colouration front from the cathode. The time required for the coloured region to fill the electrode gap is found to decrease linearly with a decrease in applied voltage down to a critical voltage, below which the process was very sensitive to the ambient environment, and decrease with increase in H_2O content. Freshly evaporated films exhibit electrocolouration, but the colouration sensitivity decreases markedly with aging of the films in air or in a desiccator. On exposure to H_2O vapour at 10°C, the resistance decrease by several orders of magnitude and the electrocolouration rate increase. After a prolonged degassing at 50°C and 10^{-3} Pa, the resistance increases markedly, and no colouration

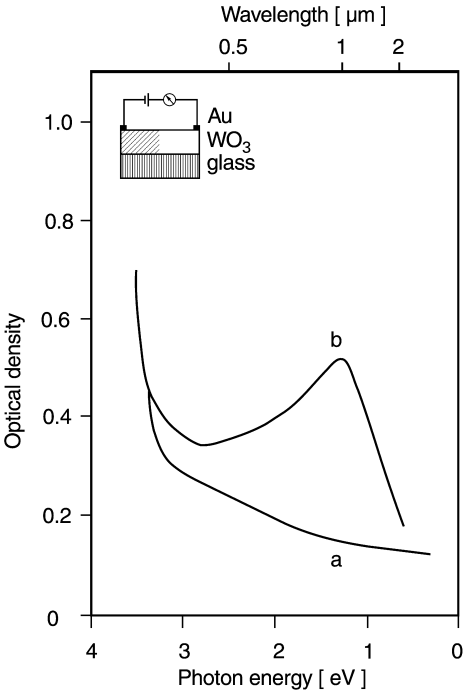

Fig. 60. Optical density of tungsten oxide film before (a) and after (b) electrocolouration. From [149].

is observed at prebreakdown fields [122]. From this observation is concluded that the presence of H_2O plays a vital role in determining both the conductivity and the rate of colouration of electrochromic films. The increased mobility with increasing H_2O content is probably due to a "solvation" effect, since H^+ ions move more readily along chains of H_2O molecules, so that the diffusion activation energy decreases with increasing H_2O content [122].

In order to test whether the conductivity in the tungsten oxide film is electronic or ionic in nature, concentrated sulphuric acid is used as an anode [125]. Also in such type of experiments, the colouration starts at the cathode, and no effects are observed at the tungsten oxide/electrolyte interface. This result convincingly demonstrates that the conductivity is almost exclusively ionic. It is further reported that the conductivity increases about two orders of magnitude upon colouration [149]. But this result is disputed [125], because the experiments are not carried out under controlled humidity conditions.

Current–voltage characteristics are measured both on uncoloured and on the electrically coloured Au/tungsten oxide/Au systems, with applied field parallel to the film plane. The current–voltage characteristic is ohmic for the uncoloured film up to an applied field strength of $\sim 10^4$ Vcm^{-1}. The electrically coloured sample shows an ohmic region at low voltages. Above a threshold voltage, the current follows by a square law dependency [149].

The optical absorption spectra of electrically coloured tungsten oxide films are measured in the wavelength range of 0.3–1.9 μm. The resulting spectra are shown in Fig. 60. Apparently, the absorption spectra are almost identical to those obtained by the other colouration processes.

A comparison of colouration efficiencies obtained by different geometries of the electrochromic cell shows that, in experiments with the field applied parallel to the film plane, the charge required to produce a given colouration is about one order of magnitude higher than with the field perpendicular to the film plane. It is concluded that, in the parallel geometry, most of the electrical current is used to electrolyse water, and only little to inject electrons. In order to vary the ratio of injected electrons to discharged protons, various cathode materials with vastly different hydrogen exchange currents are used, e.g. platinum and lead. Since no significant difference is found in the colouration parameters, the results of experiments with fields applied in parallel are therefore summarized as follows [125]:

- The electron mobility strongly depends on the degree of colouration or reduction.
- The electronic conductivity is small, compared to the ionic conductivity, even in the coloured region.
- The Coulomb efficiency of electron injection is small.

From the facts that in the parallel film case the Coulomb efficiency of electron injection is small and that the Coulomb efficiency for tungsten oxide reduction is electrode-independent, it is concluded that not only H_2 production, but also tungsten oxide reduction involves an H^0 intermediate [125].

So far, the electrocolouration phenomena of tungsten oxide films have been described by applying the electrical field parallel to the film plane. The required field strength for colouration ($\sim 10^4$ Vcm^{-1}) can also be realized by depositing a sandwich structure. In such a geometry it is possible to obtain the same field strength, applying 1 V across a 1-μm-thick tungsten oxide film.

Different types of sandwich structures are prepared. They usually consist of an ITO or SnO_2-coated glass on which the tungsten oxide film is deposited, followed by an evaporated thin transparent gold film on top of it. Using the gold as a cathode and applying 2 V across the film, the tungsten oxide layer develops a deep blue colour in a few seconds. By slowly varying the potential, typical current–voltage characteristics are obtained, which are depicted in Fig. 61 [149] for different modes of polarity. With gold as a cathode, there is a slow increase in current up to 2 V, followed by a rapid increase of current and the appearance of strong colouration in the electrochromic layer (curve a). The current–voltage curve, after one minute of correlation, is shown also in Fig. 61 (curve b). With progressive colouration, there is a gradual decrease of the threshold voltage for rapid current rise, and as the colouration reaches the saturation value the current–voltage curve takes the form of curve c shown in Fig. 61.

The structure behaves like a rectifying diode, with colouration occurring in the reversed bias condition. No bleaching occurs on reversing the polarity. Obviously, there exists a threshold voltage for colouration, and if this is taken as a measure of a barrier height of the metal oxide contact, it is evident that the barrier decreases with

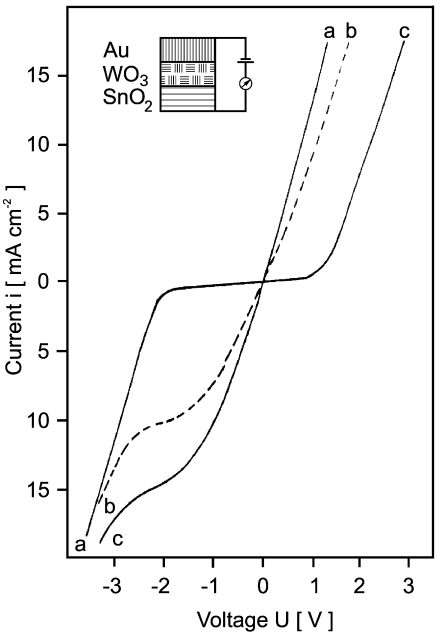

Fig. 61. Current–voltage characteristics of an Au/tungsten oxide/SnO_2 sandwich structure. From [149].

increasing colouration. The shown results suggest that the initially low conductivity in the tungsten oxide film is increased, either by the colouration of tungsten oxide or the diffusion of Au in the tungsten oxide films.

3.2.3.4. Colouration with solid state electrolytes. Most of the fundamental research on electrochromic material is realized in liquid electrolyte experiments, because it is possible to obtain controlled, defined conditions which can quickly be changed additionally. In contrast, most technical applications use solid-state electrolytes and possess only two electrodes [278,279]. The very different chemical environment of the electrochromic film may influence the electrochromism of tungsten oxide films. Electrochromic systems working with a solid electrolyte may be divided into two distinct classes: "open" systems are those that interact with the surrounding atmosphere and "closed" systems, which are constructed in a way to prevent influence by the ambient atmosphere. The second class exhibits similar reversible processes as liquid electrolyte devices.

Early devices belong to the first category, to the "*open*" *systems*, and are based on similar processes described in Section 3.2.3.3. In principle, in all-solid state configurations, the liquid electrolyte is replaced by a solid. One of the first electrolytes consists of a SiOx layer evaporated over the tungsten oxide layer on SnO_2-coated glass and a gold electrode evaporated over the SiO_x [149]. The role played by water in this sandwich arrangement was not obvious immediately. But it was realized that water

possesses a certain influence on the electric-field colouration of tungsten oxide in the planar geometry with metal electrodes (Section 3.2.3.3), specifially since no colouration occured in vacuum of 10^{-5} Torr. In the geometry described in Section 3.2.3.3, the tungsten oxide film is in a direct contact with the ambient atmosphere, and the used high voltages can dissociate water on the surface of the tungsten oxide film.

The dominant role of water has been studied in a solid-state sandwich cell structure consisting of ITO/tungsten oxide/SiO_x/Au clarifying the situation [280–282]. In this open structure, weight changes during colouring and bleaching have been measured, indicating adsorption and desorption of H_2O between the cells and their surroundings. Mass-spectrometer measurements show that O_2 left the cell during colouration, and H_2 left during bleaching [282]. Additionally, colouration does not occur until a threshold voltage is reached across the electrolyte layer which corresponds to that of the electrolysis of water. It is suggested that the insulating layer contains water that can be dissociated by the electrical field, thereby providing the charged species necessary for colouration of tungsten oxide film. It is argued that this explains why higher colouration voltages are always found for open solid-state cells, compared with liquid electrolyte cells [283]. Also data of solid-state devices have been reported which do not depend on the surrounding humidity [281,284]. The devices are working with trapped water and are unaffected by ambient conditions, including vacuum, because the water is tightly bound.

Solid-state electrolytes of "*closed*" *systems* should have much in common with liquid electrolytes, because these seem to be a nearly ideal choice for a number of processes relevant for the electrochromic behaviour of tungsten oxide films. So, for example, liquid electrolytes are good ion conductors and insulators for electrons. In addition, they form the reservoir for the charged, ionic species which is necessary for the charge compensation in the tungsten oxide films during the electrochromic process. In the liquid electrolyte experiments, this reservoir contains an infinite number of available charged species which can be injected or ejected in the electrochromic film. The number of the available charged species can influence the colouration rate. Additionally, the transport mechanism at the tungsten oxide/liquid electrolyte interface is controlled by the concentration of the needed ionic species. It is well known that, for example, the H^+ or OH^- concentration determines, via the Nernst equation, the potential in the electrolyte. For the electrochromic effect, it is observed that a variation of the H^+ concentration shifts the colouration potential linearly (beginning of the colouration) [150,238]. This behaviour is explained by the "Fermi level" concept for liquid electrolytes [285], i.e. as a function of the position of the liquid electrolyte Fermi level, different potentials have to be applied to bring the flat band potential of the tungsten oxide layer to the same level as that of the solution caused by a charged transfer process at the interface [285].

For these reasons, the first significant step in the development of a thin-film solid-state electrolyte for a closed system is the simulation of the electrochromic characteristics obtained with liquid electrolytes. Comparable or identical properties are desired, principally, for thin-film solid-state electrolytes. Additionally, a high transparency is necessary for the application in technical devices. The choice in the preparation of an appropriate solid-state electrolyte is one the main challenges in the

production of all solid-state devices. Very different solid electrolytes have been developed and tested so far. Various materials have been investigated, e.g. ZrO_2, HfO_2, SiO_2, Ta_2O_5, but also fluorides, e.g. CaF_2, MgF_2 and CeF_3 [279,286]. A common property of these inorganic ionic conductors is that the ion conduction is not a solid-state bulk effect. The functioning of these solid electrolytes and, in particular, the so called "ionic conductivity" is due to the presence of crystal boundaries in the microcrystallized layers or the porous structure of the amorphous oxide layers. These allow, depending on the deposition conditions, controlled uptake of a certain amount of water which, in part, gives rise to hydroxyl groups adsorbed at the internal surfaces and, so, to a rather large mobility of H^+, OH^- and other dissoziation products of water. So, for example, it is found out that tantalum oxide films contained 0.3 H_2O/Ta_2O_5 for evaporated films [150,210]. The reason for this large water uptake is the low density in the films that have to be created by appropriate deposition conditions. For operating in electrochromic systems, it is necessary to prepare films deliberated with a low packing density, and stabilize the films in that nonequilibrium state. Such materials are sometimes described as hydrated oxides, for example as $Ta_2O_5 \cdot H_2O$ or tantalic acid.

To illustrate the electrochromic behaviour, Figs. 62 and 63 compare optical and electrical data of "standard" tungsten oxide films obtained in liquid electrolyte and in solid-state environment. The results for Fig. 62 are obtained with the two-electrode

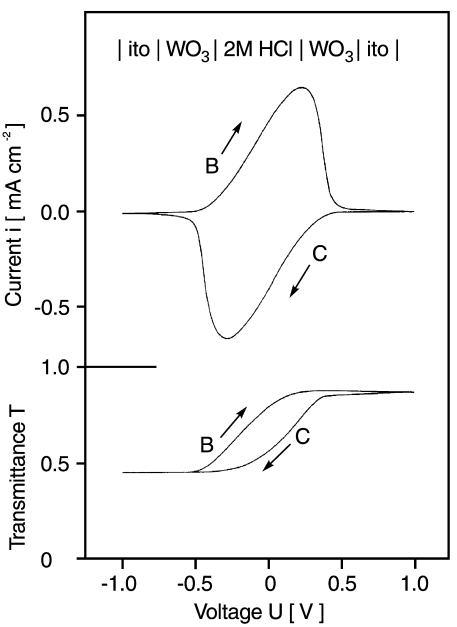

Fig. 62. Current and transmittance (at 541 nm) versus the applied voltage during colouration (C) and bleaching (B) in liquid electrolyte system.

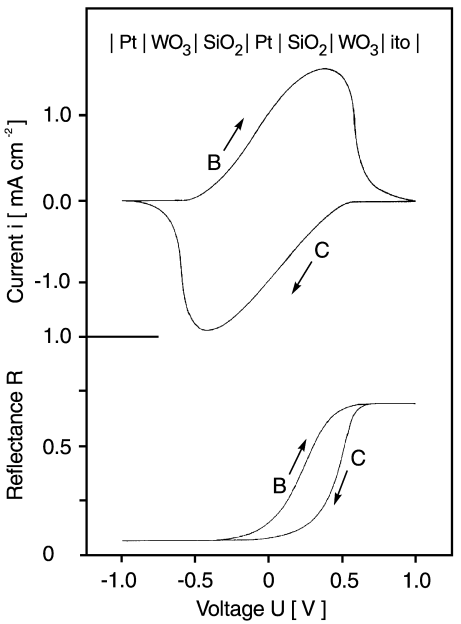

Fig. 63. Current and reflectance (at 550 nm) versus the applied voltage during C and B with a solid electrolyte.

configuration consisting of ITO/WO_3/2 M HCl/WO_3/ITO. The transmittance is recorded only for one WO_3 layer, and the measurements were taken with a sweep rate of 50 mV s^{-1} at a wavelength of 541 nm. Instead of the liquid electrolyte, a porous SiO_2 layer is sandwiched between the two tungsten oxide films for the data in Fig. 53. Additionally, one ITO layer is replaced by platinum film and to make visible the electrochromic effect of only one layer, a thin platinum film, is placed inside the electrolytes. The current and reflectance versus the voltage are taken with a sweep rate of 100 mV s^{-1}, and the reflectance is measured at a wavelength of 550 nm.

Despite the very different chemical environments, a fairly similar behaviour is obtained in electrical and optical properties. It may be guessed that, by an innovative choice of the appropriate deposition conditions, very comparable processes occur in the tungsten oxide films. In contrast with liquid electrolytes, thin oxide films possess only a limited number of transportable species, i.e. the amount of water is limited. One possibility to vary the number of insertable and extractable particles is to create solid electrolyte films with different thicknesses. It was demonstrated that thicker electrolyte films create an enhanced current in the current voltage graphs [238]. The crucial role of the thickness of the insulating layer is also observed for MgF_2 [287]. At very low thicknesses ($\sim$ 8 nm), the devices show very little colouration and an optimum is found in a thickness range of 100–200 nm.

The function of solid electrolytes is strongly related to the device design. For a symmetric device depicted in Fig. 63, a very high hydrogen content (H/Si ratio of

approximately 0.5) is analysed by NRA [171,207,209,210,238]. This concentration is much higher than that found in single layers and double layers. During the colouration and bleaching, no changes in the hydrogen concentration are observed in the solid electrolyte film, which indicates that no hydrogen transport occurs during the switching.

A different behaviour is obtained in solid electrolytes for asymmetric systems (Section 2.4). For such devices, a hydrogen transport can be analysed from the hydrogen depth profile for all layers in the system, i.e. changes in the insulating layers are likewise found [207,209]. A reversible hydrogen content, which suggests hydrogen transport, is obtained, depending on the applied potential of that type of all-solid state devices.

3.3. Coloured state

This section considers the coloured state of tungsten oxide films, which represents, in principle, a new film material with microscopic and macroscopic properties different from those of as-deposited or bleached films. The obviously changed macroscopic characteristic feature is the colour, i.e. the absorption. Different models describing the optical absorption in the tungsten oxide films are discussed briefly (Section 3.3.1). Changes in the local structure of our highly disordered standard tungsten oxide films are observed (Section 3.3.2), and the decrease in the intensity of the terminal W=O vibration indicates a local rearrangement. Colouration-induced changes in the density of states of the valence band, the conduction band, and the core levels are discussed (Section 3.3.3). For tungsten oxide films prepared with "standard" parameters, we find a linear relation between the injected charge and the amount of W^{5+}, and changes in optical density. Variations in the film composition evoked by colouration are considered (Section 3.3.4). No changes in hydrogen content are found, but colouration produces an increase in the oxygen deficit in "standard" films. The obtained results are explained with models which also take into account the observed influence of the composition of the respective reservoir.

3.3.1. Optical properties

Colouration of "amorphous" tungsten oxide films takes place upon the employment of very different procedures described in Section 3.2. Independent of the used colouration process, a similar blue colour is observed in the films, which is created by a broad and intense absorption band. The maximum of the absorption curves is centred at an energy of approximately 1.3 eV for evaporated "amorphous" films coloured by thermochromism (Fig. 27), photochromism (Figs. 34, 36 and 38), ion and electron beam irradiation (Figs. 40 and 42), and by the different types of electrochromism (Figs. 46, 53, 59 and 60). The results indicate that the coloured states of the film seem to be fairly independent of the different ways of colouring tungsten oxide, which suggests that the underlying physics is similar, so that the broad presentation of the colouring schemes, especially of the spectral absorption coefficient, may pave the way towards a unifying theoretical description. But this colouration behaviour may also indicate that several colouration mechanisms operate in parallel.

Very different models have been proposed to give an account of the optical absorption in tungsten oxide films. Based on the early work on the properties of the colour centres in tungsten oxide formed by optical and electrical excitation, a model has been proposed, which involves trapping of electrons in oxygen ion vacancies [149]. This model is analogous to the formation of F or F^- centers in other ionic solids, like alkali halides. The fact that as soon as the colour centres have been bleached by heating in oxygen at high temperature they cannot be regenerated, strongly argued in favour of this model.

A more favourable model to explain the optical absorption in amorphous tungsten oxide films involves intervalence charge transfer [244]. The optical absorption arises from a transition of an electron from one W^{6+} trapping side to an adjacent tungsten ion side. According to this model, electrons injected during the electrochromic colouration process are trapped at transition metal sites, i.e. optical absorption is due to resonance transfer of the trapped electrons among the equivalent tungsten atoms. Band shape, energy, and oscillator strength can be explained, at least qualitatively, in terms of this model.

An alternative model involves the formation of small polarons [269,288]. The small-polaron concept offers a possibility to formulate a quantitative theory for the optical absorption. Small polarons are created when electrons polarize their surroundings, so that localization of the wave function takes place, essentially to one lattice site. A small overlap between wave functions corresponding to adjacent sites, as well as strong disorder are conducive to polaron formation [288]. This model, which is basically the same as the intervalence charge transfer model, uses in addition a local structural distortion brought about by the electron trapping and W^{5+} formation. This is lowering the energy of the occupied state relative to the unocuppied state of the surrounding W^{6+}. Thus, transfer of an electron from this W^{5+} to a neighbouring W^{6+} is not necessarily a resonance process. The agreement between theory and experiment for the spectral optical density of "amorphous" tungsten oxide films is good [288] and is comparable to those obtained from the intervalence charge transfer theory [244,289].

The optical absorption in the heavily disordered tungsten oxide films can also be explained with the schematic bandstructure depicted in Fig. 9. In the fully transparent state, the Fermi level lies between the O 2p and the t_{2g} bands. Insertion of electrons shifts the Fermi level upwards and populates the lower part of the t_{2g} with excess electrons, and the material exhibits absorption.

Coloured crystalline tungsten oxide films can be treated as heavily doped semiconductors. The inserted electrons make the material infrared-reflecting, and the unavoidable ion-electron scattering limits the metallic properties [289]. Free electron theory can be employed to describe the optical properties. Drude theory can be used for a qualitative work, but is unable to give quantitative predictions [241]. Instead, the Gerlach theory for ionized impurities scattering is of much value [242].

3.3.2. Structure

Structural information can be obtained by Raman spectroscopy, especially on vibration modes of the metal–oxygen framework. For "amorphous" tungsten oxide

films, the W=O terminal bond at 950 cm^{-1} is of particular interest, as discussed in Section 3.1. Detailed studies are available for films prepared by sputtering [183] and anodic oxidation [129], but not many data have been published so far on Raman spectroscopy investigations on evaporated tungsten oxide films.

Fig. 64 exhibits the effect of colouration by In/HCl procedure (Section 3.2.3.1) on the Raman spectra for "standard" films. The vibration features of as-deposited (a) and coloured state (b) are depicted, and for comparison spectra are shown from a polycrystalline film (c). Different scales are used for depicting the counts. It is obvious that the intensity of the terminal W=O vibration is decreased by the colouration, and it seems that the feature at approximately 950 cm^{-1} shifts additionally to smaller wavenumbers. Similar results for electrochromic colouration of tungsten oxide films are reported by Berndt [154]. The shift of the peak at 950 cm^{-1} by colouration is explained by an increasing number of W^{5+} ions influencing the W=O bond, i.e. the strength of the terminal oxygen depends on the valency of the tungsten.

Analogous studies of films made by low-voltage anodic oxidation and electrochemically coloured in H-containing electrolyte gave qualitatively similar results [129,130]. With increasing amount of injected charge, the Raman signal at 950 cm^{-1} decreases and finally disappears. Contradictory results are obtained for anodic tungsten oxide films produced by high–voltage anodization ($U_a = 70$ V) and subsequently treated with Li^+ electrolyte [128], and also for rf-sputtered tungsten oxide films

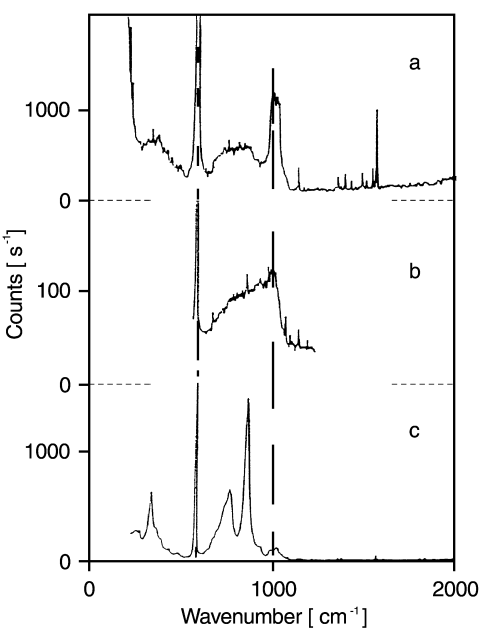

Fig. 64. Raman spectra of tungsten oxide in transparent (a) and coloured (b) state, and for polycrystalline transparent (c) film.

coloured in 1 N H_2SO_4 solution [183]. An increase of the Raman intensity at 950 cm^{-1} is analysed with the colouration. No quantitative assessment of this effect is given, but it is evident that the inserted charge leads to local structures with W=O terminal groups. Fairly recently, Raman microprobe studies of electrochromic and photochromic tungsten oxide films have been reported for layers deposited by vacuum evaporation [290]. For the film coloured in 0.1 M $LiClO_4$ solution, and with UV irradiation in air, no changes are obtained in the Raman spectra. These results obtained by Raman spectroscopy suggest that colouration of tungsten oxide films can either create or eliminate W=O bonds, depending on the preparation conditions and, in particular, on the degree of crystallinity.

For examining changes in the bonding state of OH^- ions and H_2O in tungsten oxide films during colouring and bleaching processes, infrared absorption spectroscopy is a powerful technique. The data obtained so far are not very consistent, and one should avoid to far-reaching conclusions from the published results. The IR spectrum of evaporated tungsten oxide films in contact with H_2SO_4 is rather unaffected by the colouration and bleaching process, and, in particular, the absorption of the O–H stretching mode (at 3400 cm^{-1}) is not changed [291]. This is interpreted as an evidence that intercalated protons do not bind to a Bronsted sites at the internal surfaces [291].

In studies using alkali-containing electrolytes (Li^+, Na^+, K^+) [292], an increase of the O–H stretching mode intensity occurs in direct correspondence with the quantity of inserted charge. Colouration and bleaching changes reversibly the absorption at 3400 cm^{-1}, and the amount of molecular water keeps constant, independent of the injected charge. Results reported of tungsten oxide films made by rf sputtering and coloured in 1 N H_2SO_4 are somewhat contradictory, in spite of the similar sample fabrication [183,293]. In one work, colouration leads to the evolution of an intense, broad absorption band centered at 2400 cm^{-1} and a simultaneous small decrease of a band at 3400 cm^{-1} [293], while, in the other study, colouration is associated with a growth of an absorption band at about 1620 cm^{-1} and the occurrence of a narrow absorption band at 950 cm^{-1} [183].

Interesting results are also reported for the IR absorption related to ion exchange reactions, upon immersion of evaporated tungsten oxide films in different electrolytes [294,295]. The data give evidence for alkali ions replacing protons on pore surfaces of evaporated tungsten oxide films. Studies are done with Li^-, Na^- and K-containing solutions. The OH vibration becomes less pronounced upon treatment with different solutions, whereas the H–O–H scissor modes stemming from the molecular water are not significantly changed. In chemisorption experiments, it is proved that interior surfaces of evaporated porous tungsten oxide films are covered with acidic Bronsted sites (proton donors), which are identical with the sites for exchange between protons and alkali ions.

In crystalline tungsten oxide films, XRD can give useful structural information on the atomic arrangement and its modification upon colouration and bleaching. A detailed study has been carried out for films prepared by evaporation on substrates, with different temperatures followed by an annealing procedure in air [296]. It is shown

that photochromic processes form structures similar to tungsten oxide films coloured by electrochromic processes.

To obtain information on the structural changes during colouration and bleaching in heavily disordered materials, like "amorphous" tungsten oxide films, other X-ray techniques can be used [294]. In both EXAFS and XANES spectra colouration-depending effects can be traced [297]. Evaporated tungsten oxide films, coloured in aqueous H_2SO_4 electrolyte, exhibit local structural changes in "amorphous" films under colouration in X-ray absorption spectra [297]. A strong resonance near the WL_3 absorption edge is observed and is attributed to $2p \rightarrow 5d$ transition, i.e. the final state of the photoelectron is in the continuum with 5d atomic character, and the core hole at the 2p level is screened by other electrons. Colouration shifts the position of the edge by about 1.5–1.8 eV to lower energy, and the amplitude of the absorption is somewhat higher. It is suggested that the influence of the bonding effect with oxygen ligands is high, and the concentration of W^{5+} in the coloured film is not dominant, which explains the small observed shift evoked by the colouration. But a quantitative explanation is not available.

Clearly visible differences between the bleached and the coloured state are observed in EXAFS (extended X-ray absorption fine structure) curves. In the Fourier transform of the EXAFS signals, there are three clearly separated peaks, which are attributed to single-scattering processes in the first coordination shell formed by oxygen, to multiple-scattering contribution from the first shell, and to complex contribution from the signals in the second shell. The largest difference in the frequency of the EXAFS curves is observed in the first shell between transparent and coloured state [297]. The experimental data indicate that the colouration process creates W^{5+} states by electron insertion what leads to local structural changes, which mainly results in an increase of the average tungsten–oxygen bond length. Taking into account that only some of the tungsten ions transform into the W^{5+} state, the atomic separation of oxygen and tungsten have an average distance of 0.1767 nm for the transparent film, i.e. for the W^{6+} sites, and 0.1881 nm for the coloured film, i.e. for the W^{5+} states. The EXAFS results suggest that the tungsten–oxygen distance is increased, when the tungsten ion charge is decreased by the localization of one extra electron [297].

The agreement between the calculated EXAFS signal and the experimental data can be improved by including more than two components in the fitting procedure. Besides the distribution of the W–O distance for the W^{6+} and W^{5+} states, there are several more or less well-defined groups of distances which correspond to short terminal W=O groups, middle bridging W–O–W bonds, and long non-bridging $W–OH_2$ bonds. The total EXAFS signal from the first shell is the sum of the contribution from distances in each group. Including such an a priori known structural information with the model, a best-fit analysis is obtained by a four-component fit [297]. The calculated average tungsten-oxygen distance obtained by this approach is somewhat larger than in the two-component model, and is equal to 0.1881 nm for the W^{6+} state and 0.1992 nm for the W^{5+} state, i.e. the difference between the bond length of W^{6+} and W^{5+} is equal to 0.011 nm. It is suggested that the large changes of about 6% of the W^{6+}–O distance by the localization of one electron, i.e. by the

formation of W^{5+} ions, lead to a significant distortion of the lattice, and the displacement of the oxygen around tungsten ions under colouration corresponds to the formation of small-radius polarons [297].

To obtain structural information, RDF of coloured, highly disordered, evaporated tungsten oxide films are evaluated in the manner mentioned in Section 3.1.5 from the intensity curves of scattered electrons [180]. The film colouration is carried out by reduction in vacuum by heating up to $\sim 200°C$ for 15 min (Section 3.2.1), as well as by products of the chemical reaction between Zn and HCl (Section 3.2.3.1). The RDF of the chemically coloured film indicates a weak transformation of neighbouring atomic order structure. The basic octahedral configuration seems to remain. This may be concluded from the radii of the first coordination spheres (0.192 nm) identical for the coloured and the bleached films. But changes are obtained in the next coordinational environment. Instead of spheres with radii $r = 0.460$ nm (W–O) and $r = 0.541$ nm (O–O) for the bleached state, the new radii for the coloured film appear at $r = 0.517$ nm and $r = 0.606$ nm. Also the mean W–W distance seems to increase from $r = 0.373$ to 0.377 nm. It is conjectured that the colouration is associated with structural transformations from a state with non-linear arrangement of corner-sharing octahedra to a state with a planar arrangement of such octahedra [180]. It must be emphasized again that data obtained by the interaction of electrons with the film can contain artefacts (Section 3.1.5).

RDFs are also reported for thermochromically coloured films [180]. The data suggest that a transformation takes place, affecting the main structure unit determined by the mutual arrangement of oxygen and tungsten atoms in the WO_6 octahedra. The first coordination sphere with the radius $r = 0.192$ nm separates into two with $r = 0.158$ and 0.210 nm, which is interpreted as the axial deformation of the octahedron. The tungsten environment of six oxygen atoms is conserved, and the transformation in the second coordination sphere probably reflects the tendency of the formation of regular three-dimensional framework from octahedra. The shown data suggest further that transparent films stored in air with high humidity exhibit a similar RDF as films coloured by heating in vacuum. It is described that the "aging" effect may be accelerated by heating [180]. Since comparable data are obtained for films stored in high relative humidity ("aging"), the effect of colouration in vacuum is not clear.

3.3.3. Electronic configuration

In order to explain the colouration behaviour, especially the optical absorption in "amorphous" tungsten oxide films, several models for the electron configuration have been proposed and are discussed in Section 3.3.1. It is very difficult to form an opinion on the relevant mechanism in tungsten oxide films on the basis of macroscopic data. Microscopic information is necessary to select the right model.

Colouration-induced changes in the density of states of the valence band, the conduction band or the core levels can be obtained by UPS (ultraviolet photoelectron spectroscopy), XPS (X-ray photoelectron spectroscopy), or ESCA, XRF (X-ray fluorescence), or EELS (electron energy loss spectroscopy). UPS spectra of evaporated tungsten oxide films are taken with HeI photons (21.2 eV) [298]. For films deposited

by thermal evaporation, a strong peak at ~ 4.5 eV is observed, which mainly represents the occupied O 2p states in the valence band. A smaller peak near 7 eV is also detected. This second valence band peak completely disappears after exposing the evaporated film to 10^5 l oxygen [298]. Another characteristic feature of as-deposited films is the appearance of states in the gap. A narrow peak at 0.8 eV and a broader one at 2 eV below the Fermi level can be seen. After oxygen exposure, the peak at 0.8 eV in the gap disappears, too. By extrapolation of the onset of the valence band to zero intensity, the position of the top of the valence band relative to the Fermi level is determined to be 3.15 eV [298].

Annealing in vacuum, which is combined with the thermochromic colouration (Section 3.2.1), leads to an increase in the intensity of the second valence band peak at 7 eV in the UPS curves. It seems that thermochromic colouration of evaporated films in vacuum increases the oxygen deficit of the substoichiometric film, and for $T_a > 500^\circ$C spectras, are obtained that are interpreted as metallic films, which are most likely WO_2 [298]. Additionally, the annealing behaviour of the work function and also the position of the top of the valence band relative to the Fermi energy are given [298].

The valence and conduction bands of evaporated tungsten oxide films coloured by use of H_2SO_4 electrolyte are investigated by XPS. Fig. 65 reproduces data of as-deposited films, light-coloured (LC) or dark-coloured (DC) state [299]. A broad band

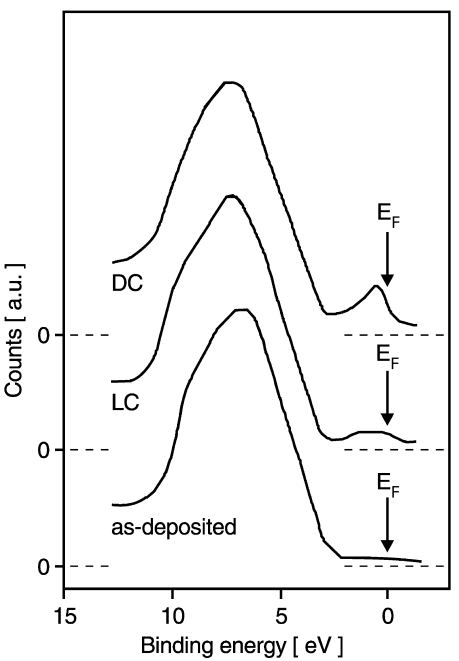

Fig. 65. X-ray photoelectron spectra for valence and conduction band electrons for evaporated tungsten oxide films in different colouration states. From [299].

lies between 4 and 10 eV, and a narrow peak, slightly below the Fermi energy, increases in intensity with the colouration. The feature between 4 and 10 eV is interpreted as the occupied O 2p dominated valence band, and the peak closely below E_F is caused by electrons occupying the otherwise empty lower part of the conduction band derived from W 5d orbitals or a defect band localized in the band gap [299]. Spectra in qualitative agreement with those in Fig. 65 have been reported in other works for colouration of evaporated films with hydrogen-containing electrolytes [180,246,299], as well as in such films coloured with L^+, Na^+, K^+-containing electrolyte [299,300]. Similar valence and conduction band data are obtained for films coloured with the Zn/HCl mixture [180]. Data are also available for evaporated tungsten oxide films after UV irradiation [301] or by electrocolouration. Fig. 66 exhibits, for comparison, the photoelectron count rate versus the electron energy for films before and after UV irradiation.

For evaporated tungsten oxide films, the obtained spectra of the valence and conduction band electrons seem to be independent of the colouration procedure. There is general agreement that the main feature between 4 and 10 eV is evoked by the O 2p-dominated valence band, and that the peak near the Fermi energy is considered attributable to the fact, that electrons occupy, during the colouration of the film, the otherwise empty lower part of the conduction band derived from the W 5d orbitals, or populate a defect band in the gap.

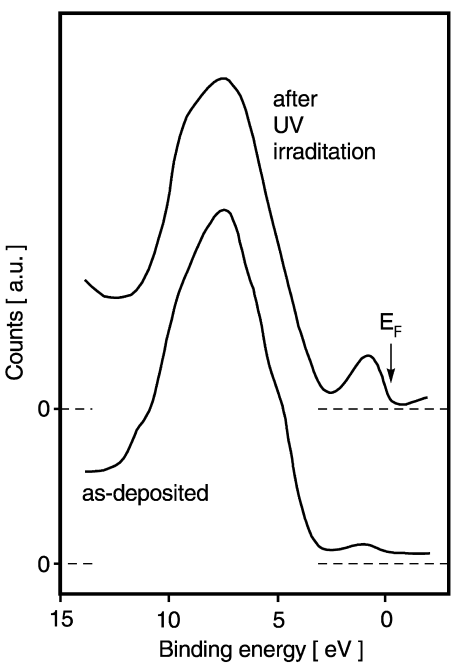

Fig. 66. X-ray photoelectron spectra of the films coloured by UV irradiation. From [301].

Also XRF spectra of evaporated films coloured with Zn/HCl mixture exhibit band features [180] in overall agreement with those shown in Fig. 65. The X-ray emission spectroscopy technique, which has been used for the determination of the partial density of O 2p states in the valence band, indicates a two-peak structure at 8 eV and ~ 9.5 eV, which shows differences depending on the colouration. These effects are discussed in terms of model clusters having octahedral coordination [180].

Since the induced electrochromic colouration is correlated with the transport of charge, changes in the valence of the elements in the tungsten oxide films can be expected. Such kind of information can be obtained from ESCA data. For that reason, different colouration states of our "standard" tungsten oxide films have been analyzed by ESCA [162,204,302]. Four typical ESCA spectra for a W 4f state are shown in Fig. 67. A tungsten oxide film annealed at 150°C for 20 h in air is used as a reference. The shown data indicate that, after annealing, the tungsten oxide layer is completely oxidized. The W $4f_{7/2}$ peak appears at a binding energy of 35.85 eV, the $4f_{5/2}$ one at 38.0 eV. Relative to the metal state (31.0 eV), the measured W 4f doublet is shifted to higher binding energies by approximately 5 eV and represents the oxidation state W^{6+}. Transparent, as-deposited tungsten oxide film is labelled $x = 0$ in Fig. 67. The slight broadening of the spectrum and the shoulder at a smaller binding energy suggests that the as-deposited film is not fully oxidized, i.e. the surface contains small amounts of W^{5+}. The two additional spectra in Fig. 67 represent coloured states with

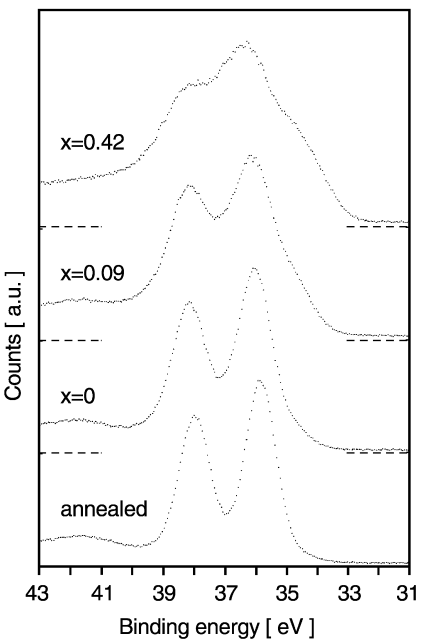

Fig. 67. ESCA spectra of W 4f doublet for annealed "standard" tungsten oxide, as-deposited film ($x = 0$), and in two colouration states with $x = 0.1$ and 0.4.

$x = 0.1$ and 0.4, respectively. The injected charge creates a new additional oxidation state with a different binding energy which is leading to more complex spectra by superimposing a W^{5+} doublet with a W^{6+}. Binding energies of the W 4f doublet, qualitatively similar to those in Fig. 67 have been reported also in other studies on films coloured with H^+, Li^+ and Na^+ [299], and for UV-irradiated films [301]. A large amount of consistent data has been gathered, particularly for evaporated films.

Deconvolution of the ESCA spectra makes it possible to obtain quantitative information on the relative number of tungsten atoms in different valence states. The procedure of analysing the spectra is described elsewhere [303]. In Fig. 68, the resulting correlation of W^{5+}/W_{tot} to the introduced charge is depicted. An almost linear dependence is observed for the amount of W^{5+} for $x < 0.25$. The shown error bars demonstrate the range of the different fitting solution. The fitting uncertainties increase with a more complex structure of higher x-values. A small offset can be recognized between the theoretical line and experimental data points. For the expected theoretical line, the assumption is used that all the injected charge should create additional W^{5+}.

For electrochromic coloured tungsten oxide films, two linear relationships exist versus the injected charge. One is shown in Fig. 47, where the extinction coefficient exhibits linear dependence for $x < 0.2$, while the second one is depicted in Fig. 68. Connecting these two results, it can be concluded that the extinction coefficient for each wavelength is proportional to the amount of W^{5+} species in WO_3. This is an experimental proof of the direct relationship between the W oxidation state and the optical absorption for WO_3 films and must be considerd in a model discussion of the electrochromic process.

For assessing the valence state of the tungsten ions, electron spin resonance (ESR) is also of large value, since W^{5+} ($5d^1$ configuration) gives the signal due to its unpaired

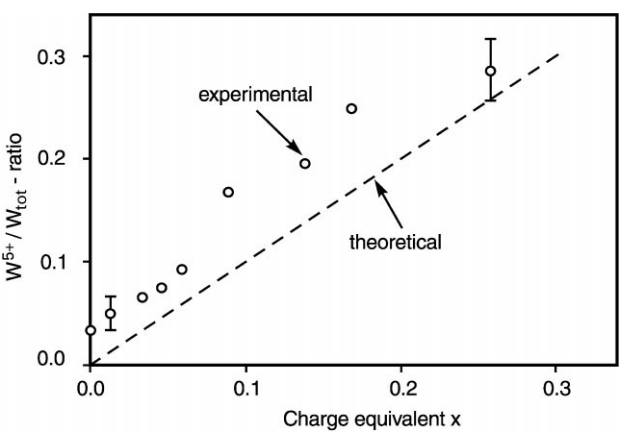

Fig. 68. W^{5+}/W_{tot}-ratio determined from ESCA measurements, as a function of the injected charge. The cycles are results of the data analysis of the ESCA spectra and the dashed line representing the expected theoretical dependence.

electron, whereas W^{6+} ($5d^0$ configuration) does not give any signal. ESR spectra of freshly prepared non-coloured tungsten oxide films generally contain one asymmetric signal around the g-factor 1.9 [182,206,304–306]. This signal belongs to Mo contamination in the tungsten oxide films. In some investigations, also a weak broad feature at $g \sim 2$ is reported, which is attributed to surface electrons [206,306]. Coloured "amorphous" tungsten oxide films show a broad asymmetric resonance line around the g-parameter 1.7 at temperatures from 77 K to RT. This signal can be unambiguously ascribed to W^{5+} ions and appears for the different colouration procedures described in Section 3.2, i.e. for films coloured by thermochromism, UV irradiation, electrochemical, by spill-over (hydrogen), or by selecting suitable preparation conditions [306]. The g-signal at about 1.7 is very weak, but exists also in virgin films. The W^{5+} ESR signal strongly depends on the amount of the sample and its colouring intensity. As depicted in Fig. 69, the intensity of the W^{5+} ESR signal varies linearly with the intensity of the optical absorption at the band maximum around 1.3 eV [182]. The ESR signal from the W^{5+} ions is detected only in the coloured state of "amorphous" tungsten oxide films and is not possible be measured from W^{5+} ions in the coloured state of polycrystalline and oriented polycrystalline material down to 10 K [304].

The presence of the ESR signal at $g \sim 1.7$, the ESCA doublet from W^{5+} ions in coloured "amorphous" films, and the direct proportionality between the W^{5+} ESCA

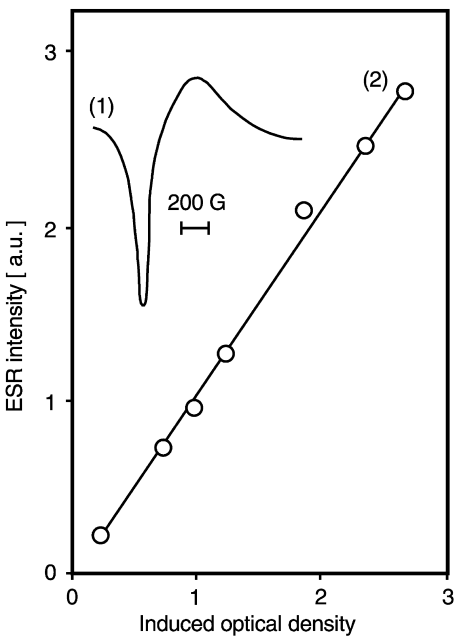

Fig. 69. The ESR signal of W^{5+} ion (1) and the relation between the intensity and the induced optical density of amorphous tungsten oxide films coloured to different levels (2). From [182].

and ESR signals, and the induced optical density allow to assume that chromogenic colouration in the tungsten oxide films is connected with the W^{5+} ions. It is guessed that the W^{5+} ion is located in octahedrally coordinated oxygen ligands with C_{4v} axial symmetry, and that, for observing charge transfer to a neighbouring W^{6+} ion – which is necessary for the colouration – only a few per cent of overlapping 5d t_{2g} states needed. It is affirmed that the axially distorted WO_6 octahedra with a terminal oxygen are a site for electron localization in coloured tungsten oxide films. Intervalence charge transfer transition may occur inside the clusters or between adjacent clusters linked by W–O–W bonds. It may further be guessed that the cluster consists of at least two types of WO_6 octahedra: one with a terminal oxygen and one without it, which represent axially distorted and generally distorted octahedral respectively. The large distance between equal orbitals in differently distorted octahedra gives broad localized states at the bottom of the conduction band and on top of the valence band. The appearance of colouration (or nonstoichiometry) produces electrons which fill these defect states. Since the introduced electrons do not seem to change the position of states in the band, the possibility of polaron formation in the tungsten oxide films is denied on the basis of ESR data [182]. In this model, the ground state of a localized electron in the 5d states is viewed as being localized on one tungsten site (W^{5+}), and the first excited state of such an electron overlaps with empty 5d states of the neighbouring tungsten ions (W^{6+}) [182].

The various results indicate that the electron structure of tungsten oxide films is changed by colouration. Independent of the colouration procedure, a band appears near the Fermi level and increases with colouration. Both ESCA and ESR exhibit a linear increase of the W^{5+} state with colouration. The inserted electrons increase the electron density in the tungsten oxide films, i.e. the Fermi level is moved upwards in the presumed rigid band scheme in Fig. 9. In this picture, the excess electrons must enter the t_{2g} band, when the material is transformed from a transparent to an absorbing state. When the electrons are extracted, the material returns to its original transparent state.

In another model, it has been concluded that the injected electrons occupy the conduction band after colouration, and that electrochromism of "amorphous" tungsten oxide films is due to an intraband transition between an electron injected in the conduction band and an empty state [300]. This explanation is derived from results of XPS and EELS investigation on evaporated tungsten oxide films coloured in lithium-containing electrolyte. An energy shift of the Fermi level, as a function of the amount of injected charge, is analysed, but the band gap between the top of the valence band and the bottom of the state below the Fermi level is the same, even if the film is coloured [300]. The interpretation is that the bottom of the state, which is observed below the Fermi level, is pinned and the top of the occupied state is shifted to low energies by colouration. It is guessed that the peak at the Fermi level, as seen in the coloured film, is caused by the electron near the bottom of the calculated conduction band, i.e. the injected electrons occupy the lowest state of the conduction band and the band becomes wider. For that reason, the unoccupied state of the conduction band is analysed by EELS. It is found that the signal of the final state of the transition from O 1s to W 5d, namely the bottom of the conduction band, decreases in the coloured

film, because the injected electrons fill the state even in the "amorphous" tungsten oxide film. The decrease in the intensity of this transition peak seems to be consistent with the appearance of the state just below the Fermi level observed in photoelectron spectroscopy after colouration. From the fact that the transition from the O 1s to W 5d is forbidden by the selection rules of EELS but is seen in the EELS spectra, the conclusion is drawn that the conduction band is hybridized with W 5d and O 2p and that the electron injected by the colouration may not be strongly localized at the tungsten atoms [300].

3.3.4. Composition and influence of the reservoir

The generation of colouration in tungsten oxide films can be connected with different transport mechanisms which, in part, are necessary for the charge balancing of the injected electrons. Thus, reversible electrochromism is usually explained by the double charge injection model described in reaction (1.1), which should lead to an increase in hydrogen content. In the case of using lithium-containing electrolytes, Li intercalation and deintercalation are analysed by SIMS [292], which is superimposed by a general upward tendency of permanent Li^+ incorporation. But the experimental results for the H^+ intercalation are not conclusive for the proposed model. On the basis of the double charge injection model, the increase in the hydrogen content in the coloured tungsten oxide films (δH/W) should be the same size as the charge equivalent ($x = e^-/W$).

To verify the double-charge injection model, our "standard" tungsten oxide films are coloured electrochemically in 2 M HCl with various charge equivalent x and are investigated by NRA. Deeply coloured films typically contain $x = 0.3$, and the *hydrogen* concentration should be changed by this amount ($\delta H/W = 0.3$). In Fig. 70,

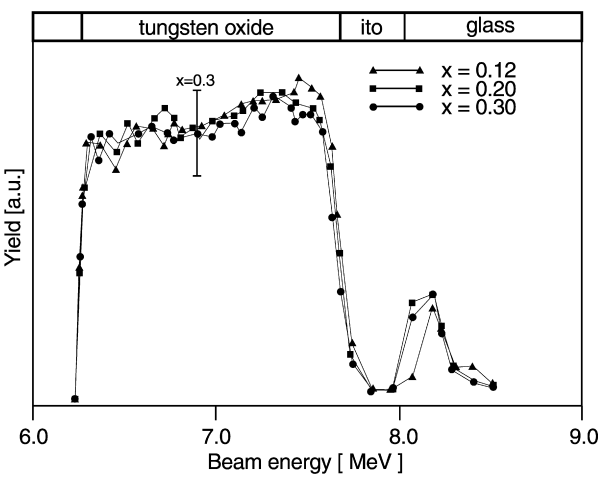

Fig. 70. Hydrogen depth profile of tungsten oxide films coloured in 2 M HCl liquid electrolyte with different amounts of injected charge. The increase in hydrogen concentration expected from double charge injection model of $x = 0.3$ is indicated.

hydrogen depth profiles are depicted, taken immediately after colouration. The analyzed hydrogen content in films with different colouration is identical within the experimental uncertainties. The expected change in the hydrogen concentration is indicated for $x = 0.3$.

For in situ gas-phase experiments (Section 3.2.3.2), similar results are obtained in the NRA investigations on "standard" films [271]. Only a small increase is obtained in the hydrogen content of the tungsten oxide film after colouration with 1% H_2/99% Ar gas. The small increase cannot explain the measured colouration effect and is interpreted as the adsorption of hydrogen at internal surfaces of the porous film. Comparable results are reported for electrochemical and gas phase experiments obtained with the ^{11}B-technique, another NRA method [206].

Another interesting observation is realized for our electrochemically coloured tungsten oxide films are stored in air. Fig. 71 exhibits that the films adsorb different amounts of water, depending on the colouration state. The data show the hydrogen content after storaging for one day in air with a r.h. of $\sim 60\%$. Starting with the same hydrogen content after the colouration, the deeply coloured films ($x = 0.24$) exhibit a higher H/W ratio than the nearly transparent film ($x = 0.04$). From the changes in energy loss, i.e. from the broadening of the spectra, it can be concluded that additional water is adsorbed in the film [207]. The reason for the different rate in water uptake is not clear yet.

Colouration of tungsten oxide films can be produced also by an *oxygen* deficit. A blue colour is reported for films prepared under specially selected deposition conditions [206,306]. Therefore, a second way of interpreting the colouration is that of an electrochemical extraction of a negative species, O^-, or by desorption of oxygen in the thermochromic and photochromic processes, with a coloured product being more substoichiometrical than WO_{3-z} [149]. For that reason, the oxygen contents in

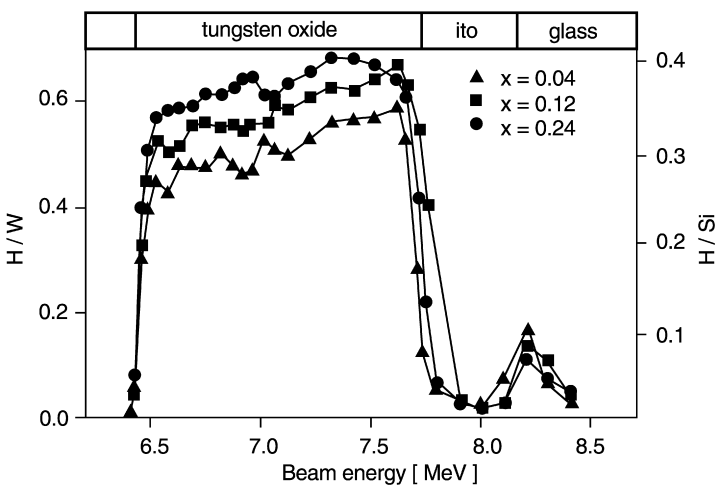

Fig. 71. Water uptake of tungsten oxide films with different colours stored for one day in air (r.h. $\sim 60\%$).

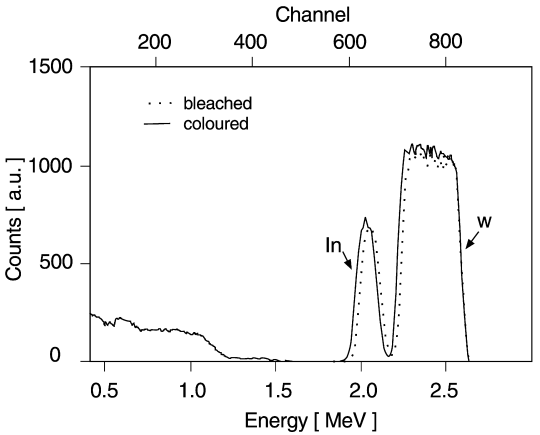

Fig. 72. RBS spectra for transparent tungsten oxide film (dashed line) and a deeply coloured sample (solid line).

the coloured and the bleached film are compared. Fig. 72 exhibits RBS data of "standard" films deposited by evaporation on ITO-coated glass. Between the bleached and coloured state, only small changes are observed which may be explained by the reduction of the oxygen content. For the used experimental set-up and given uncertainties, the δO/W ratio may be decreased by 0.25 for a film coloured with $x = 0.5$ [150,207].

The oxygen content of tungsten oxide films can also be analyzed from the O 1s signal at a binding energy of approximately 531 eV in ESCA. Fig. 73 depicts ESCA spectra of the O 1s region of films in different colouration states ($0.02 > x > 0.25$). With increasing colouration, the O 1s peak decreases. It seems that the oxygen content of the film surface is influenced by the electrochemical colouration. In Fig. 74, the changes in the O 1s yield are shown. The data are normalized to $x = 0$. With increasing x, the oxygen content decreases linearly [150]. The obtained data should not be overinterpreted, and a quantitative analysis should be avoided because of the experimental uncertainties, which are: (i) ESCA detects only about the uppermost 3 nm of tungsten oxide films; (ii) the films are coloured in aqueous electrolyte which can modify the surface, and (iii) the samples are transported in air to the UHV system for analysis, and during the transport reactions may occur at the surface. In that way the ESCA data can only give a tendency for the colouration process.

RBS data, which describe the bulk properties of the film, as well as ESCA measurements, which are surface-sensitive, suggest that tungsten oxide films coloured in HCl electrolyte change the O/W ratio, depending on the injected charge. With increasing colouration, the film substoichiometry seems to correlate with the film absorption.

In hydrogen-containing electrolyte, electrochemically coloured films do not seem change the OH or the H_2O content. This can be concluded from results obtained by

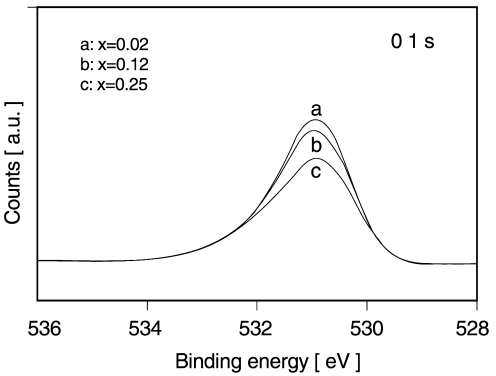

Fig. 73. ESCA spectra of the O 1s binding energy region for tungsten oxide films with different colouration.

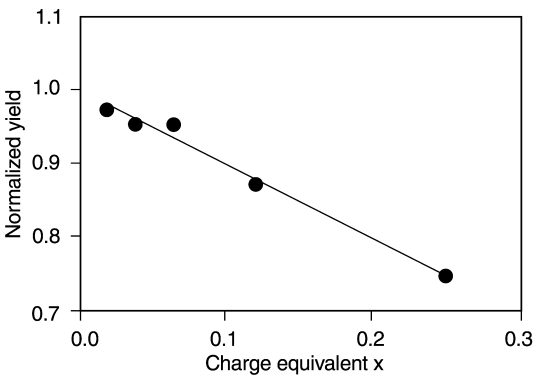

Fig. 74. Changes in the oxygen content, normalized to $x = 0$, as a function of the injected charge.

IR spectroscopy [294], described in Section 3.3.2, but also from NRA results in Fig. 70. But in studies using alkali-containing electrolytes, an increase in the O–H vibration mode intensity is reported [292]. In order to explain the data, a phenomenological model is formulated involving alkali ions replacing hydrogen on the internal surfaces, insertion of liberated hydrogen in interstitial positions in the tungsten oxide lattice, and adsorption of H_2O molecules next to the W=O bond. These processes seem to be different by the use of an hydrogen-containing electrolyte.

Certain conclusions on changes of the film composition can be drawn also from measuring the *reaction products leaving the film* during the colouration, or from the dependence of the colouration behaviour on the *surrounding medium* and its composition. The influence of the ambient environment can be compared to results obtained in the immersion experiments, where a diffusion is observed in an equilibrium state for the concentration of certain elements for the whole system, i.e. the contacting media create a reservoir for species which can be transported in and out of the film. Additionally, the ambient atmosphere influences the potential at the interface. For

example, hydrogen exposure greatly reduces the barrier height and favors the electron injection. These effects are discussed in Section 3.4.

A reduction of the oxygen concentration in tungsten oxide films is supported by the following reported experimental results. During the thermochromic colouration (Section 3.2.1), oxygen desorption is measured with a mass spectrometer [213]. This is supported by UPS data in which an increase in the oxygen deficit is detected during the heating of tungsten oxide films [298]. A similar result is obtained for open solid-state systems (Section 3.2.3.4). Mass spectrometer measurements show that O_2 left during the electrochromic colouration of the device [282]. The oxygen content in the film surface is decreased also by preferential sputtering during ion beam bombardment (Section 3.2.2.2), and irreversible colouration is obtained [229]. Comparable effects are produced by electron beam [229,236], where the oxygen content is reduced by electron-stimulated desorption processes (Section 3.2.2.3). Such non-reversible colouration is fairly similar to that of films obtained by special deposition conditions in which substoichiometric films are created (Section 3.1.6).

Another experimental fact, which is independent of the used colouration procedure, is the influence of the *reservoir* composition on the colouration processes. Thermochromic colouration (Section 3.2.1) is only observed in oxygen-free atmosphere, and oxygen is necessary for bleaching [163,213]. The intensity of the photochromic colouration (Section 3.2.2.1) is decreased in the presence of oxygen [216,217]. Especially for the bleaching process of UV-coloured films, oxygen exhibits a large influence. In our gas phase experiments described in Section 3.2.3.2, oxygen-containing gases are used for the bleaching [219,271]. The electrochromic efficiency is also influenced by the presence of oxygen in liquid electrolyte experiments [268]. The anodic reaction, i.e. the bleaching efficiency, is increased in aerated solutions. This is explained by taking into account the fact that the oxygen, dissolved in the liquid electrolyte, oxidizes the coloured tungsten oxide films, and water is produced [268]. From the results obtained by the very different colouration processes, it can be concluded that oxygen in the surrounding atmosphere increases the tendency to bleach coloured films.

But also hydrogen-containing environment of the film possesses a certain influence on the chromogenic behaviour. High relative humidities increase the probability of electrocolouration (Section 3.2.3.3) [125]. A faster and a larger response is observed for the photochromic colouration in the presence of water vapour and is also enhanced in the presence of alcohols (Section 3.2.2.1) [220–224]. In the gas phase experiments described in Section 3.2.3.2, beside hydrogen also the water vapour, which is called cocatalyzer, is necessary for the colouration [219,271]. The results can be summarized as follows: hydrogen-containing species favour the colouration process.

The reported data on the changes in film composition during the chromogenic colouration processes in the presence of oxygen- and hydrogen-containing reservoirs can be summarized:

- The oxygen content of the film is reduced by the colouration, and the presence of oxygen in the surrounding atmosphere decreases the colouration effect.

- No changes are observed in the hydrogen content of the film between the bleached and the coloured state, i.e. the total amount of hydrogen-containing species remains constant.
- The water content and the number of hydroxyl groups remain constant in the tungsten oxide film; but the presence of hydrogen-containing species in the reservoir is necessary for the colouration or enhancing the effect.
- Additionally, the number of the W=O bonds seem to decrease during the colouration of "standard" films, and the O–H species remain constant (but they increase by using alkali-containing electrolytes).

As described in Section 3.2, the wavelength-dependent changes in optical absorption are essentially independent of the used colouration technique. This experimental result suggests that the chemistry, underlying the optical properties should be basically the same, i.e. a *unified model* with similar reactions may prevail for the different colouration techniques, which explains the various findings on film composition and the influence of the composition of the reservoir.

Different models for material transport and for charge compensation can be used to explain the observed results. But certainly, the double charge injection model is not valid, because it suggests an increase of hydrogen content in the coloured material. The simplest way to explain the changes in the film composition during chromogenic colouration is

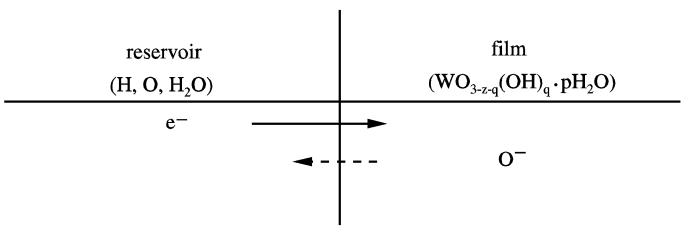

(R1)

The reservoir can contain hydrogen, oxygen, water, and dissociation products of water in different concentrations, and the tungsten oxide film consists of complex composites of $WO_{3-z-q}(OH)_q \cdot pH_2O$ [307], where the variables z, q, p are determined by the preparation conditions and film treatment. During the colouration process, an electron, e^-, is injected in the film and an oxygen ion diffuses across the film interface in the reservoir. In this model, the oxygen concentration in the bleached state is lower than in the coloured state, as suggested by RBS and ESCA, the hydrogen content and all other composition components in the film remaining constant. Charge neutrality is to be realized by the insertion of one electron in the film and extraction of one oxygen ion, which is probably removed from WO_{3-z-q} species.

Some results of not completely reversible colouration procedures may be explained by that simple mechanism. The models allow the explanation of the data obtained by thermochromism [213], by ion beam [229] and electron bombardment [229]. But this one channel model for oxygen cannot explain the measured hydrogen diffusion (Section 3.2.3.1) nor can it the injection of alkali species in the film by use of

alkali-containing electrolyte obtained with different experimental conditions. Additionally, the influence of hydrogen-containing vapour cannot be described.

To obtain a better agreement with the experimental results, hydrogen transport across the film interface has to be added. A more realistic description of the chromogenic colouration process may be given by

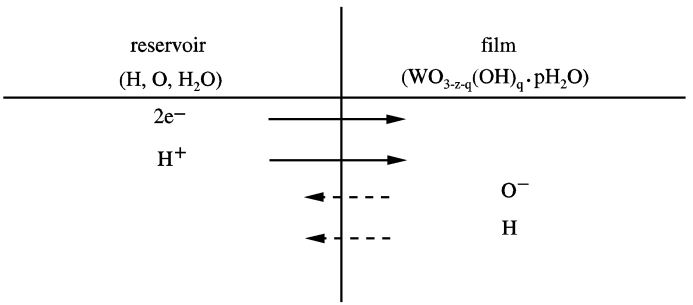

(R2)

This reaction also explains the measured changes in composition. Hydrogen diffusion takes place, but the H content is not changed in the film and the oxygen concentration is decreased in the coloured state by the amount indicated by our RBS studies on electrochemically coloured material. Results from films coloured by the use of alkali electrolyte suggest that, for example, Li^+ replacing H adsorbed at internal surfaces [292]. A similar mechanism may occur by the use of hydrogen-containing electrolytes. The injected H^+ ion replaces H adsorbed at internal surfaces, and the film behaves like a saturated "hydrogen alloy", and H diffuses out of the film across the film interface in the neighbouring reservoir. The second channel, the transport of H^+ in the film and H out of the film, may explain the unchanged hydrogen concentration determined by NRA. Charge compensation is realized in this model.

The influence of the reservoir composition can be demonstrated by the reactions (R1) and (R2). For example, thermochromism is observed only by heating in vacuum, i.e. the oxygen content in the reservoir is zero. If there is any oxygen in the reservoir, the oxygen desorption process is superimposed by oxygen adsorption, which avoid or hinder the colouration reaction. These influences of the oxygen in the reservoir are also to be found in photochromism and electrochromism with liquid and solid electrolyte, and especially in gas-phase experiments, where oxygen is used for bleaching.

The presence of hydrogen-containing species in the reservoir can be explained by the R2 reactions. While the H concentration in the film is unchanged, the hydrogen-containing species in the reservoir are necessary for charge compensation in the colouration process. The importance of hydrogen-containing species in the reservoir for the colouration is demonstrated for photochromism and the different types of electrochromism, i.e. in aqueous and solids electrolyte, gas phase experiments, and by the use of high electric fields.

The discussed models explain the changes in composition during the chromogenic colouration processes, and the second one describes additionally the influence of

oxygen and hydrogen in the surrounding atmosphere. But also structural changes are observed, which may be result of changes in composition, and the colouration is affected by water. The results on the changes in O–H vibration and also in the W=O mode are somewhat contradictory in the published papers. While, by the use of hydrogen-containing electrolyte, the O–H vibration mode seems to be constant, in experiments with alkali electrolytes, this feature is systematically increased with the inserted charge [292]. One way to explain that is the different rate of water uptake for coloured film, described above as being independent of the colouration process. But in the case where the increase in the OH vibration is correlated with the colouration process, this can be described simply by two mechanisms. One is the internal changes induced by the alkali uptake, and second one by a more complex species transport across the interface. Such processes may be given by

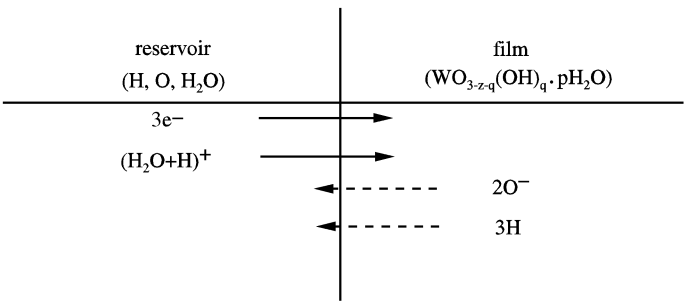

(R3)

In this reaction, $(H_2O + H)^+$ suggests the formation of a solvated proton on the surface followed by proton transport in the adsorbed phase of the "cocatalyst". For these processes, the hydrogen content continues to be constant, the oxygen content is reduced in the way found by RBS, and charge neutrality is given. The reduction of the W=O sites can be explained by reaction (R3), and also the increase in the O–H vibration. The insertion of a solvated proton (or alkalai) may give a hint why water or alcohol is necessary in the surrounding atmosphere for the colouration of the films.

3.4. Discussion

This section discusses and compares the various experimental findings, and summarizes the composition and structure models of as-deposited and coloured films. In not completely reversible processes oxygen desorption is found to be the predominant process. More complex reactions occur in the reversible processes, where defined charge transfer across the interface is necessary. The role of the interface potential in aqueous electrolyte experiments and in gas phase experiments is discussed, and the Fermi level concept for different media is described. The influence of the contacting medium as a reservoir for charge-compensating particles is presented.

As-deposited tungsten oxide films produced by evaporation are substoichiometric (WO_{3-z}) and contain water in different forms. One way to describe the complex

composition of the films may be $WO_{3-z-q}(OH)_q \cdot pH_2O$ [307,320]. The amount of water uptake in the films depends on the deposition conditions which create a low film density, and on the post-deposition treatment. Tungsten oxide films appear to be "amorphous" in TEM, Raman and XRD investigations, but results of X-ray scattering suggest a local, i.e. nearest neighbour order. A proposed structural model is based on hexagonal $WO_3 \cdot 1/3\ H_2O$, in which three-, four-, and six-membered rings of WO_6 octahedra create nanostructure clusters with a size of approximately 1.6 nm. The substoichiometry of tungsten oxide films is consistent with the structural assumption. The distance between the clusters is ~ 2.4 nm and explains the observed density for films deposited at RT. Additionally, the model is supported by the fact that in the vapour of the evaporated material, a high number of $(WO_3)_3$, are analysed. Since the size of the clusters with a local order is influenced by the partial pressure of water and substrate temperature, the number of trimers are enlarged under technically relevant conditions, where generally a high partial pressure of water is present. The optical property of as-deposited film can be ascribed as a semiconductor with an indirect, allowed transition with a bandgap of $E_g \sim 3.25$ eV.

The chromogenism of tungsten oxide films produced by evaporation is affected mainly by two factors. That is the nanostructure clusters which possess a nearest neighbour order and create low-density films. The low-density nanocomposited structure is conducted to intercalation/deintercalation processes of mobile species during the chromogenism. The second factor is the film composition, especially the non-stoichiometry in the tungsten oxygen framework with the respective hydrogen content in the film. The substoichiometric tungsten oxide films can be described by WO_{3-z} with $0.15 < z < 0.35$ and with the hydrogen tungsten ratio of $0.2 < 1.8$. A decrease in z decreases the colouration efficiency [252], while higher H/W ratios correspond to higher efficiencies [206].

Various colouration techniques can be used to change the optical properties of tungsten oxide films (Section 3.2). Most of the described processes are reversible, i.e. the film can be cycled for many times between the coloured and bleached state. But some of the processes are *not completely reversible*. For example, electron beam irradiation creates a colouration, which is associated with electron-stimulated desorption of oxygen and increases the oxygen substoichiometry with irradiation time [229]. Ion beam irradiation also produces non-reversible colouration, but the effects are more complex. They depend on the type of ions ($^1H - {}^{70}Ga$) and the used accelerating energies (4 keV–30 MeV), and the ion dose (Section 3.2.2.2). Ion implantation is suggested for Na^+ ions [227], while Ar^+ ions in the same energy range induce oxygen-deficient, substoichiometric films by preferential sputtering [229]. Also colouration evoked by temperature does not seem to be totally reversible. During the heating of films, a substantial loss in mass starts at about 50°C, which is attributed to the desorption of water [208]. Also oxygen desorption is measured during the annealing [213]. But no large changes in the O/W ratio are found by RBS [115]. An increase in the oxygen deficit of substoichiometric film is found in UPS [298]. It can be guessed that in the not fully reversible processes an increase in oxygen deficiency is created, which may be described by the one channel model (R1) for chromogenic colouration of evaporated tungsten oxide films.

The reason for the non-reversibility may be different, but it seems that the basic octahedral WO_6 building blocks are probably damaged during temperature treatment and by the interaction with electrons and ions. Electron bombardment as well as ion bombardment can lead to amorphization of the film, i.e. they can destroy the nanostructure of the clusters in the film, which is necessary for reversible chromogenic processes. In the thermochromic process, a transformation seems to take place, affecting the main structure unit. This can be concluded from RDFs in which the first coordination sphere is separated in two, which is interpreted as a strong axial deformation of the octahedra [180]. During the thermochromic process, the loss of water in the film produces a densification and creates new nanostructure which allows only a partial bleaching in a long period of time. This means, in the model given in the schematic representation (R2), that for temperature $T_a < 280^\circ C$ H_2O desorbs [208], and for temperatures $T_a > 300^\circ C$ water fragments $(OH)_q$ which are reaction products of W–OH condensation [208] are expelled. It seems that, in nonreversible chromogenism, oxygen desorption induced by electrons, ions or temperature is a predominated process. The transfer of material occurs only in one direction across the interface. It is postulated that oxygen desorbs [163,214] and the partial reversibility in colour takes place by oxidation at higher temperatures.

For *reversible* chromogenism, the main features of the structure and the composition remain far-reaching unchanged. Two injected electrons, described in reaction (R2), are combined by small changes in composition, i.e. the high oxygen concentration in the tungsten oxide film is reduced by a small amount only, and the hydrogen content remains constant. The phenomenological model in reaction (R2) also satisfies the current-doubling effect observed in the presence of water and alcohols [223], and it explains the two channels for the colouration and bleaching process found in electrochromism and photochromism [217,218,253,254].

Whether the injection of two electrons in reaction (R2), which is responsible for the colouration, is combined by a measurable local structural distortion of the lattice and the formation of a polaron, depends probably on the properties of the as-deposited state. It is reported that a lack of oxygen in the film and an increased nanocrystallinity (and probably the film density) enhance the oscillator strength of small-polaron absorption [252]. This may explain to some extent the contradictory results found in ESR [182] and EELS [300], which denies the formation of small polarons, while EXAFS results [299] suggest the displacement of the oxygen around tungsten ions with the corresponding formation of small polarons.

In most of the reversible processes, a defined charge transfer process occurs across the reservoir/tungsten oxide interface, i.e. the *potential at the interface* plays a dominant role for the chromogenism, especially for the electrochemical processes where external voltage is applied, or in the spill-over experiments, but also in the photochromic processes. Therefore, it is necessary to compare the potentials for the very different experimental situations and the respective energy levels, both in the solid and in the reservoirs.

To bridge the gap between the terminology of solid-state physics and electrochemistry, the "Fermi level" concept was introduced in liquid electrolytes for the discussion

of electron transfer processes at the interface between solid and electrolyte [285]. It was considered as a synonymous expression of the electrochemical potential of electrons. A similar theory is proposed for the chemical modulation of the Fermi level of a solid in gas phase experiments, where the partial electron transfer between a gas molecule and a semiconductor is explained [308]. In this model, a charge-transfer complex is formed between the gas molecule and an ionizable acceptor or donor state in the solid, which results in a shift of the work function. There is a formal analogy between this two relationships, which describe the potentials in the reservoir and the Nernst equation.

The situation at the interface gas reservoir/chromogenic film, for instance, may be described as follows: a gas molecule (e.g. H_2, O_2) from the reservoir contacts the surface and dissolves in an electronically conducting solid phase (Rh or tungsten oxide film), according to Henry's law. The concentration of the gas in the solid, $g(s)$, is given by the solubility coefficient α and by the partial pressure of the gas p_G, with

$$g(s) = \alpha \cdot p_G. \tag{3.15}$$

Gas molecules are electrically neutral. However, upon entering the solid interface, they dissociate and they exchange "partial electron density" (δe) with the matrix according to the equilibrium; δe is the number of moles of charge transferred from the gas to the matrix.

In the following, it is assumed that the tungsten oxide film is an n-type semiconductor with a discrete energy band structure. If the gas is an electron donor (i.e. a Lewis base) like hydrogen, the charge density is transferred to the conduction band, while for an electron-accepting gas (i.e. a Lewis acid) like oxygen, the charge-transfer complex is formed between the gas and the valence band. In either case, the direction in which the charge flows is governed by the difference of the electron affinity of the solid and the gas. This interaction can be viewed as a normal doping process, where the distribution of electrons is given by the Fermi–Dirac statistics [308].

The affinity of electrons for the gas is described by the so-called Mullikan electronegativity, χ, which is the average value of the ionization potential, I_P, and the electron affinity, E_a,

$$\chi = 0.5(I_p + E_a), \tag{3.16}$$

while the affinity of electrons for the solid, the Fermi level E_F, is the bulk component of the work function ϕ, with

$$\phi = E_F - \eta e, \tag{3.17}$$

where the second term is the work required to transfer electron across the surface dipolar layer η. It has been shown experimentally that the charge transfer is proportional to the difference between the Fermi level and the Mullikan electronegativity [309].

At a semiconductor electrolyte interface, a potential drop not only occurs across the Helmholtz layer, but also across the space charge region of the semiconductor as

a result of the low carrier density in semiconductors. The potential across the Helmholtz layer is mostly independent of the applied potential and can be changed by altering the pH value of the electrolyte [317,319]. The Helmholtz layer also remains unchanged, if a redox system is added to the electrolyte, provided that the interaction with the semiconductor is weak. Equilibrium is achieved as soon as the electrochemical potential, the Fermi level of the electrolyte and semiconductor, is equal throughout the system. A corresponding potential drop occurs across the space charge region in the semiconductor surface leading to a certain band bending [310–312]. Similarly as in solids, energy levels of a redox system are empty or are occupied by electrons. However, the energy position of empty and occupied state can be considerably different, due to the strong interaction of the redox system with the solvent. At equilibrium, the relative position of the energy levels of both sides of the interface can be measured versus a reference electrode (e.g. NHE). An externally applied potential, necessary for the colouration, only varies the potential across the space charge layer and, consequently, the band bending. A certain potential is required to make the energy bands flat (flat-band potential). The electron transfer across the interface occurs when levels of equal energy exist on both sides of the interface.

The fairly complex situation of the potentials in the respective interface is summarized in the schematic representation in Fig. 75. Different potential scales are shown, which belong to the different experimental situations. All potentials are connected to the absolute scale, the vacuum level, which is the usual scale in

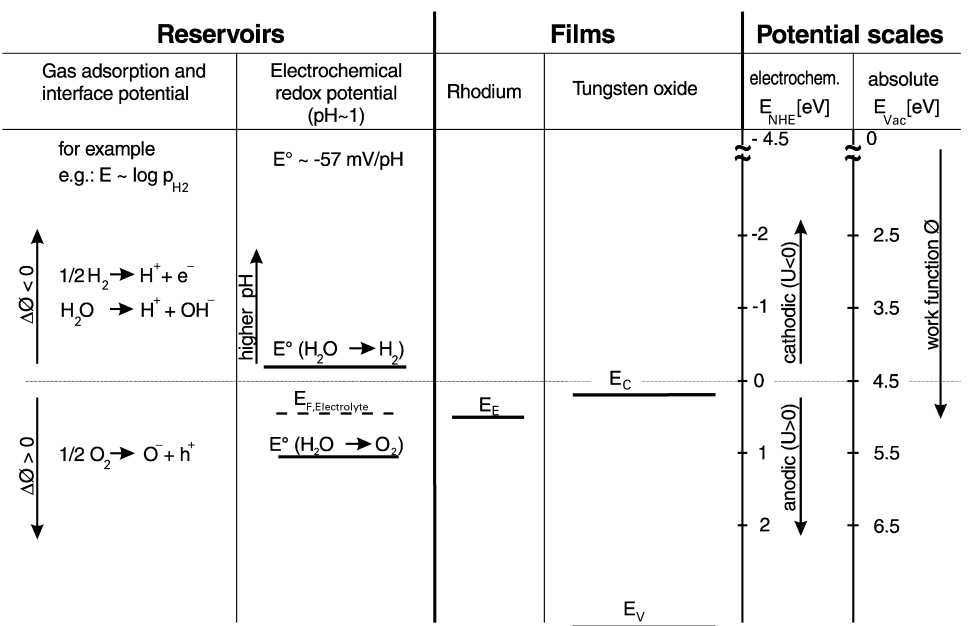

Fig. 75. Band edge positions of tungsten oxide, Fermi level E_F of Rh, and potentials in the reservoirs.

solid-state physics. Relative to the vacuum level, the Fermi energy E_F of an electronic conductor, particularly of a metal, is given by a negative work function, a quantity which can directly be measured by the threshold energy of photoelectron emission into a vacuum [313]. The band edge positions of the conduction and valence band of the tungsten oxide film are shown [311,312], and also the Fermi level for the Rh, the catalyzer necessary in the gas-phase experiments is given [270]. The depicted energies have to be considered as bulk energies, i.e. they do not represent the exact film interface values.

In electrochemical experiments, the potentials are related to the potential of a reference electrode, mostly to the normal hydrogen electrode, NHE [270,285,310,312], which is shifted by 4.5–4.7 eV relative to the vacuum level. In the electrochemical terminology, a cathodic polarization, which is necessary for colouring tungsten oxide films, means a shift of the potential to a lower work function, while anodic polarization shifts the potential to a higher work function.

A further group of data describes the situation in the reservoir. These are divided in electrochemical quantities which belong to aqueous electrolytes and gas phase data. In electrochemical reservoirs, the redox potentials are given for small pH. The potential of the redox reaction follows the Nernst equation in its pH dependence, i.e. low pH corresponds to a high work function, and high pH to a low work function [312]. In the column for the gas-phase data, no discrete values are given, but tendencies are. It is known that the adsorption of H_2O and H_2 on metals decreases the work function, while the adsorption of oxygen increases the work function, depending on the coverage [314,318], i.e. the adsobates modulate the potential in the interface in a way similar to an applied external voltage [314,318]. At room temperature, the gases (H_2, O_2, H_2O) dissociate on catalyzer, as well as on oxides. For that reason, some possible dissociation products are given in the brackets. This indicates only that in the reservoir a large number of species are available which can deliver charge. Thus, in the interaction with the solid-state surface, water and hydrogen can be described as an electron donor (Lewis base), and oxygen or the dissociation product of water, the hydroxyl groups, are electron acceptor (Lewis acid) [315]. In the Lewis acid – base picture, hydroxyl groups, tend to occupy electron-rich adsorption sites, or on ionic surfaces, they may prefer the ionic sites.

It is generally accepted that the variable absorptance in tungsten oxide film is caused by a change in the electronic structure, which is correlated by a change in the oxidation state of W from the W^{6+} to W^{5+}. This can be created either by an internal charge transfer or by a charge carrier transport across the interface. The situation of semiconducting tungsten oxide in contact with aqueous electrolytes, depicted in Fig. 76, has been well investigated so far [311]. A potential drop occurs across the Helmholtz layer and in the space charge region, leading to a band bending of the energy level in the tungsten oxide films [311,312]. For the colouration, electrons have to be transferred between solid and electrolyte, i.e. an equilibrium of both energy levels has to be achieved by an applied external voltage which changes the potential in the interface and the corresponding band bending.

For the colouration by gases, no external voltages have to be applied. The situation of the potential at the catalyzer/tungsten oxide interface is schematically depicted in

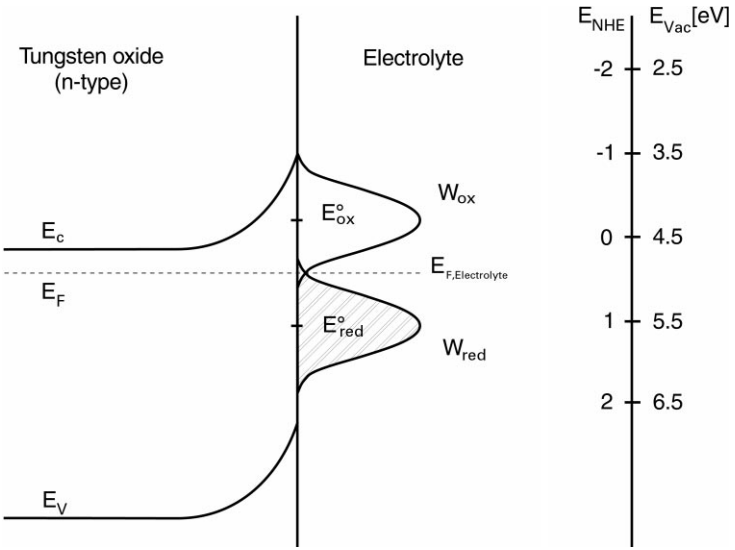

Fig. 76. Energy states of tungsten oxide/electrolyte interface.

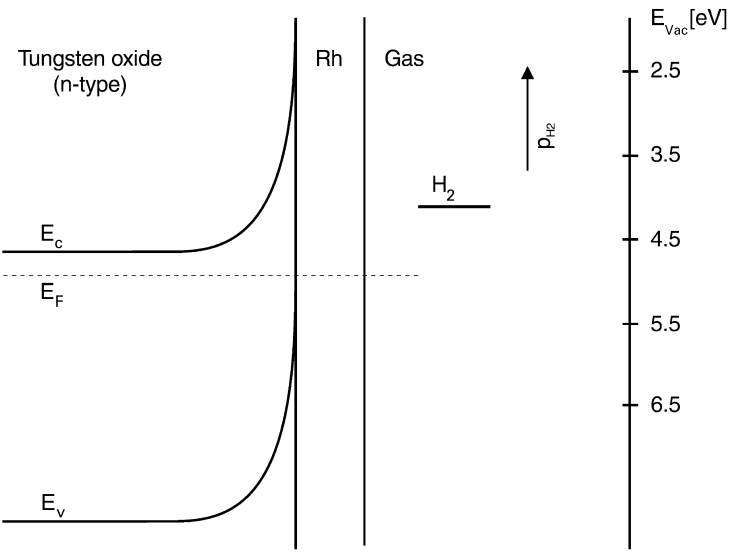

Fig. 77. Energy level diagram for the Rh/tungsten oxide interface region.

Fig. 77 for colouration evoked by gases. The barrier height of the Schottky contact is determined by the conduction band of tungsten oxide and the Fermi level of rhodium. By an exposure with hydrogen, the dissociation of H_2 at the Rh surface is followed by a rapid diffusion of H to the Rh/oxide interface where a dipole layer is created, which

results in a field across the interface, which in turn produces a sharp drop in the conduction band edge. This potential drop lowers the energy of the conducting band edge relative to the Fermi level in Fig. 77 and allows the charge transfer of electrons for the colouration of tungsten oxide. The observed dependency of the optical density on the hydrogen concentration, depicted in Fig. 55, indicates that the H-induced potential drop, in the interface of the Schottky barrier, can be described by analogy to the Nernst equation.

These considerations of the electron potentials in the film interfaces are helpful to understand the influence of the concentration of various species on the colouration. For instance, the hydrogen concentration of the gas [308] or of the electrolyte determines the "Fermi level" [285] of the contacting medium via the Nernst equation, i.e. the H concentration influences the potential in the interface and controls the colouration and bleaching process in photochromism and electrochromism. But the medium contacting the film surfaces operates not only as a potential modifier, it also creates the reservoir for particles, injected or ejected in tungsten oxide films during chromogenic reactions. The population of the reservoir and the influence on the chromogenism of tungsten oxide film may be understood in a very simple way: All elements in the contacting atmosphere can be principally transported in the film and different film components in the reservoir. Some species can support colouration (e.g. hydrogen, which is an electron donor) and increase the colouration probability, and other elements in the contacting medium – which can also diffuse from the reservoir in the film during the colouration (e.g. oxygen) – will decrease the colouration probability, i.e. the absence of hydrogen favours the bleaching, because no species for the colouration process are in the reservoir and the presence of hydrogen supports colouration.

For oxygen in the reservoir contacting the film interface, very similar arguments can be used, as described for the hydrogen above. Oxygen in the gas phase induces bleaching in photochromic, thermochromic, and electrochromic reactions, because oxygen diffuses in the film, removes an e^- from coloured W^{5+} state, and can occupy oxygen vacancy, which also gives a certain contribution to the film colouration, as can be concluded from substoichiometric films. Tendencies for the bleaching in the presence of oxygen in the surrounding atmosphere can be found in results obtained by photochromism, thermochromism, and also electrochromism, and especially in the gas phase experiment. The transport of oxygen shown in reaction (R2) during the colouration also explains RBS findings, which indicate that for one injected electron 0.5 O is removed.

The role of water in such processes is very crucial. From adsorption experiments of water on solid-state surfaces it is known that adsorption of water lowers the work function and electron affinity at the interface of metals and semiconductors, respectively [241,315]. The changes in the potential at the interface may influence the charge transfer process across the interface by modifying the potential barrier. But the role of water in the reservoir is certainly not only that of a potential modifier; it is much more complex. One way to explain the influence of water (or alcohols) on the colouration reaction is illustrated in reaction (R3), which describes the transport of a proton in its hydration shell. But it is also reported that water may dissociate at a catalyzer and

oxide surfaces [315]. If that occurs, OH^- and H^+ are present at the surface. The OH^- ions generated by the dissociation of the adsorbed water may be oxidized and yield to OH radicals, and the electron is injected into the conduction band of the tungsten oxide film and can contribute toward the colouration. The decomposition of water by irradiation with light and into hydrogen and oxygen is also reported for liquid electrolyte in contact with tungsten oxide [311,316]. This photoelectrolysis starts by the generation of electron–hole pairs by irradiating with UV light. The hole weakens the O–H bond of water molecules, which leads to the decomposition into proton and highly reactive oxygen atoms. Water is inevitably present in the solvent or is adsorbed at the internal surface of the tungsten oxide films. Thus, H^+ ions are generated through the oxidation of water and accumulate in the films, together with the photogenerated or catalytically generated electrons; hence, water can cause some chromogenic effects.

4. Summary

This section summarizes the chromogenism of coatings, with the focus being on optically active tungsten oxide films. The chemical composition and the structure of tungsten oxide films deposited by evaporation are given briefly. Various colouration procedures are mentioned. The most probable models describing the change in optical densities are cited, and the proportionality of W^{5+} to the colouration is given. Different channels for reversible chromogenic colouration are named.

Chromogenic behaviour of coatings is observed for a broad spectrum of materials, and various mechanisms are responsible for the changes in the optical properties in the visible wavelength range. Very different deposition conditions and layer designs can be used to prepare organic and inorganic, optically active thin-film systems altering their optical characteristics as a function of external conditions. Numerous physical and chemical processes are interrelated during the colouration and bleaching reaction, i.e. the optical switching process is highly complex.

The various mechanisms, reactions, and processes of optically active coatings are demonstrated on tungsten oxide films, which are the materials best investigated so far. Especially, tungsten oxide films deposited by evaporation are considered in larger detail in this case study, because they offer, in principle, nearly "ideal" chromogenic behaviour, and a wealth of information is available. As-deposited films are sub-stoichiometric and contain water or water fragments. No long-range order exists in the layers, but a short-range order is indicated by SAXS, and a nanostructure is proposed based on hexagonal $WO_3 \cdot 1/3\ H_2O$ in which three-, four- and six-membered rings of WO_6 octahedra form the local order. This structural model is consistent with the substoichiometry and the low density in the film. It can explain also the terminal W=O bonds and the presence of water. The optical properties of the transparent as-deposited material can be described as a semiconductor with an indirect, allowed transition ($E_g \sim 3.25$ eV).

Numerous procedures are used for the colouration of tungsten oxide films. The obtained spectral absorption is essentially identical, i.e. it is fairly independent of

the colouration technique for nanocomposited materials deposited at low substrate temperature. Ten different procedures are described which create the typical blue colour in tungsten oxide films. They may be divided in two classes. Colouration created by preparation, by temperature, ion beam, and electron beam irradiation belongs to the first class of not completely reversible processes. The observed absorption is associated with an increased oxygen deficit, and the basic octahedral WO_6 building blocks are probably damaged by these colouration procedures.

The second type, the reversible chromogenism, is observed via different electrochromic procedures and also via the photochromic technique, as demonstrated for very thin layers. In the electrochromic processes, potentials control the reactions. External voltages are applied for electrocolouration, and in experiments with solid-state or liquid electrolytes. Internal changes in the involved potentials are evoked by the gases in the spill-over technique and local fields produced in Zn/HCl or In/H_2SO_4 mixture experiments. The reversible colouration reactions exhibit a strong influence on the water content in the neighbouring reservoir, i.e. high water content is a favourable condition for colouration.

The changes in the optical density during the colouration are best described theoretically by the small polaron concept, or by the intervalence charge transfer model. Local structural distortion of the lattice and the formation of a polaron are more pronounced in films with high oxygen deficit and an increased nanocrystallinity. Some experimental results suggest that the tungsten–oxygen distance is increased by the localization of one extra electron. Investigations on evaporated films with high oxygen content and/or "amorphous", less dense structure exhibit no measurable changes in structure, probably because the oscillator strength of small-polaron absorption is decreased, i.e. obtained results depend remarkably on the film preparation conditions. For similar reasons, the intensity of terminal W=O vibrations is decreased by colouration of "standard" films, while an increase is observed for films with a higher degree of crystallinity.

The various colouration procedures produce doubtlessly the same changes in the electronic structure of tungsten oxide films. The changes in the optical density are directly proportional to the amount of W^{5+}, as analysed on "standard" films and other materials by different methods. Independent of the colouration procedure, a band appears near the Fermi level and increases with the colouration. The inserted electron increases the electron density, i.e. the Fermi level is moved upwards and the excess electrons enter the otherwise empty lower part of the 5d t_{2g} band or a defect band localized in the band gap.

The colouration reactions of the various procedures are explained by a unified model with a minimum of two different reaction channels. The double charge injection model in the simple version is not valid, because the generation of colour is not connected to an increase in hydrogen concentration in the tungsten oxide film. Beside electron injection responsible for the colouration of tungsten oxide films by the creation of W^{5+}, a path for material transport for charge compensation has to be considered. Channel one is responsible for the reduction of the oxygen content in the tungsten oxide films during colouration. Oxygen desorption or ejection is sufficient

for explaining the effects of not completely reversible colouration techniques. In the reversible processes, a second channel is active. Charge-carrying hydrogen-containing species, i.e. a proton or a solvated proton, are injected in the film, but the same amount of electrically neutral hydrogen diffuses out of the film. In this way, the hydrogen concentration continues to be constant during the colouration.

The two-channel models also explain the influence of the composition of the reservoir. The tungsten oxide films and the reservoir have to be considered as one system, i.e. as a unit which has the tendency to equalize the concentration of species that can diffuse in the whole system. Therefore, the presence of hydrogen or water in the reservoir is favourable for the colouration processes of channel two, while oxygen in the reservoir hinders the colouration reaction of channel one. The potential in the interface reservoir/tungsten oxide film plays a dominant role in the various electrochromic colouration techniques. A unified view on absolute potential scale explains the potentials in different processes in photochromism and electrochromism in which the reservoir consists of gases, liquids or solids. The influence of the interface potential on the space-charge layer of the tungsten oxide film is described in terms of band bending.

References

[1] C.M. Lampert, C.G. Granqvist (Eds.), Large-Area Chromogenics: Materials and Devices for Transmittance Control, vol. 54, SPIE Opt. Eng. Press, Washington, 1990.
[2] C.G. Granqvist, Handbook on Inorganic Electrochromic Materials, Elsevier Science B.V., Amsterdam, 1995.
[3] B.W. Faughnan, R.S. Crandall, P.M. Heyman, RCA Rev. 36 (1975) 177. R.S. Crandall, B.W. Faughnan, Appl. Phys. Lett. 28 (1976) 95.
[4] V. Wittwer, O.F. Schirmer, P. Schlotter, Solid State Commun. 25 (1978) 977. O.F. Schirmer, V. Wittwer, G. Baur, G. Brandt, J. Electrochem. Soc. 124 (1977) 749.
[5] S.K. Deb, Philos. Mag. 27 (1973) 801.
[6] J.V. Gabrusenoks, P.D. Cikmach, A.R. Lusis, J.J. Kleperis, G.M. Ramans, Solid State Ionics 14 (1984) 25.
[7] S. Hashimoto, M. Masuoka, J. Appl. Phys. 69 (1991) 933; J. Electrochem. Soc. 138 (1991) 2403.
[8] B.W. Faughnan, R.S. Crandall, in: J.I. Pankow (Ed.), Display Devices, Topics in Applied Physics, vol. 40, Springer, Berlin, 1980, p. 181.
[9] P. Gérard, A. Deneuville, R. Courths, Thin Solid Films 71 (1980) 221. A. Deneuville, P. Gérard, J. Electron. Mater. 7 (1978) 559.
[10] T. Nanba, I. Yasui, J. Solid State Chem. 83 (1989) 304.
[11] See for example [1] and references therein.
[12] F.J. Morin, Phys. Rev. Lett. 3 (1959) 34.
[13] M.F. Rubner, Polym. Mater. Sci. Eng. 54 (1986) 665.
[14] J.H. Day, R.D. Willett, in: C.M. Lampert, C.G. Granqvist (Eds.), Large-Area Chromogenics: Materials and Devices for Transmittance Control, vol. 54, SPIE Opt. Eng. Press, Washington, 1990, p. 122.
[15] O. Inganas, G. Gustafsso, W.R. Salaneck, J.E. Oesterholm, J. Laakso, Synth. Met. 22 (1988) 395.
[16] S.D.D.V. Rughooputh, S. Hotta, A.J. Heeger, F. Wadl, J. Polym. Sci. 25 (1987) 1071.
[17] J.S. Moore, S.I. Stupp, Macromolecules 19 (1986) 1815.
[18] T. Sato, Y. Yutani, T.J. Otsu, Macromol. Sci. Chem. A 23 (1989) 749.

[19] A.J. Lovinger, Macromolecules 19 (1986) 2657.
[20] E. Hadjoudis, M. Vittorakis, I. Moustakoli, Tetrahedron 43 (1987) 1345.
[21] D.A. Hinckleg, P.G. Seybold, J. Chem. Educ. 64 (1987) 362.
[22] H.R. Jaw, M.A. Mooney, T. Novinson, W.C. Kaska, J.I. Zink, Inorg. Chem 26 (1987) 1387.
[23] V. Fernandez, F. Jaque, J.M. Calleja, Solid State Commun. 59 (1986) 803.
[24] G.V. Jorgenson, Electrochromic and thermodynamic materials for solar energy applications with emphasis on niobium and vanadium oxides, Lawrence Berkeley Laboratory Report, LBL 18299 Berkeley, USA, 1984.
[25] G.V. Jorgenson, Thermochromic materials research for optical switching films, Department of Energy Report, DOE/SF/15295-T1 San Franzisco, USA, 1986.
[26] A.N. Kozlou, L.A. Maksimow, Sov. Phys. JETP 21 (1965) 790.
[27] J.C. Hubbard, Proc. Roy. Soc. A 276 (1963) 238.
[28] N.F. Mott, Metal–Insulator Transitions, Taylor and Francis Ltd., London, 1974.
[29] D. Adler, Solid State Phys. 21 (1974) 1.
[30] K.A. Kahn, G.A. Niklasso, C.G. Granqvist, J. Appl. Phys. 64 (1988) 3327.
[31] Razavi, T. Hughes, J. Antinovitch, J. Hoffman, J. Vac. Sci. Technnol. A 7 (1989) 1310.
[32] K.A. Kahn, C.G. Granqvist, Appl. Phys. Lett. 55 (1989) 4.
[33] F.C. Francine, J. Vac. Sci. Technol. A 7 (1989) 1194.
[34] P. Jin, S. Tanemura, Jpn. J. Appl. Phys. 33 (1994) 1478.
[35] G.H. Brown (Ed.), Photochromism, Wiley, New York, 1971. G.H. Dorion, A.F. Wiebe, Photochromism, The Focal Press, London, New York, 1970.
[36] N.Y.C. Chy, in: C.M. Lampert, C.G. Granqvist (Eds.), Large-Area Chromogenics: Materials and Devices for Transmittance Control, vol. 54, SPIE Opt. Eng. Press, Washington, 1990, p. 102.
[37] T. Yoshida, A. Morinaka, N. Funakoshi, J. Chem. Soc. Chem. Commun. 437 (1988) 23.
[38] A. Morinaka, T. Yoshida, N. Fumakoshi, Jpn. J. Appl. Phys. 26 (Suppl. 26-4) (1987) 87.
[39] K. Matsui, S. Yoshida, J. Appl. Phys. 64 (1988) 2607.
[40] E. Ando, J. Miyazaki, K. Morimoto, H. Nakahara, K. Fukuda, Thin Solid Films 133 (1985) 25.
[41] E. Ando, J. Hibino, T. Hashida, K. Morimoto, Thin Solid Films 160 (1988) 279.
[42] M. Mizuhashi, S. Furuuchi, Thin Solid Films 30 (1975) 259; Report Res. Lab. Asahi Glass Co., Ltd., vol. 26, 1976, p. 17.
[43] A.A. Kuz'michev, V.V. Sviridov, Inorg. Mater. 15 (1979) 1240.
[44] T. Hirono, T. Yamada, J. Appl. Phys. 59 (1986) 948.
[45] R.J. Colton, A.M. Guzman, J.W. Rabalais, J. Am. Chem. Soc. 11 (1978) 171.
[46] T.C. Arnoldussen, J. Electrochem. Soc. 123 (1976) 527.
[47] J.P. Ziegler, J.C. Hemminger, J. Electrochem. Soc. 134 (1987) 358.
[48] C.M. Lampert, Solar Energy Mater. 11 (1984) 1 and references therein.
[49] T. Oi, Nucl. Annu. Rev. 16 (1986) 185.
[50] A. Donnadieu, Mater. Sci. Eng. B 3 (1989) 185.
[51] H. Shirakawa, E.J. Louis, A.G. Mac Diarmid, C.K. Chiang, A.J. Heeger, J. Chem. Soc. Chem. Commun. 1 (1977) 578.
[52] S.C. Yang, in: C.M. Lampert, C.G. Granqvist (Eds.), Large-Area Chromogenics: Materials and Devices for Transmittance Control, vol. 54, SPIE Opt. Eng. Press, Washington, 1990, p. 335.
[53] G. Kaindl, G. Wartmann, S. Roth, K. Menke, Solid State Commun. 41 (1982) 75.
[54] R.J. Cushman, P.M. Mc Manus, S.C. Yang, J. Electroanal. Chem. 291 (1986) 335.
[55] K. Mücke, F. Böhm, T. Gambke, C. Ottermann, K. Bange, SPIE 1323 (1990) 188.
[56] C. Ottermann, J. Segner, K. Bange, Proc. SPIE 1728 (1992) 211.
[57] C.G. Granqvist, Solid State Ionics 70/71 (1994) 678.
[58] C.G. Granqvist, Sol. Energy Mater. Sol. Cells 32 (1994) 369.
[59] W.C. Dautremont-Smith, Display 4 (1982) 67.
[60] S. Gottesfeld, J.D.E. Mc Intyre, G. Beni, J.L. Shay, Appl. Phys. Lett 33 (1978) 208.
[61] L.M. Schiavone, W.C. Dautremont-Smith, G. Beni, J.L. Say, Appl. Phys. Lett. 34 (1979) 823.
[62] D. Michell, D.A.J. Rand, R. Woods, J. Electroanal. Chem. 84 (1977) 117.
[63] G. Blondeau, M. Froelicher, M. Froment, A. Hugot-Le Goff, Phys. Status Solidi A 26 (1974) 181.

[64] Z. Orel, M.G. Hutchins, G. McMeckins, Sol. Energy Mater. Sol. Cell 30 (4) (1993) 327.
[65] M.K. Carpenter, R.S. Conell, D.A. Corrigan, Sol. Energy Mater. 16 (1987) 333.
[66] T. Maruyama, S. Arai, Sol. Energy Mater. Sol. Cells 30 (3) (1993) 257.
[67] A.M. Andersson, W. Estrada, C.G. Granqvist, Proc. SPIE 1272 (1990) 96. W. Estrada, A.M. Andersson, C.G. Granqvist, A. Gorenstein, F. Decker, J. Mater. Res. 6 (1991) 1715.
[68] K. Bange, F.G.K. Baucke, B. Metz, Proc. SPIE 1016 (1989) 170.
[69] K. Bange, C. Ottermann, From Galileo's Occhialino to Optoelectronics, vol. 9128, World Scientific. Publ. Co., Singapore, 1993, p. 14.
[70] J. Nagai, Sol. Energy Mater. Sol. Cell 31 (1993) 291.
[71] A. Nemetz, A. Temmink, K. Bange, S.C. de Torresi, C. Gabrielli, R. Torresi, A. Hugot-Le Goff, Sol. Energy Mater. Sol. Cell 25 (1992) 93.
[72] K. Bange, U. Martens, A. Nemetz, A. Temmink, in: M.K. Carpenter, D.A. Corrigan, (Eds.), Electrochromic Materials, The Electrochemical Society, Pennington, USA, 1990, Proc. vol 90-2, p. 334.
[73] N.R. Lynam, H.R. Habib, Proc. SPIE 1016 (1989) 63.
[74] C. Ottermann, A. Temmink, K. Bange, Proc. SPIE 1272 (1990) 111.
[75] S. Yamada, T. Yoshioka, M. Miyashita, K. Urabe, M. Kiato, J. Appl. Phys. 63 (1988) 2116.
[76] B. Orel, M. Macek, F. Svegl, K. Kalcher, Thin Solid Films 246 (1994) 131.
[77] S. Gottesfeld, J. Electrochem. Soc. 127 (1980) 272.
[78] L.D. Durke, O.J. Murphy, J. Electroanal. Chem. 109 (1980) 373.
[79] U.L. Stangar, B. Orel, I. Grabec, B. Ogorevc, K. Kalcher, Sol. Energy Mater. Sol. Cells 31 (1993) 171.
[80] Y. Fujita, K. Miyazaki, C. Tatsuyama, Jpn. J. Appl. Phys. 24 (1985) 1082.
[81] C.R. Aita, Y. Liu, M.L. Kao, S. Hansen, J. Appl. Phys. 60 (1986) 749.
[82] S.F. Cogan, in: C.M. Lampert, C.G. Granqvist (Eds.), Large-Area Chromogenics: Materials and Devices for Transmittance Control, vol. 54, SPIE Opt. Eng. Press, Washington, 1990, p. 313.
[83] A. Talledo, A.M. Andersson, C.G. Granqvist, J. Appl. Phys. 69 (1991) 3261.
[84] M.S.R. Kahn, K.A. Kahn, W. Estrada, C.G. Granqvist, J. Appl. Phys. 69 (1991) 3231.
[85] K. Nagase, Y. Shimizu, N. Miura, N. Yamazoe, Appl. Phys. Lett. 64 (9) (1994) 1059. S. Sato, Y. Seino, J. Electron. Commun. Soc. J 65-L (1982) 629.
[86] W.C. Dautremont-Smith, Displays 1 (1982) 3.
[87] B.W. Faughnan, R.S. Crandall, R.S. Heyman, RCA Rev. 36 (1975) 177.
[88] M.L. Hitchman, J. Electroanal. Chem. 85 (1977) 135.
[89] S.K. Deb, J.A. Chopoorian, J. Appl. Phys. 37 (1966) 4818.
[90] N. Miyata, S. Akiyoshi, J. Appl. Phys. 58 (1985) 1651.
[91] A. Donnadieu, D. Davazoglou, A. Abdellaoui, Thin Solid Films 164 (1988) 333.
[92] C.E. Tracy, D.K. Benson, J. Vac. Sci. Technol. A 4 (1986) 2377.
[93] K. Kitao, S. Yamada, Y. Hiruta, N. Suzuki, K. Urabe, Appl. Surf. Sci. 33/34 (1988) 812.
[94] S. Yamada, M. Kitao, in: C.M. Lampert, C.G. Granqvist (Eds.), Large-Area Chromogenics: Materials and Devices for Transmittance Control, vol. 54, SPIE Opt. Eng. Press, Washington, 1990, p. 246.
[95] A. Pennisi, F. Simone, C.M. Lampert, Sol. Energy Mater. Sol. Cells 28 (3) (1992) 233.
[96] J. Götsche, A. Hinsch, V. Wittwer, Sol. Energy Mater. Sol. Cells 31 (3) (1993) 415.
[97] A. Azens, B. Stjerna, C.G. Granqvist, J. Gabrusenoks, A. Lusis, Appl. Phys. Lett. 65 (1994) 1998.
[98] A. Azens, C.G. Granqvist, E. Pentjuss, J. Gabrusenoks, J. Barczynska, to be published.
[99] C.K. Dyer, J.S. Lech, J. Electrochem. Soc. 135 (1978) 23.
[100] A. Gutarra, A. Azens, B. Stjerna, C.G. Granqvist, Appl. Phys. Lett. 64 (13) (1994) 1604.
[101] N. Özer, F. Tepehan, Sol. Energy Mater. Sol. Cells 30 (1) (1993) 13.
[102] K. Bange, T. Gambke, Adv. Mater. 2 (1990) 10.
[103] A. Agrawal, J.P. Cronin, R. Zhang, Sol. Energy Mater. Sol. Cells 31 (1993) 9.
[104] C.G. Granqvist, Solid State Ionics 53–56 (1992) 479.
[105] C.M. Lampert, Thin Solid Films 236 (1993) 6.
[106] C.M. Lampert, Sol. Energy Mater. Sol. Cells 32 (1994) 307.

[107] C.M. Lampert, S.J. Visco, M.M. Doeff, Y.P. Ma, Y. He, J.-C. Giron, Sol. Energy Mater. Sol. Cells 33 (1994) 91.
[108] S.K. Deb, Appl. Opt. Suppl. 3 (1969) 192.
[109] F.G.K. Baucke, K. Bange, T. Gambke, Displays 10 (1988) 179.
[110] K. Bange, T. Gambke, G. Sparschuh, in: R.E. Hummel, K.H. Guenther (Eds.), Handbook of Optical Properties, vol. I, CRC Press, Boca Raton, 1995, p. 105.
[111] R.C. Ottermann, A. Temmink, K. Bange, Thin Solid Films 193/194 (1990) 409.
[112] N.R. Lynam, SAE Tech. Paper Ser. 870636 (1987) 1.
[113] S.E. Selkowitz, C.M. Lampert, in: C.M. Lampert, C.G. Granqvist (Eds.), Large-Area Chromogenics: Materials and Devices for Transmittance Control, vol. 54, SPIE Opt. Eng. Press, Washington, 1990, p. 22.
[114] N.R. Lynam, in: C.M. Lampert, C.G. Granqvist (Eds.), Large-Area Chromogenics: Materials and Devices for Transmittance Control, vol. 54, SPIE Opt. Eng. Press, Washington, 1990, p. 47.
[115] A. Deneuville, P. Gerard, J. Electron. Mater. 7 (1978) 559.
[116] K. Mücke, F. Böhm, T. Gambke, C. Ottermann, K. Bange, SPIE 1323 (1990) 188.
[117] B.P. Hichwa, G. Caskey, D.F. Betz, J.D. Harlow, J. Vac. Sci. Technol. A 5 (1987) 1775.
[118] G.L. Harding, Thin Solid Films 138 (1986) 279.
[119] A. Donnadieu, D. Davazoglou, Proc. SPIE 653 (1986) 63.
[120] D. Davazoglou, A. Donnadieu, R. Fourcade, A. Hugot-LeGoff, P. Delichere, A. Perez, Rev. Phys. Appl. 23 (1988) 265.
[121] D. Davazoglou, G. Leveque, A. Donnadieu, Sol. Energy Mater. 17 (1988) 379.
[122] R. Hurditch, Electron Lett. 11 (1975) 142.
[123] D. Craigen, A. Mackintosh, J. Hickman, K. Colbow, J. Electrochem. Soc. 133 (1986) 1529.
[124] J. Zhang, K. Colbow, Appl. Phys. Lett. 58 (1991) 1013.
[125] H.R. Zeller, M.U. Beyeler, Appl. Phys. 13 (1977) 231.
[126] D.K. Benson, C.E. Tracy, Proc. SPIE 562 (1985) 46. C.E. Tracy, D.K. Benson, J. Vac. Sci. Technol. A 4 (1986) 2377. J.S.E.M. Svensson, D.K. Benson, C.E. Tracy, Proc. SPIE 1016 (1988) 19.
[127] F. Di Quarto, A. Di Paola, S. Piazza, C. Sunseri, Sol. Energy Mater. 11 (1985) 419.
[128] P. Delichere, P. Falaras, M. Froment, A. Hugot-LeGoff, B. Agius, Thin Solid Films 161 (1988) 35.
[129] T. Ohtsuka, N. Goto, N. Sato, K. Kunimatsu, Ber. Bunsenges. Phys. Chem. 91 (1987) 313.
[130] T. Ohtsuka, N. Goto, N. Sato, J. Electroanal. Chem. 287 (1990) 249.
[131] K. Machida, M. Enyo, J. Electrochem. Soc. 137 (1990) 1169.
[132] A. Chemseddine, F. Barbonneau, J. Livage, J. Non-Cryst. Solids 91 (1987) 271.
[133] A. Di Paola, F. Di Quarto, C. Sunseri, Corrosion Sci. 20 (1980) 1067.
[134] D.V. Sviridov, A.I. Kulak, Thin Solid Films 198 (1991) 191.
[135] H. Unuma, K. Tonooka, Y. Suzuki, T. Furusaki, K. Kodaira, T. Matsushita, J. Mater. Sci. Lett. 5 (1986) 1248.
[136] J.M. Bell, D.C. Green, A. Patterson, G.B. Smith, K.A. MacDonald, K. Lee, L. Kirkup, J.D. Cullen, B.O. West, L. Spiccia, M.J. Kenny, L.S. Wielunski, Proc. SPIE 1536 (1991) 29.
[137] K. Yamanaka, H. Oakamoto, H. Kidou, T. Kudo, Jpn. J. Appl. Phys. 25 (1986) 1420.
[138] T. Kudo, S. Takano, A. Kishimoto, Y. Aikawa, Denki Kagaku 59 (1991) 718.
[139] M.A. Habib, S.P. Maheswari, M.K. Carpenter, J. Appl. Electrochem. 21 (1991) 203.
[140] M.I. Yanovskaya, I.E. Obvintseva, V.G. Kessler, B.Sh. Galyamov, S.I. Kucheiko, R.R. Shifrina, N.Ya. Turova, J. Non-Cryst. Solids 124 (1990) 155.
[141] J. Götsche, A. Hinsch, V. Wittwer, Sol. Energy Mater. Sol. Cells 31 (3) (1993) 415.
[142] A. Agrawal, J.P. Cronin, R. Zhang, Sol. Energy Mater. Sol. Cells 31 (1) (1993) 9 and references therein.
[143] J.P. Cronin, D.J. Tarico, J.C.L. Tonazzi, A. Agrawal, S.R. Kennedy, Sol. Energy Mater. Sol. Cells 29 (4) (1993) 371.
[144] N. Baba, T. Yohino, J. Appl. Electrochem. 12 (1982) 607.
[145] M.H. Miles, D.E. Stilwell, R.A. Hollins, R.A. Henry, in: M.K. Carpenter, D.A. Corrigan (Eds.), Electrochromic Materials, The Electrochemical Society, Pennington, USA, 1990, Proc. vol. 90-2, p. 137.

[146] G.K. Wertheim, M. Campagna, J.-N. Chazalviel, D.N.E. Buchanan, H.R. Shanks, Appl. Phys. 13 (1977) 225.
[147] G. Gerand, G. Nowogrocki, J. Guenot, M. Figlarz, J. Solid State Chem. 29 (1979) 429.
[148] T. Nanba, I. Yasui, J. Solid State Chem. 83 (1989) 304.
[149] S.K. Deb, Appl. Opt. (Suppl. 3) (1969) 192. S.K. Deb, Philos. Mag. 27 (1973) 801.
[150] K. Bange, et al., BMFT Final Report FKZ 13 N 5476, 1991.
[151] M.S. Whittingham, MRS Bull. 9 (1989) 31.
[152] J.B. Goodenough, in: H. Reiss (Ed.), Progress in Solid State Chemistry, Pergamon Press, Oxford, 1971.
[153] J.M. Honig, in: S. Trasatti (Ed.), Electrodes of Conductive Metallic Oxides, Elsevier, Amsterdam, 1980.
[154] E.U. Berndt, Ph.D. Thesis, Universität Münster, 1986.
[155] R.J. Ackermann, E.G. Rauh, J. Phys. Chem. 67 (1963) 2596. J.H. Norman, H.G. Staley, J. Chem. Phys. 43 (1965) 3804.
[156] J. Berkowitz, W.A. Chupka, M.G. Ingharm, J. Chem. Phys. 27 (1957) 85.
[157] O. Glemser, R. v. Haeseler, Z. Anorg. Allg. Chem. 316 (1962) 168. S.S. Lu, J. Electrochem. Soc. 127 (1980) 1108.
[158] A. Azens, M. Kitenbergs, U. Kanders, Vacuum 47 (1995) 745.
[159] L. Pickelmann, P. Schlotter, C. Vogel, BMFT Report FKZ FB-T 83-212, 1983.
[160] G. Baur et al., Forschungsbericht BMFT-FB-T 80-196,1980. G. Baur et al., Abschlußbericht BMFT-FB, Förderungskennzeichen NT2536/3, 1982. P. Schlotter, L. Pickelmann, J. Elektron. Mater. 11 (1982) 207.
[161] Y. Shigesato, Y. Hayashi, A. Masui, T. Haranou, Jpn. J. Appl. Phys. 30 (1991) 814. Y. Shigesato, A. Murayama, T. Kamimori, K. Matsuhiro, Appl. Surf. Sci. 33/34 (1988) 804.
[162] K. Bange, H. Hantsche, C. Ottermann, X. Yu, Proc. SURTEC 5, C. Hanser Verlag, München, 1989, p. 397.
[163] V.I. Kukuev, E.A. Tutov, E.P. Domashevskaya, M.I. Yanovskaya, I.E. Obvintseva, Yu.N. Venevtsev, Zh. Tekh. Fiz. 57 (1987) 1957 [Soviet Phys. Tech. Phys. 32 (1987) 1176].
[164] D. Green, Properties of tungsten oxide and trigonally bonded compounds, Ph.D. Thesis, University of Sydney, Australia, 1991.
[165] K. Miyake, H. Kaneko, M. Sano, N. Suedomi, J. Appl. Phys. 55 (1984) 2747.
[166] Y. Wang, N. Herron, J. Chem. Phys. 95 (1991) 525.
[167] Y. Shigesato, Jpn. J. Appl. Phys. 30 (1991) 1457.
[168] H. Morita, H. Washida, Jpn. J. Appl. Phys. 23 (1984) 754.
[169] M. Hüppauff, K. Bange, B. Lengeler, Thin Solid Films 230 (1993) 191.
[170] K. Matsuhiro, Y. Masuda, Proc. SID 21 (1980) 101. Y. Shigesato, A. Murayama, T. Kamimori, K. Matsuhiro, Rep. Res. Lab. Asahi Glass Co., vol. 38, 1988, p. 39.
[171] Gmelin, Handbuch der anorganischen Chemie, Ergänzungsbände Wolfram B2, B3, 8. Auflage, Springer, Berlin, 1979.
[172] W. Wagner, F. Rauch, R. Feile, C. Ottermann, K. Bange, Thin Solid Films 235 (1993) 228.
[173] O. Becker, K. Bange, Ultramicroscopy 52 (1993) 73.
[174] R. Messier, J. Vac. Sci. Technol. A 4 (1986) 490.
[175] S.A. Agnihotry, K.K. Saini, T.K. Saxena, S. Chandra, Thin Solid Films 141 (1986) 183.
[176] T. Motohiro, Y. Taga, Appl. Opt. 28 (1989) 2466.
[177] M. Shiojiri, T. Miyano, C. Kaito, Jpn. J. Appl. Phys. 18 (1979) 1937.
[178] C. Kaito, T. Shimizu, Y. Nakata, Y. Saito, Jpn. J. Appl. Phys. 24 (1985) 117.
[179] G.M. Ramans, J.V. Gabrusenoks, A.R. Lusis, A.A. Patamalnieks, J. Non-Cryst. Solids 90 (1987) 637.
[180] V.I. Kukuyev, L.F. Komolova, M.V. Lesovoy, Y.Y. Tomaspolsky, J. Microsc. Spectrosc. Electron. 14 (1989) 471.
[181] G.M. Ramans, J.V. Gabrusenoks, A.A. Veispals, Phys. Status Solidi 74 (1982) K41.
[182] J.V. Gabrusenoks, P.D. Cikmach, A.R. Lusis, J.J. Kleperis, G.M. Ramans, Solid State Ionics 14 (1984) 25.
[183] M.F. Daniel, B. Desbat, J.C. Lassegues, R. Garie, J. Solid State Chem. 73 (1988) 127.

[184] M. Pham Thi, G. Velasco, Solid State Ionics 14 (1984) 217. M. Pham, Thi, G. Velasco, Rev. de Chimie minérale 22 (1985) 195.
[185] P. Delichère, P. Falaras, M. Froment, A. Hugot-le Goff, B. Agius, Thin Solid Films 161 (1988) 35. P. Delichère, P. Falaras, A. Hugot-le Goff, Thin Solid Films 161 (1988) 47. P. Delichère, P. Falaras, A. Hugot-le Goff, Sol. Energy Mater. 19 (1989) 323. P. Delichère, P. Falaras, A. Hugot-le Goff, Proc. SPIE 1016 (1988) 12.
[186] M. Green, Z. Hussain, J. Appl. Phys. 69 (1991) 7788.
[187] R. Mercier, O. Bohnké, Cl. Bohnké, G. Robert, B. Carquille, M.-F Mercier, Mat. Res. Bull. 18 (1983) 1.
[188] M. Pham Thi, Chem. Phys. Lett. 115 (1985) 130.
[189] T. Ohtsuka, N. Goto, N. Sato, K. Kunimatsu, Ber. Bunsenges. Phys. Chem. 91 (1987) 313.
[190] M.F. Daniel, B. Desbat, J.G. Lassegues, B. Gerand, M. Figlarz, J. Solid State Chem. 67 (1987) 235.
[191] T. Nanba, Y. Nishiyama, I. Yasui, J. Mater. Res. 6 (1991) 1324.
[192] E. Salje, K. Viswannathan, Acta Crystallogr. A 31 (1975) 356. E. Salje, Acta Crystallogr. A 31 (1975) 360. E. Salje, Ferroelectrics 12 (1976) 215.
[193] S. Mohan, A. Mukunthan, Curr. Sci. 54 (1985) 858.
[194] J.M. Stencel, L.E. Makovsky, J.R. Diehl, T.A. Sarkus, J. Raman Spectrosc. 15 (1984) 282.
[195] Y. Shigesato, Y. Hayashi, A. Masui, T. Haranou, Jpn. J. Appl. Phys. 30 (1991) 282.
[196] N. Yoshiike, S. Kondo, J. Electrochem. Soc. 130 (1983) 2283. N. Yoshiike, S. Kondo, J. Electrochem. Soc. 131 (1984) 809. N. Yoshiike, S. Kondo, J. Electrochem. Soc. 131 (1984) 2600.
[197] T.C. Arnoldussen, J. Electrochem. Soc. 128 (1981) 117.
[198] A. Balerna, E. Bernieri, E. Burattini, A. Kuzmin, A. Lusis, J. Purans, P. Cikmach, Nucl. Instr. and Meth. Phys. Res. A 308 (1991) 234.
[199] A. Balerna, E. Bernieri, E. Burattini, A. Kuzmin, A. Lusis, J. Purans, P. Cikmach, Nucl. Instr. and Meth. Phys. Res. A 308 (1991) 240.
[200] B. Gerand, G. Nowogrocki, M. Figlarz, J. Solid State Chem. 38 (1981) 312.
[201] C.A. Bishop, G. Edge, I. Sutherlad, R.P. Howson, Vacuum 37 (1987) 279.
[202] J. Nagai, T. Kamimori, M. Mizuhashi, Proc. SPIE 502 (1984) 59. J. Nagai, T. Kamimori, M. Mizuhashi, Sol. Energy Mater. 13 (1986) 279. T. Kamimori, J. Nagai, M. Mizuhashi, Sol. Energy Mater. 16 (1987) 27.
[203] J. Nagai, Proc. SPIE 1016 (1988) 28.
[204] A. Temmink, O. Anderson, K. Bange, H. Hantsche, X. Yu, Thin Solid Films 192 (1990) 211.
[205] M.R. Goulding, C.B. Thomas, Thin Solid Films 62 (1979) 175.
[206] P. Gérard, A. Deneuville, R. Courths, Thin Solid Films 71 (1980) 221. A. Deneuville, P. Gérard, J. Electron. Mater. 7 (1978) 559.
[207] W. Wagner, Ph. D. Thesis, Universität Frankfurt, 1990.
[208] A. Agrawal, H. Habibi, Thin Solid Films 169 (1989) 257.
[209] F. Rauch, W. Wagner, K. Bange, Nucl. Instr. and Meth. B 42 (1989) 264.
[210] W. Wagner, F. Rauch, K. Bange, Fresenius Z. Anal. Chem. 333 (1989) 478.
[211] S. Badilescu, P.V. Ashrit, F.E. Girouard, V. Truong, J. Electrochem. Soc. 136 (1989) 3599.
[212] P. Schlotter, L. Pickelmann, J. Electron. Mater. 11 (1982) 207.
[213] M.R. Goulding, C.B. Thomas, R.J. Hurditch, Solid State Commun. 46 (1983) 451.
[214] H. Niehus, Surf. Sci. 78 (1978) 667.
[215] C. Bechinger, S. Herminghaus, P. Leiderer, Thin Solid Films 239 (1994) 156.
[216] C.S. Bechinger, Ph.D. Thesis, Universität Konstanz, Germany, 1993.
[217] C.S. Bechinger, G. Oetinger, S. Herminghaus, P. Leiderer, J. Appl. Phys. 74 (1993) 4527.
[218] J.R. Sambles, G.W. Bradberry, F. Yang, Contemp. Phys. 32 (1991) 173.
[219] R. Keller, Diploma Thesis, University Mainz, 1987.
[220] A.I. Garrilynk, B.P. Zakarchenya, F.A. Chudnovskii, Sov. Tech. Phys. Lett. 6 (1980) 512.
[221] A.I. Garrilynk, T.G. Lanskaya, F. Chudnovskii, Sov. Tech. Phys. Lett. 32 (1987) 964.
[222] M. Nagasu, N. Koshida, Appl. Phys. Lett. 57 (1990) 1324.
[223] E. Kikuchi, K. Iida, A. Fujishima, K. Itoh, J. Electroanalyt Chem. 351 (1993) 105.
[224] J.N. Yao, B.H. Loo, A. Fujishima, Ber. Bunsenges. Phys. Chem. 94 (1990) 13.

[225] M. Nagasu, N. Koshida, J. Appl. Phys. 71 (1988) 398.
[226] N.N. Dinh, V.T. Bich, N.H. Hoang, L.Q. Minh, Phys. Stat. Soli. 108 (1988) K157.
[227] N. Koshida, O. Tomita, Jpn. J. Appl. Phys. 24 (1985) 92. N. Koshida, O. Tomita, Y. Iketsu, Ext. Abstr. 17th Conf. Sol. State Dev. Mat., Tokyo, 1985, p. 369. N. Koshida, Y. Ichinase, K. Ohtaka, M. Komuro, N. Atoda, J. Vac. Sci. Technol. B 8 (1990) 1093.
[228] S. Walck, A.D. Buonaquisti, J. Vac. Sci. Technol. A 3 (1985) 2214.
[229] H. Morita, T. Miura, H. Washida, Jpn. J. Appl. Phys. 20 (1981) 323.
[230] A.E. Antropov, O.F. Afonin, A.I. Gavrilynk, B.P. Zakharchenya, F.A. Chuclnoskii, N.K. Shaver, Sov. Tech. Phys. Lett. 4 (1978) 224.
[231] P.K. Gupta, K.L. Chopra, J. Appl. Phys. 62 (1987) 4273.
[232] M. Koitabashi, H. Kimura, S. Shimoji, M. Yamamoto, IEEE Trans. Eletron. Dev. 37 (1990) 2644.
[233] M.R. McCartney, D.J. Smith, Surf. Sci. 221 (1989) 214.
[234] D. Papadopoulos, C. Manolikas, J. Spyridelis, Mater. Res. Bull. 10 (1975) 847.
[235] M. Baba, T. Ikeda, Jpn. J. Appl. Phys. 20 (1981) L149.
[236] T.T. Lin, D. Lichtmann, J. Appl. Phys. 50 (1979) 1298.
[237] I.A. Konovalov, Y.A. Kulyupin, V.B. Nechitailo, V.I. Stepkin, Sov. Phys. Tech. Phys. 30 (1985) 966.
[238] K. Bange, U. Martens, A. Nemetz, A. Temmink, in: M.K. Carpenter, D.A. Corrigan (Eds.) Electrochromic Materials, Proc. vol. 90-2, The Electrochemical Society, Pennington, USA, 1990, p. 334.
[239] C.M. Lampert, Sol. Energy Mater. 11 (1984) 1.
[240] W.C. Dautremont-Smith, Displays 3 (1982) 67.
[241] I.F. Chang, B.L. Gilbert, T.I. Sun, J. Electrochem. Soc. 122 (1975) 955.
[242] P.G. Dickens, M.S. Whittingham, Q. Rev. Chem. Soc. 22 (1968) 30.
[243] M.S. Whittingham, MRS Bull. (1989) 31.
[244] B.W. Faughnan, R.S. Crandall, P.M. Heyman, RCA Rev. 36 (1975) 177. R.S. Crandall, B.W. Faughnan, Appl. Phys. Lett. 28 (1976) 95.
[245] M. Green, W.C. Smith, J.A. Weiner, Thin Solid Films 38 (1976) 89.
[246] H.N. Hersh, W.E. Kramer, J.H. McGee, Appl. Phys. Lett. 27 (1975) 646.
[247] M. Green, K.S. Kang, Thin Solid Films 40 (1977) L19.
[248] W.C. Dautremont-Smith, M. Green, K.S. Kang, Electrochem. Acta 22 (1977) 751.
[249] L.M. Schiavone, W.C. Dautremont-Smith, G. Beni, J.L. Shay, Appl. Phys. Lett. 34 (1979) 823.
[250] S. Yamada, Y. Hiruta, N. Suzuki, K. Urabe, M. Kitao, K. Toyoda, Jpn. J. Appl. Phys. 24 (Suppl. 3) (1985) 142.
[251] H. Morita, Jpn. J. Appl. Phys. 24 (1985) 750.
[252] T. Yoshimura, J. Appl. Phys. 57 (1985) 911.
[253] A. Vértes, R. Schiller, J. Appl. Phys. 54 (1983) 199.
[254] G. Bajars, Ya.A. Pitkevich, J. Straumens, A. Lusis, Sov. Electrochem. 25 (1989) 749.
[255] T. Kamimori, J. Nagai, M. Mizuhashi, Proc. SPIE 428 (1983) 51.
[256] M.L. Hitchman, Thin Solid Films 61 (1979) 341.
[257] B. Reichman, A.J. Bard, J. Electrochem. Soc. 126 (1979) 583.
[258] B. Reichman, A.J. Bard, D. Laser, J. Electrochem. Soc. 127 (1980) 647.
[259] R.S. Crandall, B.W. Faughnan, Appl. Phys. Lett. 26 (1975) 120.
[260] B.W. Faughnan, R.S. Crandall, M.A. Lampert, Appl. Phys. Lett. 27 (1975) 275.
[261] R.S. Crandall, P.J. Wojtowicz, B.W. Faughnan, Solid State Commun. 18 (1976) 1409.
[262] A.R. Haranahalli, P.H. Holloway, J. Electron. Mater. 10 (1981) 141.
[263] L. Zhongkuan, D. Zishang, J. Zhoughua, J. Non-Cryst. Solids 112 (1989) 309.
[264] H. Morita, Jpn. J. Appl. Phys. 24 (1985) 723.
[265] S.K. Mohapatra, J. Electrochem. Soc. 125 (1978) 284.
[266] H. Morita, H. Washida, Jpn. J. Appl. Phys. 19 (1980) L228.
[267] R. Kötz, C. Barbero, O. Haas, J. Electroanal. Chem. 296 (1990) 37.
[268] S.I. Córdoba-Torresi, A. Gorenstein, R.M. Torresi, M.V. Vasquez, J. Electroanal. Chem. 318 (1991) 131.
[269] V. Wittwer, O.F. Schirmer, P. Schlotter, Solid State Commun. 25 (1978) 977.
[270] D.E. Aspnes, A. Heller, J. Phys. Chem. 87 (1983) 4919.

[271] K. Bange, R. Keller, W. Wagner, F. Rauch, Proc. SPIE 1016 (1988) 50.
[272] R.D. Rauh, Solid State Ionics 28–30 (1988) 1479.
[273] K. Ito, T. Kubo, in: S. Kataoka (Ed.), Proc. 4th Sensor Symp.
[274] S.J. Khoobar, J. Phys. Chem. 68 (1964) 411.
[275] M. Boudart, M.A. Vannice, J.E. Benson, Z. Phys. Chem. Neue Folge 64 (1969) 171.
[276] R.B. Levi, M. Boudart, J. Catal. 32 (1974) 304.
[277] R.R. Rye, A.J. Ricco, J. Appl. Phys. 62 (1987) 1084.
[278] K. Bange, T. Gambke, Adv. Mater. 2 (1990) 10.
[279] F.G.K. Baucke, K. Bange, T. Gambke, Displays 10 (1988) 179.
[280] A.J. Hughes, P. Lloys, Program of the 19th Electronic Materials Conf., Cornell University Ithaca, NY, 1977, p. 44.
[281] H.J. Stocker, S. Singh, L.G. Van Uitert, G. Zydzik, Program of the 20th Electronic Materials Conf., Santa Barbara, CA, 1978, p. 12.
[282] Y. Hajimoto, M. Matsushima, S. Ogura, Program of the 20th Electronic Materials Conf., Santa Barbara, CA, 1978, p. 12.
[283] B.W. Faughnan, R.S. Crandall, Display Devices, in: J.I. Pankow (Ed.), Springer Topics in Appl. Phys., vol. 40, Springer, Berlin, 1980, p. 181.
[284] I. Shimizu, M. Shizukuishi, E. Inoue, J. Appl. Phys. 50 (1979) 4027. M. Shizukuishi, I. Shimizu, E. Inoue, J. Appl. Phys. 20 (1981) 575 (19) (1980) 2121.
[285] H. Gerischer, Electrochim. Acta 34 (1989) 1005. H. Gerischer, W. Eckhardt, Appl. Phys. Lett. 43 (1983) 393.
[286] C. Ottermann, J. Segner, K. Bange, Proc. SPIE 1728 (1992) 211.
[287] S.K. Deb, Proc. SPIE 692 (1986) 19.
[288] O.F. Schirmer, V. Wittwer, G. Baur, G. Brandt, J. Electrochem. Soc. 124 (1977) 749. O.F. Schirmer, J. Phys. (Paris), Colloque 6 (1980) 479.
[289] C.G. Granqvist, Appl. Phys. A 57 (1993) 3.
[290] B.H. Loo, J.N. Yao, H. Dwain Coble, K. Hashimoto, A. Fujishima, Appl. Surf. Scie. 81 (1994) 175.
[291] L. Pickelmann, P. Schlotter, Proc. 1st Europ. Disp. Res. Conf. Eurodisplay, 1981, p. 87.
[292] N. Yoshiike, S. Kondo, Denki Kagaku 54 (1986) 423.
[293] H. Akram, H. Tatsuoka, M. Kitao, S. Yamada, J. Appl. Phys. 62 (1987) 2039.
[294] P. Schlotter, L. Pickelmann, J. Electron. Mater. 11 (1982) 207.
[295] N. Yoshiike, Y. Mizuno, S. Kondo, J. Electrochem. Soc. 131 (1984) 2634.
[296] A.I. Gavrilyuk, V.G. Prokhavtilov, F.A. Chudnovskil, Sov. Phys. Solid State 24 (1982) 558.
[297] A. Kuzmin, J. Purans, J. Phys.: Condens. Matter 5 (1993) 2333; 5 (1993) 267.
[298] H. Höchst, R.D. Bringans, Appl. Surf. Sci. 11/12 (1982) 768.
[299] R.J. Colton, A.M. Guzman, J.W. Rabalais, J. Appl. Phys. 49 (1978) 409; Acc. Chem. Res. 11 (1978) 170.
[300] S. Hashimoto, M. Masuoka, J. Appl. Phys. 69 (1991) 933; J. Electrochem. Soc. 138 (1991) 2403.
[301] G. Hollinger, T.M. Duc, A. Deneuville, Phys. Rev. Lett. 37 (1976) 1564.
[302] A. Temmink, O. Anderson, K. Bange, H. Hantsche, X. Yu, Vacuum 41 (1990) 1144.
[303] O. Anderson, Vacuum 41 (1990) 7.
[304] P.D. Cikmach, J.J. Kleperis, A.R. Lusis, G.M. Ramans, Phys. Status Solidi A 90 (1985) K1.
[305] S.K. Deb, Phys. Rev. B 16 (1977) 1020.
[306] A. Deneuville, P. Gérard, B.K. Chakraverty, Proc. 12th Int. Conf. Amorphous and Liquid Semicond., Edinburgh, 1977, p. 668.
[307] C.G. Granqvist, Renewable Energy 5 (1994) 141.
[308] J. Janata, Anal. Chem. 63 (1991) 2546.
[309] D. Blackwood, M.J. Josowicz, J. Phys. Chem. 95 (1991) 493.
[310] R. Memming, Electrochim. Acta 25 (1980) 77.
[311] M.A. Butler, J. Appl. Phys. 48 (1977) 1914.
[312] H. Gerischer, in: B.O. Chinp (Ed.), Solar energy conversion, Topics in Appl. Phys., vol. 31, Springer, Berlin, 1979, p. 115.
[313] N.D. Lang, W. Kohn, Phys. Rev. B 3 (1971) 1215.

[314] K. Bange, B. Straehler, J.K. Sass, R. Parson, J. Electroanal. Chem. 229 (1987) 87.
[315] P.A. Thiel, T.E. Madey, Surf. Sci. Rep. 7 (1987) 211.
[316] M.A. Butler, R.D. Nusby, R.K. Quinn, Solid State Commun. 19 (1976) 1011.
[317] J.O.M. Bockris, A.K.N. Reddy (Eds.), Modern Electrochemistry, Plenum Press, New York, 1970.
[318] K. Bange, D.E. Grider, T.E. Madey, J.K. Sass, Surf. Sci. 136 (1984) 38. K. Bange, T.E. Madey, J. K. Sass, E.M. Stuve, Surf. Sci. 183 (1987) 334.
[319] R. Williams, M.E. Labib, Appl. Phys. Lett. 51 (1987) 1860.
[320] C.G. Granqvist, in: M.H. Francombe, J.L. Vossen (Eds.), Physics in Thin Films, vol. 17, Academic Press. Inc., San Diego, 1993, p. 301.